UNIVERSITY OF CALIFORNIA

Los Angeles

Autonomic Dysfunction following Myocardial Infarction:

Mechanisms and Therapies

A dissertation submitted in partial satisfaction of the

requirements for the degree Doctor of Philosophy

in Molecular, Cellular, and Integrative Physiology

by

Joseph Elias Hadaya

2022

ABSTRACT OF THE DISSERTATION

Autonomic Dysfunction following Myocardial Infarction:

Mechanisms and Therapies

by

Joseph Elias Hadaya

Doctor of Philosophy in Molecular, Cellular, and Integrative Physiology

University of California, Los Angeles, 2022

Professor Kalyanam Shivkumar, Chair

Dysfunction of the autonomic nervous system has been implicated in the progression of most cardiovascular disorders, including congestive heart failure, myocardial infarction, and ventricular arrhythmias. Central to cardiovascular disease progression are the tenets of reflexive sympathoexcitation and reduced parasympathetic tone; indeed, beta blockade and inhibition of the renin-angiotensin-aldosterone system are the mainstays of medical treatment for most cardiovascular disorders. In Yucatan minipigs, myocardial infarction (MI) led to substantial impairments in left ventricular mechanical function and high susceptibility to ventricular tachycardia and fibrillation. At the tissue level, MI

promoted anisotropic electrical conduction, while also leading to greater repolarization heterogeneity and steep repolarization gradients at the border-zone. Myocytes from MI animals exhibited myofibril disarray and a high degree of myocytolysis, a characteristic finding in autopsy specimens of patients with sudden cardiac death. Moreover, extracardiac neural remodeling of the stellate ganglia, the principal efferent sympathetic input to the heart, included greater neuropeptide Y expression, cholinergic transdifferentiation, and a high degree of satellite glial cell activation. Similarly, the thoracic dorsal root ganglia, which serve as the primary source of general visceral afferent fibers to the heart, demonstrated high levels of neuronal nitric oxide synthase expression as well as activation of glial cells. In healthy minipigs, sympathetic afferent and efferent block reduced the effects of sympatho-activation by blunting interstitial norepinephrine release in the left ventricular myocardium. In minipigs with MI, chronic vagal nerve stimulation substantially improved cardiac mechanical function and reduced ventricular arrhythmias following MI, partly by stabilizing activation and repolarization in the border-zone. Finally, MI-associated extracardiac neural remodeling, particularly glial activation in the stellate and dorsal root ganglia, was mitigated by chronic VNS. In conclusion, this work suggests that restoration of parasympathetic function, whether pharmacologically or through neuromodulation, is an attractive therapeutic strategy for post-MI cardiac dysfunction. Furthermore, an improved understanding of cardiac autonomic dysfunction may lead to rationale, neuroscientifically-inspired approaches to treat cardiovascular disease.

The dissertation of Joseph Elias Hadaya is approved.

Jeffrey Laurence Ardell

Thomas J. O'Dell

Yvette Taché

Kalyanam Shivkumar, Committee Chair

University of California, Los Angeles

2022

DEDICATION

To my family, friends, colleagues, and mentors, who have served as a constant source of inspiration, encouragement, and wisdom.

TABLE OF CONTENTS

LIST OF FIGURES

LIST OF TABLES

LIST OF ACRONYMS

ACEi	Angiotensin-converting enzyme inhibitor
AF	Atrial fibrillation
AMT	Axonal modulation therapy
ANTHEM-HF	Autonomic Neural Therapy to Enhance Myocardial Function in Heart Failure
APD	Action potential duration
ARI	Activation recovery interval
ATRAMI	Autonomic Tone and Reflexes After Myocardial Infarction
BSS	Bilateral sympathetic stimulation
CBDCC	Charge balanced direct current carousel
CGRP	Calcitonin gene-related peptide
CHF	Congestive heart failure
CI	Confidence interval
Ctrl	Control
cVNS	Chronic vagal nerve stimulation
DREADDs	Designer receptors specifically activated by designer drugs
DRG	Dorsal root ganglia
ELISA	Enzyme-linked immunosorbent assay
ERP	Effective refractory period
FSCV	Fast scanning cyclic voltammetry
GFAP	Glial fibrillary acidic protein
HFpEF	Heart failure with preserved ejection fraction
HR	Heart rate
IACUC	Institutional Animal Care and Use Committee
ICD	Implantable cardioverter defibrillator
ICNS	Intrinsic cardiac nervous system
INOVATE-HF	Increase of Vagal Tone in Heart Failure
KHFAC	Kilohertz frequency alternating current

LAD	Left anterior descending coronary artery
LV dP/dt	Rate of change of left ventricular pressure
LV dP/dt_{max}	Maximum rate of change of left ventricular pressure
LV dP/dt_{min}	Minimum rate of change of left ventricular pressure
LV	Left ventricle
LVESV	Left ventricular end diastolic volume
LVEF	Left ventricular ejection fraction
LVESV	Left ventricular end systolic volume
LVIDd	Left ventricular internal diameter in diastole
LVIDs	Left ventricular internal diameter in systole
LVP	Left ventricular pressure
MI	Myocardial infarction
NE	Norepinephrine
NECTAR-HF	Neural Cardiac Therapy For HF
nNOS	Neuronal nitric oxide synthase
NPY	Neuropeptide Y
NSVT	Non-sustained ventricular tachycardia
PBS	Phosphate buffered saline
PES	Programmed electrical stimulation
PGP9.5	Protein gene product 9.5
PW	Pulse width
RAGP	Right atrial ganglionated plexus
RASSL	Receptor activated solely by a synthetic ligand
ROI	Region of interest
RG	Repolarization gradient
RSS	Right sympathetic stimulation
RT90	Repolarization time at 90% repolarization
S100B	S100 calcium binding protein B
SCD	Sudden cardiac death
SCS	Spinal cord stimulation

SG	Stellate ganglia
TH	Tyrosine hydroxylase
TRPV1	Transient receptor potential cation subfamily V member 1
TZB	Tolerance zone boundary
VA	Ventricular arrhythmia
VAChT	Vesicular acetylcholine transporter
VF	Ventricular fibrillation
VIVGP	Ventral interventricular ganglionated plexus
VNS	Vagal nerve stimulation
VT	Ventricular tachycardia

PREFACE

Chapter 1. A version of this manuscript is published: Hadaya J, Ardell JL. Autonomic Modulation for Cardiovascular Disease. Frontiers in Physiology. 2020 Dec 22;11:617459. Doi: 10.3389/fphys.2020.617459. PMID: 33414727; PMCID: PMC7783451.

Chapter 2. A version of this manuscript is published: Hadaya J, Buckley U, Gurel NZ, Chan CA, Swid MA, Bhadra N, Vrabec TL, Hoang JD, Smith C, Shivkumar K, Ardell JL. Scalable and reversible axonal neuromodulation of the sympathetic chain for cardiac control. American Journal of Physiology-Heart and Circulatory Physiology. 2022 Jan 1;322(1):H105-H115. Doi: 10.1152/ajpheart.00568.2021. Epub 2021 Dec 3. PMID: 34860595; PMCID: PMC8714250.

Chapter 3. A version of this manuscript is in preparation for publication.

Chapter 4. A portion of this manuscript is accepted for publication: Hadaya J, Ardell JL. Renal Dysfunction in Heart Failure: The Role of Cardiac Afferent Fibers. Journal of the American College of Cardiology: Basic to Translational Science. 2022.

This work was supported by the National Institutes of Health (NIH) through the Office of the Director and Common Fund's Stimulating Peripheral Activity to Relieve Conditions Program, Grant OT2 OD023848 (PI: K. Shivkumar); NIH National Institute of Biomedical Imaging and Bioengineering Grant U01 EB025138 (PI: J. Ardell); NIH National Heart, Lung, and Blood Institute (NHLBI) Grant HL150136 (PI: T. Vrabec); NIH NHLBI Ruth L. Kirschstein Postdoctoral Individual National Research Service Award F32 HL160163 (PI: J. Hadaya); and American Heart Association Postdoctoral Fellowship 836169 (PI: J. Hadaya).

VITA

Education

2008-2012 University of California, Los Angeles (UCLA), Bachelor of Science in Physiological Science, Cum Laude, College Honors
2015-2016 Broad Institute of Harvard and MIT, Predoctoral Fellowship (Sarnoff Cardiovascular Research Fellowship) in Cardiovascular Genetics
2012-2017 Cleveland Clinic Lerner College of Medicine, Doctor of Medicine

Clinical Training

2017- UCLA Health System, General Surgery Internship and Residency

Honors and Awards

2008-2012 Dean's Honor List, UCLA College of Letters and Science
2011-2012 Wasserman Research Fellowship, UCLA College of Letters and Science
2012 Chancellor's Service Award, UCLA College of Letters and Science
2012-2017 Full Tuition Scholarship, Cleveland Clinic Lerner College of Medicine
2014 Featured Poster, Heart Rhythm Society Scientific Sessions 2014
2014 Tylenol Future Care Scholarship, Johnson & Johnson
2015-2016 Sarnoff Fellowship, Sarnoff Cardiovascular Research Foundation
2016 NIH Medical Research Scholars Program (declined due to award terms)
2016 Academy of Medicine Education Foundation Scholarship
2016 Vascular Annual Meeting Travel Scholarship, Society for Vascular Surgery
2016 Academic Surgery Leadership Scholarship, University of Michigan
2017 Cleveland Clinic Foundation Dean's Award
2017 Andrew J. Fishleder Leadership Award, Cleveland Clinic Foundation
2019- Specialty Training and Advanced Research Program, UCLA DGSOM
2020 Medical Student Teaching Award, UCLA DGSOM
2021 American Heart Association Postdoctoral Fellowship (Percentile 7)
2021- NIH Ruth L. Kirschstein National Research Service Award (Percentile 6)
2022 Cardiovascular Section Research Recognition Award, American Physiological Society
2022 Postdoctoral Translational Research Award, American Physiological Society Physiologists in Industry Committee (declined due to award terms)
2022 Young Investigator Award Finalist, American Physiological Society
2022 Emerging Scientist Award, NIH Common Fund SPARC Program
2022 Cardiac Electrophysiology Society Young Investigator Award Competition, Heart Rhythm 2022

Publications

1. Hadaya J, Ardell JL. Renal Dysfunction in Heart Failure: The Role of Cardiac Afferent Fibers. JACC Basic Transl Sci, 2022.
2. Gurel NZ, Sudarshan KB, Hadaya J, Karavos A, Temma T, Hori Y, Armour JA, Kember G, Ajijola OA. Metrics of High Cofluctuation and Entropy to Describe Control of Cardiac Function in the Stellate Ganglion. Under review.
3. Habibagahi I, Omidbeigi M, Hadaya J, Lyu H, Jang J, Ardell JL, Bari A, Babakhani A. Vagus nerve stimulation using a miniaturized wirelessly powered stimulator in pigs.

In revision.
4. Hadaya J, Buckley U, Gurel NZ, Chan CA, Swid MA, Bhadra N, Vrabec TL, Hoang JD, Smith C, Shivkumar K, Ardell JL. Scalable and reversible axonal neuromodulation of the sympathetic chain for cardiac control. Am J Physiol Heart Circ Physiol, 2022.
5. Gurel NZ, Hadaya J, Ardell JL. Stress-related dysautonomias and neurocardiology-based treatment approaches. Auton Neurosci, 2022.
6. Boukens BJD, Dacey M, Meijborg VMF, Janse MJ, Hadaya J, Hanna P, Swid MA, Opthof T, Ardell JL, Shivkumar K, Coronel R. Mechanism of ventricular premature beats elicited by left stellate ganglion stimulation during acute ischaemia of the anterior left ventricle. Cardiovasc Res, 2021.
7. Natterson-Horowitz B, Baccouche BM, Mary J, Shivkumar T, Bertelsen MF, Aalkjær C, Smerup MH, Ajijola OA, Hadaya J, Wang T. Did giraffe cardiovascular evolution solve the problem of heart failure with preserved ejection fraction? Evol Med Public Health, 2021.
8. Mori S, Hanna P, Dacey MJ, Temma T, Hadaya J, Zhu C, Chang G, Peacock WJ, Fishbein MC, Shivkumar K. Comprehensive Anatomy of the Pericardial Space and the Cardiac Hilum: Anatomical Dissections With Intact Pericardium. JACC Cardiovasc Imaging, 2021.
9. Hanna P, Dacey MJ, Brennan J, Moss A, Robbins S, Achanta S, Biscola NP, Swid MA, Rajendran PS, Mori S, Hadaya JE, Smith EH, Peirce SG, Chen J, Havton LA, Cheng ZJ, Vadigepalli R, Schwaber J, Lux RL, Efimov I, Tompkins JD, Hoover DB, Ardell JL, Shivkumar K. Innervation and Neuronal Control of the Mammalian Sinoatrial Node a Comprehensive Atlas. Circ Res, 2021.
10. Kluge N, Dacey M, Hadaya J, Shivkumar K, Chan SA, Ardell JL, Smith C. Rapid measurement of cardiac neuropeptide dynamics by capacitive immunoprobe in the porcine heart. Am J Physiol Heart Circ Physiol, 2021.
11. Hadaya J, Ardell JL. Autonomic Modulation for Cardiovascular Disease. Front Physiol, 2020.
12. Gupta RM, Hadaya J, Trehan A, Zekavat SM, Roselli C, Klarin D, Emdin CA, Hilvering CRE, Bianchi V, Mueller C, Khera AV, Ryan RJH, Engreitz JM, Issner R, Shoresh N, Epstein CB, de Laat W, Brown JD, Schnabel RB, Bernstein BE, Kathiresan S. A Genetic Variant Associated with Five Vascular Diseases Is a Distal Regulator of Endothelin-1 Gene Expression. Cell, 2017.
13. Zhou W, Yamakawa K, Benharash P, Ajijola O, Ennis D, Hadaya J, Vaseghi M, Shivkumar K, Mahajan A. Effect of stellate ganglia stimulation on global and regional left ventricular function as assessed by speckle tracking echocardiography. Am J Physiol Heart Circ Physiol, 2013.
14. Ajijola OA, Vaseghi M, Zhou W, Yamakawa K, Benharash P, Hadaya J, Lux RL, Mahajan A, Shivkumar K. Functional differences between junctional and extrajunctional adrenergic receptor activation in mammalian ventricle. Am J Physiol Heart Circ Physiol, 2013.
15. Vaseghi M, Zhou W, Shi J, Ajijola OA, Hadaya J, Shivkumar K, Mahajan A. Sympathetic innervation of the anterior left ventricular wall by the right and left stellate ganglia. Heart Rhythm, 2012.

CHAPTER 1

Introduction

Introduction

The autonomic nervous system regulates all aspects of cardiac function including chronotropy, inotropy, dromotropy, and lusitropy.[1] In the last decade, it has become increasingly evident that autonomic dysregulation plays a major role in the development and progression of major cardiovascular diseases, including myocardial infarction, heart failure, and sudden cardiac death.[1-4] While pharmacologic therapy targets cardiac disease through neurohormonal blockade, results have not been as promising as hoped.[4-6] This has led to increasing interest in neuromodulation as a new therapeutic approach, with therapies such as vagal nerve stimulation and video-assisted thoracoscopic sympathectomy showing efficacy for the treatment of heart failure and refractory ventricular arrhythmias.[7-12] Though these early studies are promising, a better understanding of the anatomy and function of the cardiac nervous system is imperative to developing and implementing precise neuromodulatory therapies.

The anatomy of the cardiac nervous system is complex and has been categorized into: 1) central components 2) intrathoracic extracardiac components and 3) intrinsic cardiac components (Figure 1).[1,2] The intrathoracic extracardiac system connects the central components to the intrinsic cardiac nervous system (ICNS), and is composed of parasympathetic and sympathetic systems that are traditionally thought to exert opposing action on cardiac electrical and mechanical function.[13,14] The parasympathetic component acts through the vagus nerve and its intrathoracic branches, using acetylcholine, nitric oxide, and vasoactive intestinal peptide as neurotransmitters.[15,16] The sympathetic component originates in the intermediolateral cell columns of the spinal cord, projects via C7 to T6 rami to the superior cervical,

middle cervical, stellate or cervicothoracic ganglia, and acts though norepinephrine and neuropeptide Y.[15,17-20] Afferent cardiac neurons, now known to be dispersed throughout the myocardium, act as mechanoreceptors and/or chemoreceptors, completing a cardiac neural circuit.[2,21,22] These afferent neurons have multimodal transduction capabilities, capable of transducing the presence of myocardial ischemia and [23]initiating reflex sympathetic activation in the setting of myocardial infarction.[24-27] The intrinsic cardiac nervous system (ICNS) is composed of clusters of ganglia referred to as ganglionated plexi distributed in epicardial fat pads.[13] These ganglionated plexi contain a diverse population of neurons, including neurons that that receive parasympathetic and sympathetic input, neurons that receive afferent information directly from myocytes, and local interneurons.[2,13] Contrary to initial studies, recent evidence has shown that the ICNS is not simply a relay station for extrinsic projections to the heart, but instead functions with higher centers to modulate regional cardiac electrical and mechanical indices on a beat-to-beat basis.[28] Moreover, the ICNS is a dynamic neural network, which remodels with disease states.[29-31] For example, in the setting of myocardial infarction, our group has shown that processing of afferent and efferent neural signals in the ICNS is impaired, with overall decreased network connectivity, suggesting an inability of neurons to respond to local myocardial stimuli.[29] Similar remodeling occurs within intrathoracic and primary sensory ganglia.[2,32-35] Given the complexity of these systems, and remodeling that occurs in disease states, a better understanding of the function of each component is necessary to improve therapeutic outcomes and reduce off-target consequences.

Herein, we provide a brief foundation for understanding the structure of, and organization of the cardiac autonomic nervous system and highlight neural control of cardiovascular function, emphasizing the roles of the sympathetic, parasympathetic, and intrinsic cardiac nervous systems. Based on this scientific foundation, an overview of current neuromodulatory therapies is presented, focusing on cardiac sympathetic denervation and vagal nerve stimulation.[4,36,37] We highlight preclinical studies of vagal nerve stimulation for structural heart disease and arrythmias. We conclude with a discussion on recently completed and in-process clinical trials of vagal nerve stimulation for heart disease, primarily congestive heart failure, driven by foundations established from preclinical studies.

Overview of Structural and Functional Organization of the Cardiovascular Neuraxis

Autonomic control of the cardiovascular system is mediated through afferent and efferent pathways and neural networks involving the brain stem, spinal cord, peripheral ganglia, and intrinsic cardiac nervous system (Figures 1 and 2).[2] Feedback systems between each of these components exist and mediate transduction of beat-to-beat information, allowing for maintenance of hemostasis and adaptation to stressors.[1,2,13] The cardiovascular neuraxis can be considered in three different levels: Level 1 is considered the heart with its own intrinsic cardiac nervous system, which is comprised of cardiac ganglia that reside at the origin of the great vessels, and posteriorly along the atria and atrioventricular junction.[2,4,13] Level 2 consists of intrathoracic components that regulate cardiac function including the middle cervical ganglia, cervicothoracic (stellate)

ganglia, and the T2-T4 portions of the sympathetic chain.[2,38,39] Level 3 can be considered as the dorsal root and nodose ganglia, which mediates the predominant proportion of afferent neurotransmission, as well as spinal cord, brainstem and higher centers.[15,40-43] Importantly, information is processed at multiple levels by interneurons, resulting in the interdependent network interactions between brainstem, spinal, intrathoracic, and cardio-cardiac reflexes.[2,28,44,45] While initially thought to exert opposing effects on cardiac electrophysiologic and mechanical function, interactions between the sympathetic and parasympathetic nervous systems mediate cooperative control and regulation of function.[1,2,46]

Cardiac Sympathetic Innervation – In Health and Disease

Canonical organization of the sympathetic nervous system traditionally consider two sets of neuronal projections, defined by location of cell bodies and neurotransmitters mediating cell to cell communication. Preganglionic neurons with cell bodies in the intermediolateral cell column of the cervical and thoracic spinal cord (C7-T6) project to the superior, middle, cervicothoracic or stellate ganglia, and the remainder of paravertebral chain, with fibers running through ventral horns.[15,21,47] Postganglionic sympathetic neurons project from these intrathoracic ganglia to atrial and ventricular myocardium, components of the conduction system, and coronary vasculature, traveling primarily as mixed cardiopulmonary nerves.[48-50] Preganglionic neurons act through acetylcholine, binding to nicotinic acetylcholine receptors, whereas postganglionic neurons release norepinephrine. Sympathetic innervation of the heart has been well characterized using immunohistochemical studies targeting tyrosine hydroxylase, the

rate-rate limiting enzyme in norepinephrine synthesis, across multiple animal models.[51,52] Although canonical neurobiology primarily emphasizes the role of norepinephrine for postganglionic neurotransmission, several co-receptors such as neuropeptide Y and galanin have been reported to be released from postganglionic nerve terminals, especially during higher levels of neural activity.[19,53,54] These peptides may mediate additional efferent effects and have been implicated in various cardiovascular disorders including heart failure.[55,56] Further study of these co-transmitters may prove of value in development of novel therapeutics.[57]

In general, sympathetic activation mediates increases in chronotropy, inotropy, dromotropy, and lusitropy.[1,58] In more contemporary porcine studies, both right and left stellate stimulation reduced activation recovery intervals, an in vivo surrogate for action potential duration.[59,60] Notably, differential shortening of activation recovery intervals in different portions of the left ventricular by right versus left stellate stimulation, was noted suggesting the presence of regional control of cardiac electrical function.[60-62] In the setting of chronic myocardial infarction, this regional regulation of cardiac electrical function is disrupted, with greater variation in repolarization and altered activation propagation.[63]

In the setting of diseased states, such as myocardial infarction and heart failure, aberrant remodeling of the sympathetic nervous system occurs and is well described.[64-67] At the level of the myocardium, cardiac sympathetic nerve density, electrical excitability, and neurotransmitter content are altered in disease states.[65,68,69] In a Langendorff-perfused mouse model of toxin-induced regional sympathetic hypoinnervation with no accompanying myocardial infarction, greater sensitivity to

circulating catecholamines and blunted responses to sympathetic nerve stimulation were observed, demonstrating the direct proarrhythmogenic effects of sympathetic nerve heterogeneity.[69] Ischemia results in release of reactive oxygen species, adenosine, and other chemical mediators, that activate afferent neurons within the myocardium.[27,70-72] Reflexes at the level of the central nervous system, stellate ganglia, and possibly the intrinsic cardiac nervous system, result in sympathoexcitation to mitigate in part the effects of ischemia on mechanical cardiac function.[73-75] This reflex sympathoexcitation is associated with structural remodeling of portions of the intrinsic cardiac nervous system as well as the stellate ganglia and an increased risk of ventricular fibrillation.[76-79] In porcine models of chronic ischemia, as well as humans with ischemic cardiomyopathy, histologic changes in stellate ganglia neurons have been observed resulting in inflammation, glial cell activation, and oxidative stress.[66,67] Cholinergic transdifferentiation has been described following myocardial infarction, and, in animal models, co-release of acetylcholine with norepinephrine may be antiarrhythmic by reducing actional potential duration dispersion.[80,81]

From a clinical perspective, this excessive sympathoexcitation is targeted pharmacologically with beta blockers as well as inhibition of the renin-angiotensin-aldosterone system in the case of heart failure.[1,5,82] Neuromodulatory approaches to decrease sympathetic tone, such as thoracic epidural anesthesia, stellate ganglion blockade, cardiac sympathetic denervation, and renal denervation have been utilized clinically to manage these disease entities.[1,4,8,82,83] In the research setting, another avenue considers application of electrical energy to reversibly block nerve conduction. For example, kilohertz frequency alternating current applied to the sympathetic chain

mitigated sympathetic outflow to the heart, reducing electrophysiologic indices associated with sympathetic chain stimulation.[84] Similarly, in animals with chronic myocardial infarction, axonal block applied to high thoracic paravertebral chain using charge-balanced direct current produced reversible block of sympathetic nerve activity and reduced ventricular tachycardia/ventricular fibrillation potential.[85] These technologies and treatment approaches warrant further study given an increasing interest of neurocardiology as a therapeutic opportunity.

Cardiac Parasympathetic Innervation – In Health and Disease

Similar to the structural organization of the sympathetic nervous system, the parasympathetic nervous system is classically described as preganglionic and postganglionic projections.[2,15] Preganglionic fibers, originating in the dorsal motor nucleus and nucleus ambiguus of the medulla project near to, or to, their target organ through the vagus nerve and intrathoracic cardiopulmonary branches.[86,87] Presynaptic fibers synapse on postsynaptic cell bodies located near or on the target organ, with neurotransmission mediated through acetylcholine and nicotinic receptors.[15] In the setting of cardiac autonomic system, a significant portion of postganglionic cell bodies are located within ganglia of the intrinsic cardiac nervous system, and then directly project to myocardium, acting through release of acetylcholine.[88-91] These groups of neurons have been well characterized using markers such as the choline acetyltransferase, and vesicular acetylcholine transporter.[92]

In addition to mediating parasympathetic efferent input to the heart and other viscera, the vagus nerve carries afferent information from intrathoracic and intraabdominal viscera to the central nervous system.[15,93,94] Of particular relevance to the cardiovascular system, bipolar neurons located in the superior and inferior (nodose) ganglia of the vagus nerve transmit sensory information from the myocardium to the nucleus tractus solitarus.[95,96] Vagal afferent fibers are predominantly unmyelinated and multimodal and with reference to bioelectric interventions are thought to be preferentially activated at lower levels of current.[45,97] Given the prevalence of afferent fibers in the vagus nerve, with some studies reporting upwards of 80% of fibers as providing afferent input to the CNS, relevance of fiber type and activation is particularly important for the use of vagal nerve stimulation for therapeutic purposes.[95,98,99]

Vagal afferent fibers carry a wide variety of information to higher centers and include atrial stretch receptors, multimodal receptors within ventricles, pulmonary stretch receptors and cardiopulmonary chemoreceptors.[100-102] Early studies, employing recordings of the vagus nerve and nodose ganglia, identified neuronal activity that was synchronous with the cardiac cycle, and affected by hemodynamic changes such as varied preload or afterload.[94,103-105] In an *in vivo* study in guinea pigs, epicardial application of substances such as nitroprusside, calcitonin gene-related peptide, histamine, and bradykinin elicited changes in nodose afferent neuronal activity, suggesting that this population of afferent neurons transduce to a wide variety of neurotransmitters and chemicals at the level of the heart.[22]

In experimental models, efferent activation of the vagus nerve produces a bradycardia and slows conduction through the atrioventricular node.[106,107] However, at

low levels of current, which primarily activates afferent pathways, a tachycardia is induced, which is abolished with transection of the vagus nerve.[45] While effects of vagal nerve stimulation on the sinus and atrioventricular node are well characterized, innervation of the ventricles by the parasympathetic system has been debated. Cholinergic neurons are present and innervate the ventricles as demonstrated by immunohistologic studies, with a greater density at the base than apex.[51,92] Functional studies in porcine models demonstrate global prolongation of activation recovery intervals with right and left sided stimulation, with no clear regional regulation by the left versus right vagus.[108] This coordination across all areas of the heart likely reflects the interganglionic interconnections occurring within the intrinsic cardiac nervous system.[2] In addition to electrophysiologic effects, vagal nerve stimulation reduces inotropy, further supporting the existence of functional innervation of the ventricle by the vagus.[108] With respect to vagal nerve stimulation, transection of afferent pathways rostral to the electrode interface markedly enhancing suppression of all cardiac functions, reflecting the dynamic interactions of afferent and efferent mediated responses whenever bioelectric interventions are imposed.[45,109,110]

Recently, selective modulation of neuronal populations has been made possible through optogenetic techniques that employ light-activated ion channels to stimulate or inhibit neurons.[111,112] For example, in a Langendorff-perused murine model, optogenetic stimulation of tyrosine-hydrolase expressing neurons on the epicardial surface of the right atrium and right ventricle resulted in greater contractile forces and heart rate, with shortening of optically-mapped action potentials.[113] A similar study in a murine Langendorff-perfused model targeting cardiac parasympathetic neurons expressing

choline acetyltransferase demonstrated bradycardia and heart block with illumination of the junction of the superior vena cava and right atrium, which was blocked by administration of atropine.[114] Other non-electrical approaches for neural stimulation including designer receptors specifically activated by designer drugs (DREADDs) or receptor activated solely by a synthetic ligand (RASSL), a family of engineered proteins that respond only to synthetic ligands and allow for modulation of G protein coupled receptor signaling.[115] Using excitatory DREADDs in a rat model of heart failure, Garrott et al. activated a population of oxytocin and glutamate co-releasing neurons in the hypothalamus that stimulated cardiac vagal neurons, which mitigated myocyte hypertrophy, collagen deposition, and ventricular dysfunction.[116] These novel approaches highlight pre-clinical advances that may allow for subselective evaluation of specific parasympathetic neuronal populations.

In the setting of myocardial injury and disease, structural and functional remodeling occur at multiple levels of the cardiac nervous system.[2,4,117] While myocardial injury generally results in a net increase in sympathoexcitation, central parasympathetic tone is reduced, driving an interest in restoring parasympathetic tone to treat disease.[2,4,40] Using a porcine model, Vaseghi et al. reported minimal changes in acetylcholine levels in the apex, anterior wall, and lateral wall of the left ventricle in healthy animals compared to those with chronic myocardial infarction.[118] Alterations in the basal activity and input of parasympathetic nervous within the intrinsic cardiac nervous system was also evident in the setting of myocardial infarction.[118] Specifically, neurons normally activated by vagal stimulation were reduced in the setting of myocardial infarction, while those normally suppressed became more active. Inputs to

these neurons significantly changed, with increased sympathetic input in the setting of myocardial infarction.[118] Changes in composition of the nodose ganglia has also been reported in the setting of chronic myocardial infarction, with increased neuron size as well as an increase in tyrosine hydroxylase positive and calcitonin gene-related peptide positive cells, with a decrease in neuronal nitric oxide synthase positive cells.[119] Overall, these findings suggest that intra and extra-cardiac parasympathetic remodeling occurs in the setting of myocardial infarction, with reduced parasympathetic input, but intact parasympathetic pathways.[118] As such, one therapeutic approach may be to target these intact pathways using vagal nerve stimulation.

Aberrant sensory information is a primary driver of acute autonomic responses to ischemic events and the progression of cardiac disease. Specific chemical ablation of cardiac transient receptor potential cation channel subfamily V member 1, TRPV1, receptors with epicardial resiniferatoxin mitigates progression of heart failure in preclinical models of ischemic heart disease.[34] Targeted neuromodulation has the potential to impact sensory transduction in an on-demand and reversible fashion.[2,120] Figure 3 shows the increase in nodose activity in response to transient occlusion of the left anterior descending (LAD) coronary artery. Such LAD occlusions were repeated in the presence of direct (cervical vagal, VNS) and remote (thoracic spinal cord, SCS) neuromodulation.[120] In both cases the nodose response to transient myocardial ischemia was mitigated.[120] Rather than being reflective of silent ischemia, we and others has proposed that pre-emptive neuromodulation alters the myocytes, likely via altered metabolism, and that this renders them stress-resistant.[34,121-123] As such the

milieu is stabilized during transient ischemic events and sensory afferent responses and resultant evoked autonomic reflexes mitigated.

The Intrinsic Cardiac Nervous System – Final Pathway for Cardiac Control

The intrinsic cardiac nervous system is a neural network comprised of afferent, efferent, and interneurons situated in fat pads distributed along the epicardial surface of the heart[13]. Although the intrinsic cardiac nervous system has been traditionally considered a relay station for efferent input to the heart, recent studies have identified a heterogenous population of neurons with varied putative functions.[13,28,124-126] These afferent neurons include multimodal and nociceptive afferent neurons, identified through both functional studies and immunohistochemical evaluation using antibodies against calcitonin gene-related peptide and substance P.[2,88,127,128] As such, the ICNS has a role in afferent sensory transduction, local network processing afferent-efferent input and can be considered as the final common pathway for input to the heart.[2,13] While each aggregate of neurons has a preferential sphere of influence with regards to cardiac mechanical and electrical function, there is substantial overlap in areas of the heart regulated. For example, focal activation of all ganglionated plexi results in changes in heart rate, suggesting direct and indirect input from each GP to the primary pacemaker of the heart (Figure 4).[13,28] Likewise, the nicotine micro-injections of most, but not all, ganglionated plexi can result in atrioventricular block or atrial fibrillation, and most have varied effects on ventricular mechanical function and electrophysiology.[13,28] These data reflects the ICNS role in overall coordination of cardiac function, as a result of local

circuit neurons mediating intra- and interganglionic interactions, shared efferent inputs, and convergent/divergent afferent inputs.[2]

Interactions between the ganglionated plexi and higher centers ultimately modulate regional cardiac function, rather than each system acting on its own.[2,13] The right atrial ganglionated plexus (RAGP), located posterolateral to the superior and inferior vena cava, and anterior to the right superior pulmonary vein, is one of the major atrial ganglionated plexi and mediates significant parasympathetic input to the right atrium.[28,126,129] In animal models, ablation of the RAGP results in near complete loss of evoked bradycardia induced by vagal nerve stimulation (Figure 5).[122] Sequential sympathetic and combined sympathetic-parasympathetic stimulation initially results in tachycardia followed by substantial bradycardia in the intact state.[122] As shown in Figure 5, with ablation of the RAGP, the tachycardia induced by sympathetic stimulation is preserved but returned to baseline with the addition of VNS. This residual sympathetic-parasympathetic interaction is completely abolished when atropine is added.[122] These observations suggest that interactions occur at both the level of end-organ as well as through the intrinsic cardiac nervous system, underscoring the importance of such interactions in understanding regional regulation of function.[2,122,130]

The ICNS has received significant attention clinically due to its accessibility with cardiac interventions or cardiac surgery.[4,46,131,132] Although dysfunction of the ICNS has been implicated in various cardiovascular diseases, our lack of knowledge regarding interactions among ganglionated plexi and higher centers has limited the advancement of therapeutics.[2,4] For example, in 2009, Nakagawa et al. reported percutaneous ablation of five accessible atrial GP in 63 patients with paroxysmal atrial fibrillation,

which resulted in a marked reduction of episodes of atrial fibrillation.[133] Further follow-up of these patients, as well as other trials, showed a greater need for pacemaker implantation, likely due to disruption of neurons projecting to the sinoatrial node, and an inadvertent increased risk of ventricular arrhythmias in the setting of ischemia.[134,135]

Disruptions in autonomic inputs to the ICNS are arrhythmogenic. In a series of studies, our group developed a model for reproducible transient induction of atrial fibrillation (AF).[123,136,137] This model involves, recording of intrinsic cardiac neural and cardiac electrical activity in response to bursts of electrical activity delivered to cardiac mediastinal nerves during the atrial refractory period.[123,136,137] Such bipolar stimulation reproducibly produces short periods of AF (~30 duration) with a latency of ~1 sec (Figure 6). ICNS activity, derived from extracellular recording, can be functionally defined into afferent, efferent or convergent (both afferent and efferent) related. While burst stimulation of mediastinal nerves increases activity in all three functional classes of ICNS neurons, convergent neurons were the preferential target. As demonstrated in Figure 6, pre-emptive VNS reduces the evoked ICNS neural response to mediastinal nerve stimulation, with the primary target being the convergent neurons, and the atrial arrhythmia potential was reduced in 75% of stimulations. The VNS impact on ICNS network function is further exemplified by mitigating synchrony between efferent to convergent and convergent to convergent neurons (Figure 6, Panel D and E). Finally, VNS exhibits memory (Figure 7), specifically, 3 minutes of cervical VNS reduced the arrhythmia potential to neural imbalances produced by mediastinal nerve stimulation for approximately 30 minutes. This has important implications for design of stimulation protocols for VNS.

VNS for Treatment of Cardiovascular Disease: Pre-Clinical Studies

Preclinical studies have provided substantial evidence supporting the utility of chronic vagal nerve stimulation (VNS) for the management of various cardiovascular disorders, with majority of studies focused on heart failure.[138,139] In a rat model of chronic heart failure induced by myocardial infarction through ligation of left coronary artery, 6 weeks of right vagal nerve stimulation ameliorated adverse ventricular remodeling and improved contractility.[140] Rats treated with VNS had reduced plasma norepinephrine and brain natriuretic peptide levels, and a 73% reduction in relative risk of death.[140] In a canine model of ventricular tachypacing induced heart failure, concomitant right vagal nerve stimulation, at an intensity to reduce heart rate by 20 beats per minute, attenuated the development of heart failure.[141] Canine receiving concomitant VNS had improved left ventricular ejection fraction and lower end-diastolic volumes, with greater heart rate variability and baroreflex sensitivity.[141] In a guinea pig model of chronic pressure overload designed to induce hypertension-mediated changes, chronic vagal nerve stimulation mitigated the development of cardiac hypertrophy and adverse neural remodeling (Figure 8).[142] Compared to animals receiving sham VNS, those receiving right or left cervical vagal nerve stimulation had reduced pressure overload-induced remodeling, including a reduction in left ventricular internal diameter at diastole, left ventricular end diastolic volume, and cardiac output. [142] At a cellular level, VNS consistently reduced pressure overload-induced myocyte hypertrophy and remodeling within intrinsic cardiac neurons.[142] Taken together, these animal models suggest vagal nerve stimulation can modulate pathologic responses that result in heart failure, in part

through improved autonomic balance, reduction of inflammation, alteration of energy utilization, and modulation of apoptotic pathways.[141-143]

Preclinical studies have demonstrated putative anti-arrhythmic effects of vagal nerve stimulation in the setting of acute (Figures 6 and 7) and chronic myocardial ischemia. In a study of acute coronary artery occlusion in anesthetized cats, animals who had previously undergone bilateral vagotomy or received atropine had less ventricular arrhythmias and death, suggesting that either efferent or afferent vagal tone may reduce ventricular fibrillation and death.[144] Billman et al. demonstrated that high vagal reflexes, assessed through baroreflex slopes, were associated with reduced vulnerability to ventricular fibrillation during acute coronary artery occlusion in canine with a history of healed myocardial infarction.[145] Similarly, animals that were initially susceptible to ventricular fibrillation and underwent daily exercise had improved baroreflexes and reduced susceptibility to ventricular fibrillation, attributed to improved autonomic balance.[146] In a canine model of healed anterior wall myocardial infarction, acute vagal nerve stimulation reduced the frequency of ventricular fibrillation in the setting of acute coronary artery occlusion and treadmill exercise among animals who were susceptible to ventricular fibrillation. [147] In a similar study, canine who were resistant to ventricular fibrillation received atropine prior to coronary artery occlusion, resulting in either novel occurrence of ventricular arrhythmias or worsened degree of ventricular arrhythmias.[148] Taken together, these early studies support a putative benefit of vagal nerve stimulation and restoration of vagal tone in the setting of acute myocardial ischemia. In a rat model of acute coronary ischemia, concomitant vagal nerve stimulation reduced ventricular tachyarrythmias, with abrogation of this effect with

atropine administration.[149] Immunohistochemical studies showed that the vagal nerve stimulation mitigated the MI-induced loss of Connexin-43 at gap junctions, suggesting that vagal nerve stimulation may combat electrical instability that occurs with myocardial ischemia.[149] In a contemporary, porcine study utilizing neuronal recordings from the ventral interventricular ganglionated plexus (VIVGP), a portion of the ICNS that innervates the ventricular myocardium, myocardial infarction resulted in increased sympathetic input to parasympathetic neurons in the VIVGP, with maintenance of parasympathetic neuronal networks.[118] In this model, vagal nerve stimulation reduced the burden of ventricular arrhythmias and reduced heterogeneity of repolarization in the scar-border zone, an area known to initiate arrhythmias clinically.[29] This study, and others, suggest that vagal nerve stimulation may, in part, act by stabilizing myocardial electrical activity, particularly at the scar-border zone.

Although the therapeutic molecular and cellular mechanisms underlying the therapeutic efficacy of vagal nerve stimulation are incompletely understood, mechanisms are thought to be mediated through both efferent activation of muscarinic receptors at the nerve-myocyte interface, as well as interaction with higher order systems and modulation of afferent-mediated reflexes (Figure 9).[2] At the level of the brainstem, afferent input is modified resulting in reduced central drive, as well as modulation of brainstem projections to spinal sympathetic networks.[2] At the level of the heart, activation of vagal efferent fibers results in acetylcholine release, activating M2 receptors on myocytes and conduction system cells, resulting in negative chronotropy, dromotropy, and, to a lesser degree, inotropy.[150] VNS may, in part, alter the balance between energy demand and supply in the setting of pathologic states.[151,152] Coronary

blood flow is modulated by vagal nerve stimulation with the majority of studies demonstrating parasympathetic coronary vasodilation although direct application of acetylcholine to vascular smooth muscle cells results in vasoconstriction.[153-155] In a canine model employing bilateral vagotomies and bilateral stellectomy, efferent vagal nerve stimulation resulted in coronary vasodilation when controlling for heart rate and aortic pressure, which was partly mitigated by atropine administration.[156] At the level of myocytes as well as the intrinsic cardiac nervous system, vagal nerve stimulation reduces sympathetic input, which may combat sympathoexcitation induced by disease states.[2,118,157] On a molecular level, vagal nerve stimulation has been associated with reduced pro-inflammatory cytokine release and improved nitric oxide signaling.[158-161] In addition, factors implicated in the progression of heart failure, such as norepinephrine and angiotensin are reduced with vagal nerve stimulation.[141]

VNS for Treatment of Cardiovascular Disease: Clinical Trials

Congestive heart failure is a major public health problem in the United States, with greater than 6 million Americans affected, with an increasing prevalence in the last decade.[162] Despite advances in medical therapies and interventional and surgical strategies for heart failure and comorbid conditions, mortality rates remain high as do the frequency of rehospitalizations for heart failure and associated costs.[163]

Heart failure is a heterogenous disorder, resulting from various entities including myocardial ischemia and valvular diseases, which ultimately result in an inability to meet oxygen and metabolic demands.[1,164] Homeostatic humoral regulatory mechanisms,

such as the renin-angiotensin-aldosterone system, are activated in an attempt to maintain cardiac output and end-organ perfusion. Importantly, imbalance the sympathetic and parasympathetic nervous systems develop and contribute to the pathogenesis of heart failure, with, in general, withdrawal of parasympathetic tone and heightening of sympathetic tone.[1,40,82,164] Consistent with this, the Autonomic Tone and Reflexes After Myocardial Infarction (ATRAMI) study reported an association between impaired vagal reflexes and mortality among 1,284 patients with a history of myocardial infarction, independent of left ventricular ejection fraction.[165] The majority of pharmacologic therapy for heart failure targets changes in neurohormonal axis, including beta-blockers and angiotensin-converting enzyme inhibitors.[82] Guideline directed medical therapy for most patients with heart failure with reduced ejection includes beta-blockers and angiotensin-converting enzyme (ACE) inhibitors or aldosterone receptor antagonists.[166] Large scale randomized trials demonstrate an improvement in survival for ACE inhibitors and beta-blockers, particularly in those with a history of myocardial infarction or reduced ejection fraction.[167-170] Although these agents have been efficacious in the management of heart failure, progression of disease generally continues, leading to renewed interest in neuromodulatory therapies.[4]

Vagal nerve stimulation (VNS) was initially developed for and clinically utilized for the management of depression and refractory epilepsy.[171,172] Though the mechanisms of VNS for epilepsy are poorly characterized, reduction in seizure frequency and use of anti-epileptic drugs have been noted across trials.[173] The Food and Drug Administration has already approved implantable pulse generators and leads for safe and effective treatment of epilepsy, facilitating the adaptation of similar technology to alternate

diseases.[173,174] Given the relevance of autonomic dysregulation in the development and progression of heart failure and arrhythmias, trials exploring the efficacy and safety of VNS for cardiovascular disease have received significant national attention since the initial report of its use for heart failure in 2008. [11,175-178] Initial clinical trials of VNS, in combination with medical therapy, for CHF demonstrated mixed results, attributed to variation in study design, sidedness of stimulation, and vagal nerve stimulation protocols.[179] Importantly, VNS protocols represent the total dose of "therapy" delivered to the patient as a function of current intensity, frequency, pulse width, and duty cycle (time on versus off), and thus are hypothesized to have a substantial impact on efficacy of therapy, as well as side effects.[179]

The Autonomic Neural Therapy to Enhance Myocardial Function in Heart Failure (ANTHEM-HF) evaluated the adjunct use of the Demipulse (LivaNova, Houston, TX) VNS system for left or right cervical vagal nerve stimulation in a cohort of patients with heart failure with reduced ejection fraction and New York Heart Association functional class II-III symptoms.[9,180-182] Improvement in primary endpoints including left ventricular ejection fraction, heart rate variability, and 6-minute walk tests, were noted, with follow-up at 1 year demonstrating persistent improvement (Figure 10).[9,180-182] In the setting of heart failure with preserved ejection fraction (HFpEF), a more clinically challenging entity to treat, a similar VNS protocol by the same investigators is presently enrolling.[181] Of existing and completed trials for CHF, ANTHEM-HF is the only trial reporting positive findings for both safety and efficacy of VNS, which has been attributed to both study design and VNS stimulation protocols.[179]

Two other major studies have explored the impact of VNS on cardiovascular outcomes in the setting of heart failure, with mixed results (Figure 10). The NEural Cardiac TherApy foR HF (NECTAR-HF) study randomized patients with heart failure with reduced ejection fraction (HFrEF) and left ventricular ejection fraction (LVEF) ≤ 35% to VNS therapy or sham (device without stimulation) with a different VNS protocol (intensity titrated to 20Hz, 300μs, proposed target current of 4mA).[183] At 6-months, the majority of patients did not achieve the pre-specified stimulus intensity because of off-target effects and there was no significant difference in pre-specified outcomes of left ventricular end systolic diameter.[183] Importantly, NECTAR-HF targeted vagal nerve stimulation at a frequency of 20Hz and a low current.[183] At these stimulation parameters, it is hypothesized that afferent fibers were preferentially activated, rather than efferent motor fibers, which may, in part, explain the lack of efficacy observed.[176,184]

The INcrease Of VAgal TonE in Heart Failure (INOVATE-HF) trial randomized 707 patients with HFrEF (LVEF ≤ 40%) with NYHA class III symptoms to medical therapy or medical therapy and VNS using an R-wave triggered pulse.[175] Of note, this trial utilized a vagal nerve stimulation protocol that implemented a putative afferent blockade in addition to efferent activation.[175] At a mean follow-up of 16 months, a composite primary endpoint of death, rehospitalization for CHF, or need for intravenous diuresis, was more frequent in the VNS group compared to control.[175] 6-minute walk test and quality of life measures improved in the VNS group compared to control (Figure 10). [175] The mixed findings in both of these studies may represent heterogenous cohorts and inadequate or inappropriately tailored VNS therapy delivery.[184]

Our prior work has described the concept of the neural fulcrum – an equilibrium point between activation of afferent and efferent vagus nerve pathways, resulting in a null heart response to stimulation with intact neural circuits.[109] Titration of vagal nerve stimulation parameters to reach the neural fulcrum over a period of time (3-4 weeks) is a feasible approach to achieve therapeutic levels of VNS.[109,184] Likewise, adjustment of parameters during a training period, off-target effects such as cough, GI discomfort, and dyspnea, can be minimized.[109,184] Figure 11 represents a graphical display of a frequency and intensity relationship for VNS, with the neural fulcrum defined as the minimal heart rate change with VNS (yellow shaded region), overlaid with parameters from the 3 previously discussed trials of VNS for heart failure. At a given pulse width, in this case 500μs, note the inverse relationship between frequency and intensity to achieve a null and minimal bradycardia (1-3 beats per minute) (Figure 11). Both NECTAR-HF and INOVATE-HF trials delivered VNS at parameters that were not effective in engaging all levels of the cardiac nervous system, while ANTHEM-HF operated at the fulcrum.[109,184] ANTHEM-HF is presently the only trial the has shown a net long-term benefit to VNS for heart failure, which may be related to activating the appropriate balance of afferent and efferent fibers.[2,109,184] Although there were significant variation in clinical characteristics, disease burden, and comorbidities including arrhythmias, in these 3 trials, it is likely that the choice of VNS likely impacted clinical responses. [2,109,184] As future trials of VNS are designed for heart failure and other cardiovascular disorders, it is imperative that structure-function relationships of the nervous system be considered.

Concluding Remarks and Future Directions

Multiple cardiovascular disorders including myocardial infarction and congestive heart failure result in excessive sympathoexcitation and a withdrawal of central parasympathetic tone.[2,4] The majority of existing therapies for these disorders focuses on blunting sympathetic drive to the heart, in the form of beta-adrenergic receptor blockade or inhibition of the renin-angiotensin-aldosterone axis.[4] Despite the widespread use of these medications, progression of disease occurs, creating a need for novel therapeutic approaches.[4] Therapies such as cardiac sympathetic denervation, stellate ganglion blockade, and renal artery denervation are being explored as avenues to reduce sympathetic tone associated with heart failure and ventricular arrhythmias.[4] In addition to the value of these therapies in the management of refractory ventricular arrhythmias, cardiac sympathetic denervation has also shown efficacy in the setting of inherited channelopathies including congenital long QT syndrome and catecholaminergic polymorphic ventricular tachycardia.[10,83,185] Vagal nerve stimulation has emerged as a promising therapeutic approach to combat the observed withdrawal of parasympathetic tone and to counteract the reflex mediated sympathoexcitation.[2,4] A significant body of pre-clinical studies supports the value of vagal nerve stimulation for the management of heart failure or arrhythmias.[2,4] Existing trials of vagal nerve stimulation have been confounded by substantial variation in inclusion criteria and inconsistent vagal nerve stimulation delivery. [2,4,184] A mechanistic understanding of neural cardiac remodeling, where and how to target the cardiac neuraxis, and follow-up with appropriate biomarkers is essential to achieve and maintain therapeutic efficacy. The goal for any of these therapies is to reduce sympathoexcitation, increase

parasympathetic tone and/or blunt aberrant afferent processing. VNS achieves all three goals concurrently and remains an area of intense scientific and clinical interest.

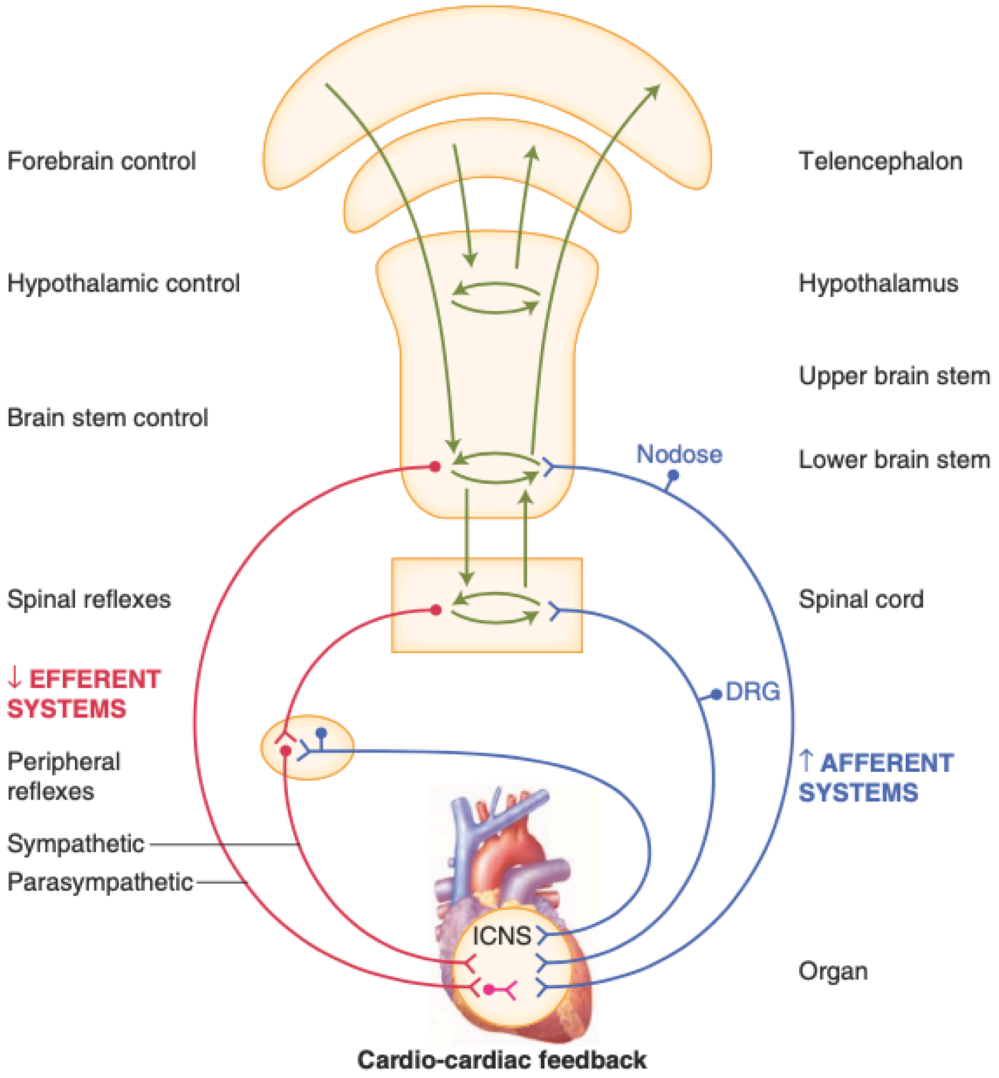

Figure 1. Neural regulation of cardiac function involves multiple nested feedback loops at the level of the heart, peripheral ganglia, and central nervous system. Afferent systems (blue) are mediated through the intrinsic cardiac nervous system, dorsal root ganglia, and nodose ganglia. Efferent systems (red) involve sympathetic, parasympathetic, and local circuit neurons. DRG, dorsal root ganglia. ICNS, intrinsic cardiac nervous system. Adapted from Janig (2016).[150]

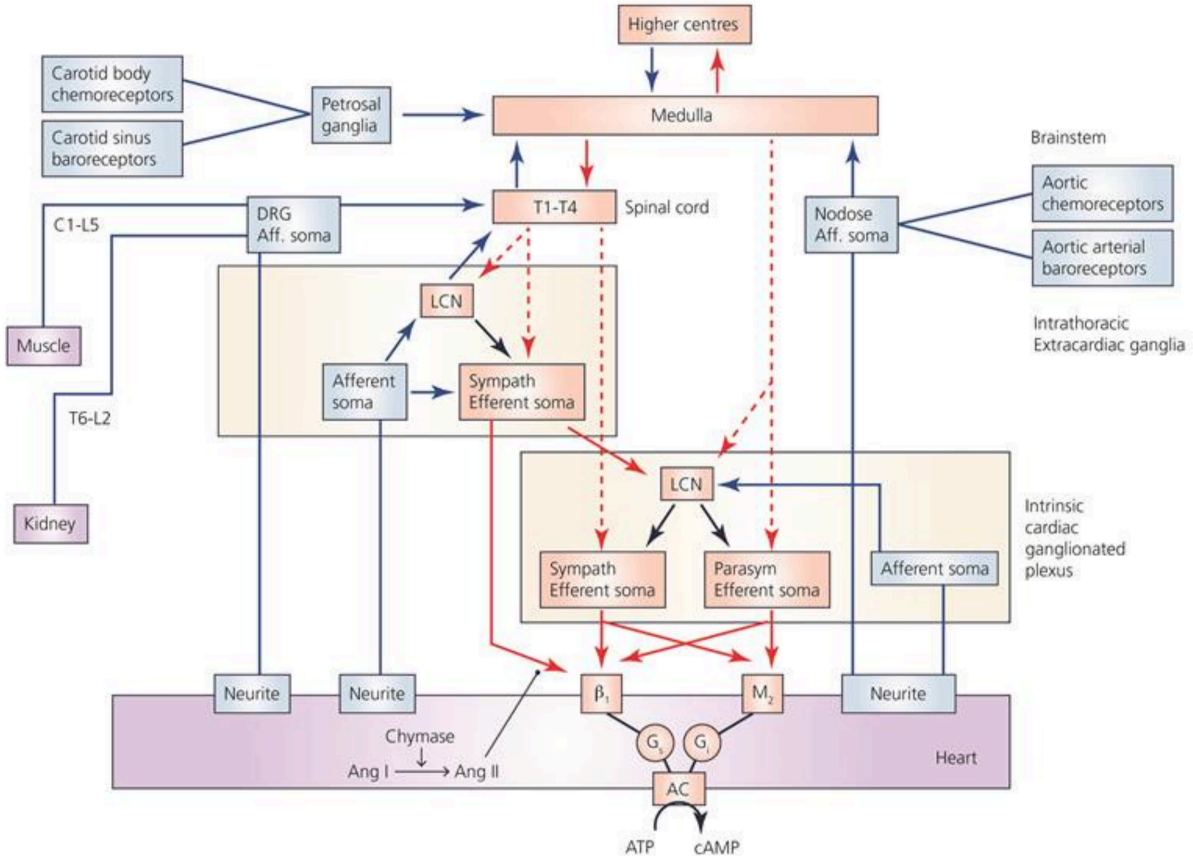

Figure 2. Interactions between central nervous system, peripheral ganglia, and the intrinsic cardiac nervous system. Multiple interdependent feedback loops regulate regional cardiac mechanical and electrical function. At the level of the heart, sensory (blue) neurons provide input directly and indirectly through the ICNS, peripheral ganglia, and spinal cord, which are capable of engaging cardiocentric reflexes. Converging inputs result in activation of adrenergic or muscarinic receptors as well as receptors for peptide co-transmitters such as neuropeptide Y (not displayed). Preganglionic sympathetic and parasympathetic efferent fibers project (red, dashed) to the ICNS, including to local circuit neurons, and postganglionic sympathetic fibers (red, solid) also directly to the myocardium. The ICNS acts as the final common pathway for

cardiac control, though interactions occur at all levels. Input from chemoreceptors, baroreceptors, as well as neurohormonal factors such as angiotensin II and circulating epinephrine (not displayed), also modulate cardiac function. Ang I, angiotensin I. Ang II, angiotensin II. LCN, local circuit neuron. Adapted from Ardell et al. (2016).[2]

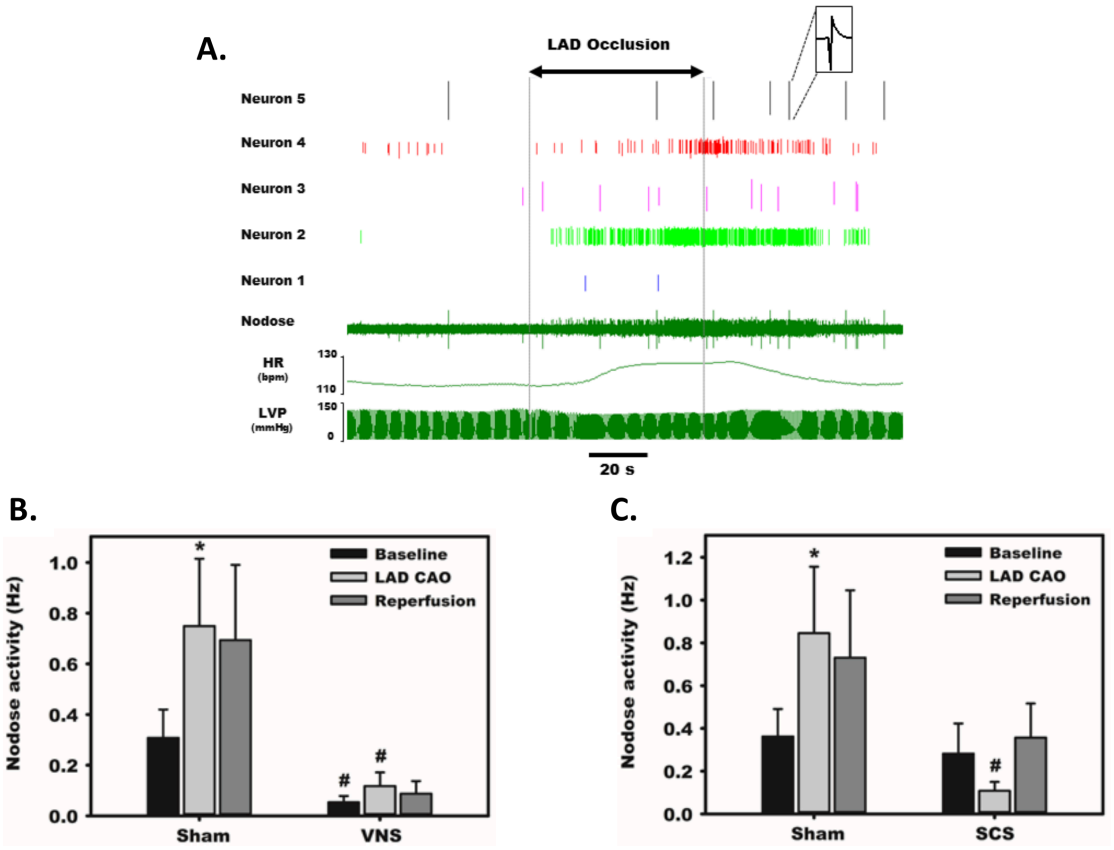

Figure 3. Afferent transduction of ischemia is modulated directly by parasympathetic input as well as remotely. Representative recordings from the nodose ganglia, one of the major parasympathetic afferent ganglia, during occlusion of the left anterior descending coronary artery. (A) Activity from 5 neurons displays substantial heterogeneity in baseline firing frequency and responses to ischemia and reperfusion. (B) Normalized, summative nodose activity at baseline, with left anterior descending artery occlusion, and reperfusion, with and without vagal nerve stimulation. In all settings, animals receiving vagal nerve stimulation displayed marked reductions in nodose activity. (C) Spinal cord stimulation also reduces nodose neural activity in response to ischemia stress. *$p < 0.05$ from baseline; $^{\#}p < 0.05$ from sham. Adapted from Salavatian et al. (2017).[120]

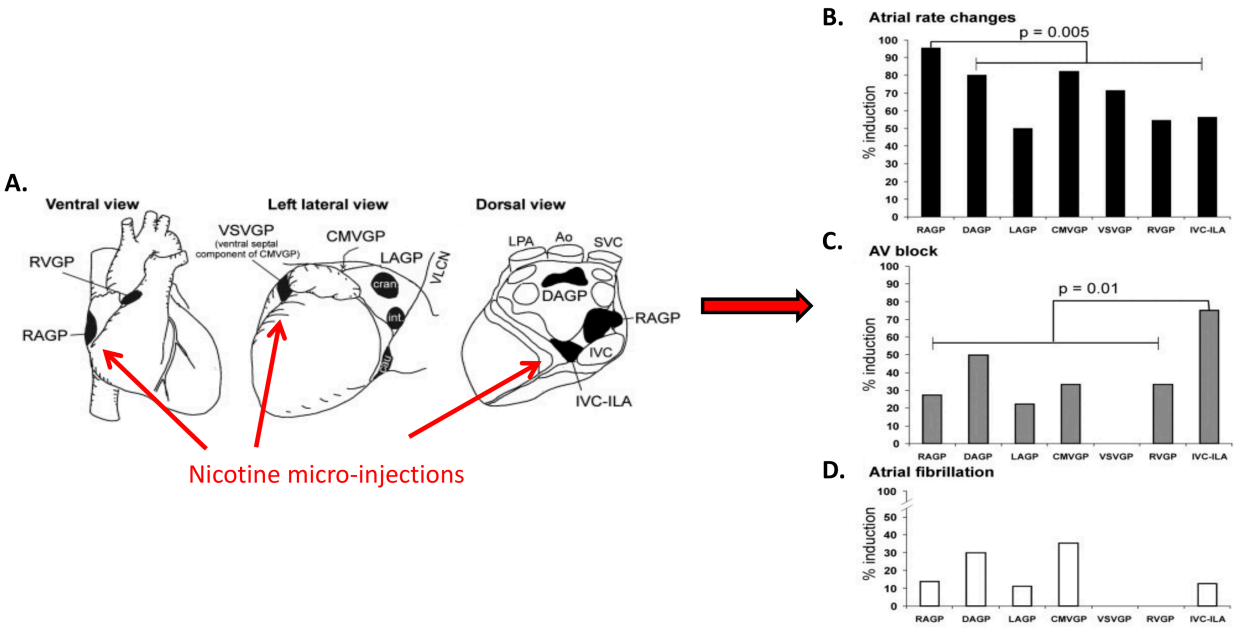

Figure 4. Aggregates of afferent, efferent, and interneurons located within epicardial fat pads comprise the intrinsic cardiac nervous system. Although each ganglionated plexus has a preferred sphere of influence, substantial overlap exists. (A) Ventral, left lateral, and dorsal views of the heart demonstrating common atrial and ventricular ganglionated plexi. Selected electrophysiologic effects of nicotine microinjections into major atrial and ventricular ganglionated plexi, (B) Heart rate, (C) Atrioventricular block, (D) atrial fibrillation. RVGP, right ventricular ganglionated plexus. RAGP, right atrial ganglionated plexus. VSVGP, ventral septal ventricular ganglionated plexus. CMVGP, cranial medial ventricular ganglionated plexus. LAGP, left atrial ganglionated plexus. DAGP, dorsal atrial ganglionated plexus. IVC-ILA, inferior vena cava-inferior atrial ganglionated plexus. Adapted from Cardinal et al. (2009).[28]

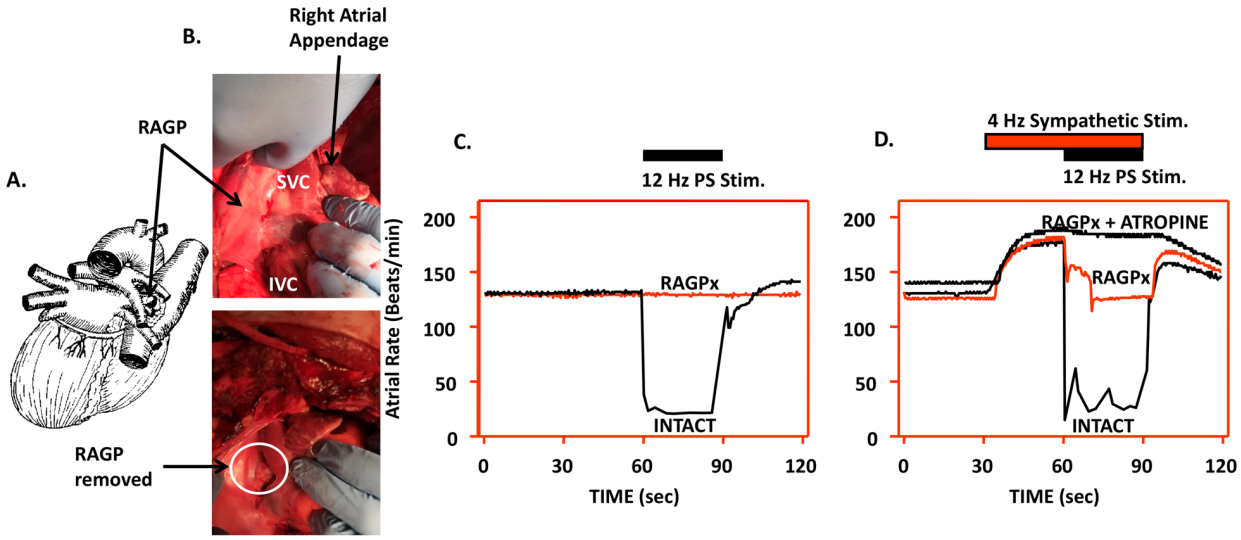

Figure 5. Interactions between sympathetic and parasympathetic system occur at end-effector as well as within the intrinsic cardiac nervous system. Disruption of the right atrial ganglionated plexus alters neural control of heart rate. (A) Diagram depicting location of right atrial ganglionated plexus, posterior to the caval veins and anterior to right pulmonary artery and right superior pulmonary vein. (B) Photographs of right atrial ganglionated plexus before and after ablation. (C) Evoked bradycardia with 12Hz parasympathetic stimulation in intact state, with loss of evoked bradycardia after RAGP ablation. (D) Combined sympathetic (4Hz) and parasympathetic (12Hz) stimulation in intact state, following RAGP ablation, and RAGP ablation with atropine administration. Adapted from McGuirt et al. (1997).[122]

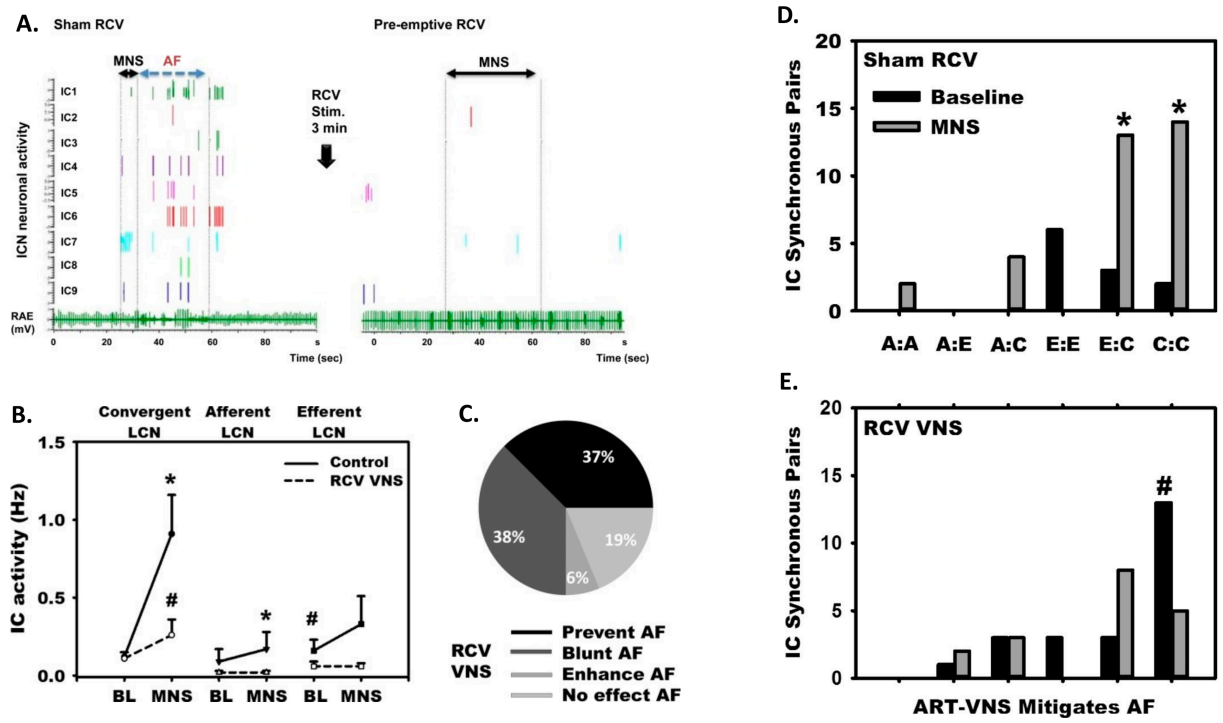

Figure 6. Vagal nerve stimulation targets local circuit neurons within the intrinsic cardiac nervous system to reduce arrhythmogenesis. (A) In response to mediastinal nerve stimulation, activity within the right atrial ganglionated plexus significantly increased and transient periods of AF were induced. (B) Increased neural activity during mediastinal nerve stimulation was primarily driven by increased activity of local circuit neurons. (C) VNS mitigated neural activity changes in response to mediastinal nerve stimulation and prevented or blunted atrial arrhythmogenesis. (D) and (E) Intrinsic cardiac neurons were classified as afferent [A], efferent [E], or convergent [C]. Mediastinal nerve stimulation resulted in increases in synchrony between efferent to convergent pairs and convergent to convergent pairs, while preemptive right cervical vagus nerve stimulation prevented such. (B): *$p < 0.05$ from baseline; #$p < 0.05$ from control (sham VNS). (D) and (E): *$p < 0.05$ from baseline; #$p < 0.01$ sham to RCV VNS state. Adapted from Salavatian et al. (2016).[123]

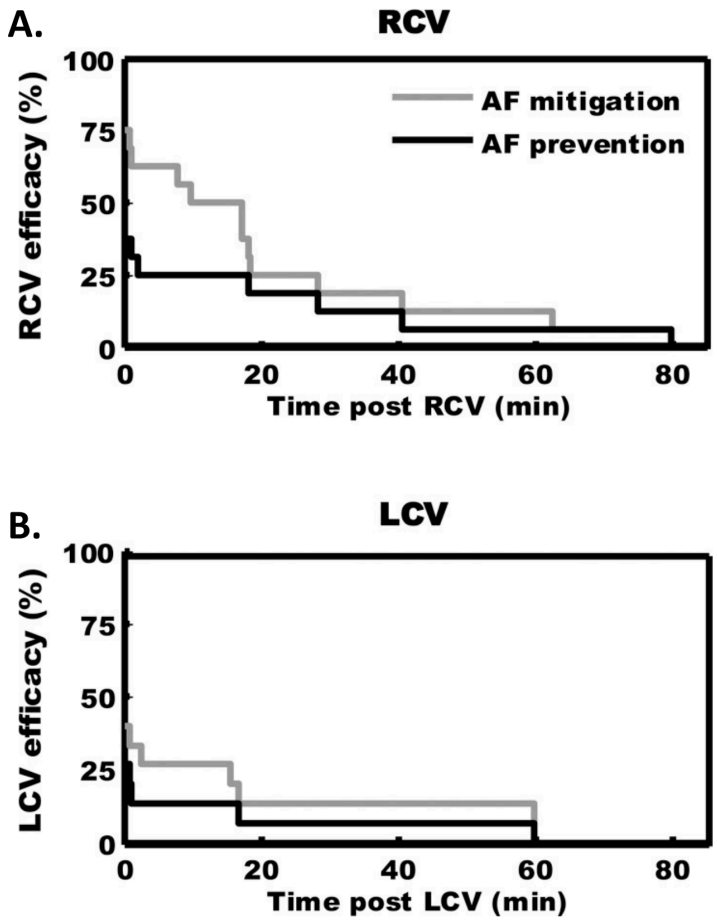

Figure 7. Kaplan-Meier curves demonstrating duration of antiarrhythmic effects of 3 minutes of preemptive cervical vagal nerve stimulation. After right (A) or left (B) sided vagal nerve stimulation, mediastinal nerve stimulation was less effective in inducing atrial fibrillation for approximately 30 minutes. Adapted from Salavatian et al. (2016).[123]

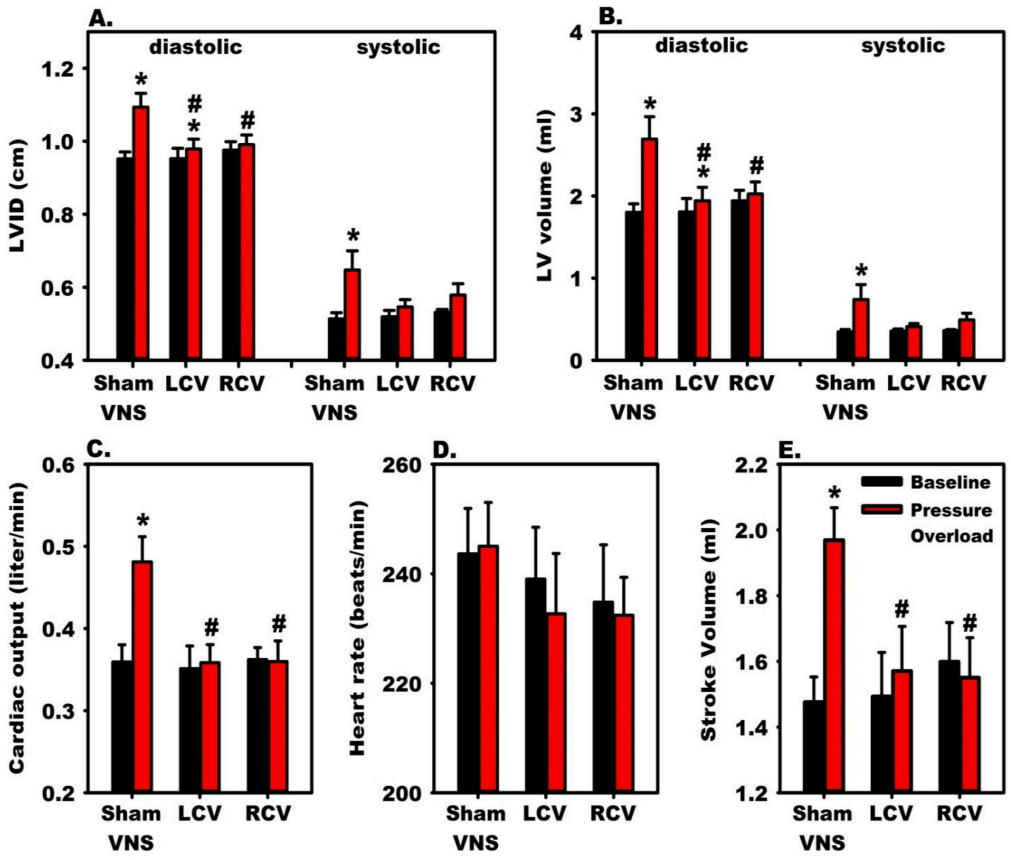

Figure 8. Vagal nerve stimulation mitigates heart failure and cardiac hypertrophy in a guinea pig model of chronic pressure-overload induced by aortic constriction. Compared to animals receiving sham vagal nerve stimulation, those receiving right or left sided vagal nerve stimulation had improvements in indices of heart failure. Significant improvements were noted in diastolic indices of (A) Left ventricular internal diameter and (B) left ventricular volume. (C) Cardiac output and (E) stroke volume normalized to baseline with left and right vagal nerve stimulation, with no changes in (D) Heart Rate. LCV, left cervical vagus stimulation. RCV, right cervical vagus stimulation. VNS, vagus nerve stimulation. LV, left ventricular. LVID, Left ventricular internal diameter. *$p < 0.05$ from baseline; $^{\#}p < 0.05$ to sham VNS. Adapted from Beaumont et al. (2016).[142]

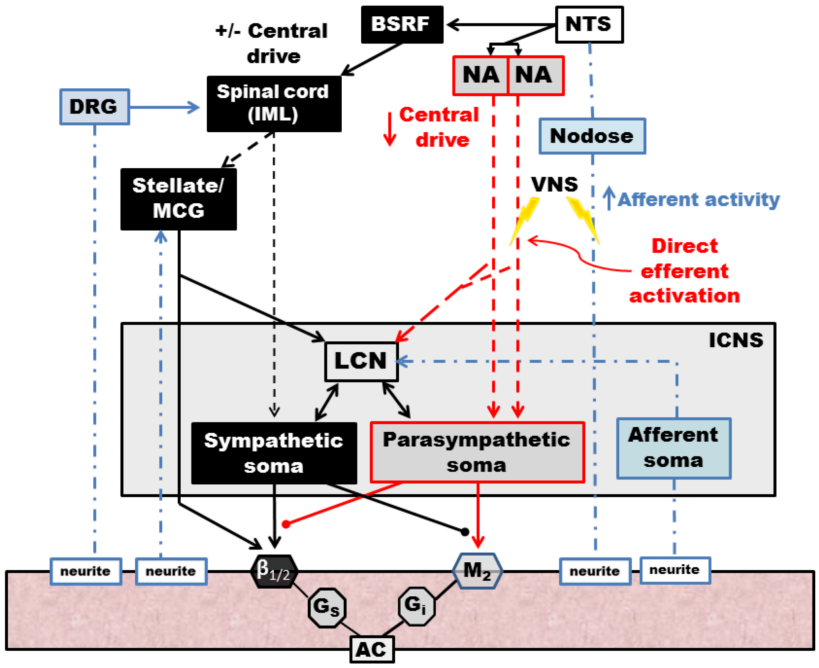

Figure 9. Schematic diagram of the effects of vagal nerve stimulation on the cardiac neuraxis. Direct efferent activation of the vagus nerve results in activation of parasympathetic postganglionic cells, located in the ICNS, which act on muscarinic receptors on the myocardium. Local circuit neurons within the ICN are activated, which modulate sympathetic reflexes with input from afferent soma, ultimately blunting reflexes within the intrinsic cardiac nervous system. Afferent activation results in reduced central drive and modulates projections to spinal sympathetic networks. Sympathetic spinal reflexes are also blunted via inhibitory projections (not shown). NTS, nucleus tractus solitarus. NA, nucleus ambiguus. BSRF, brain stem reticular formation. VNS, vagal nerve stimulation. DRG, dorsal root ganglia. IML, intermediolateral nucleus. MCG, middle cervical ganglia. LCN, local circuit neuron. ICNS, intrinsic cardiac nervous system. AC, adenylyl cyclase. Adapted from Ardell et al. (2015).[45]

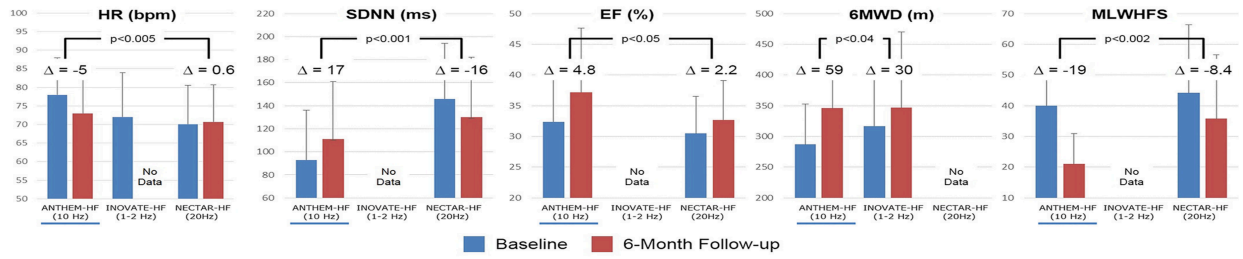

Figure 10. Clinical responses for the 3 major vagus nerve stimulation trials for HFrEF at baseline (blue) and 6-month follow up (red). Improvement for most parameters were noted for ANTHEM-HF, but unstudied or not met for INOVATE-HF or NECTAR-HF. (A) Heart rate, (B) SDNN, a standardized measurement of heart rate variability, (C) Ejection fraction, (D) 6 minute walking distance test, and (E) Minnesota Living With Heart Failure score. Adapted from Anand et al. (2020).[179]

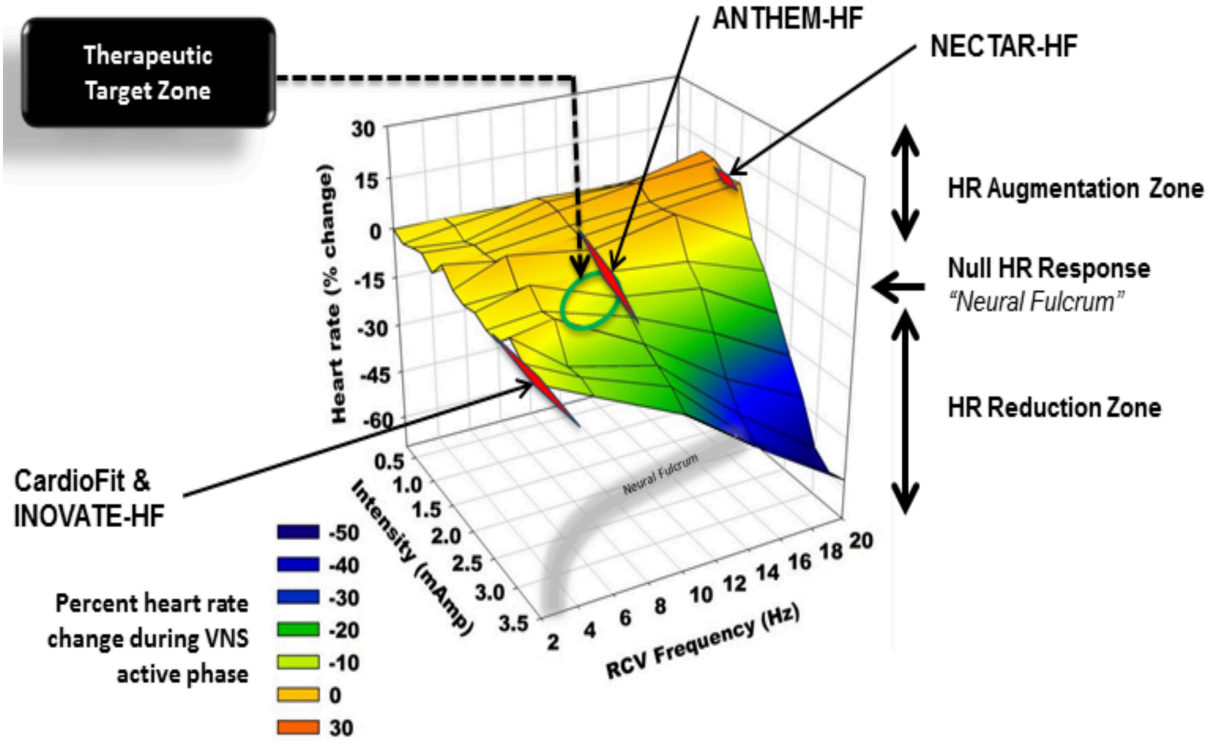

Figure 11. Heart rate responses to right cervical vagus nerve stimulation in a canine model at varying frequency and intensity (pulse width 500µs). At higher frequencies and current, vagal nerve stimulation results in predominant activation of vagomotor efferent fibers, producing a bradycardia (blue). At higher frequencies and lower current, vagal nerve stimulation results in a relative tachycardia due to preferential activation of afferent fibers (orange, red). The area at which a null heart rate response is achieved is described as the neural fulcrum (yellow surface). Achieved stimulation parameters for 3 vagus nerve stimulation trials (ANTHEM-HF, NECTAR-HF, and INOVATE-HF) are plotted as a function of frequency and intensity. Adapted from Ardell et al. (2017).[109]

References

1. Fukuda K, Kanazawa H, Aizawa Y, Ardell JL, Shivkumar K. Cardiac innervation and sudden cardiac death. *Circ Res*. 2015;116:2005-2019.
2. Ardell JL, Andresen MC, Armour JA, Billman GE, Chen PS, Foreman RD, Herring N, O'Leary DS, Sabbah HN, Schultz HD, et al. Translational neurocardiology: preclinical models and cardioneural integrative aspects. *J Physiol*. 2016;594:3877-3909.
3. Ardell JL, Armour JA. Neurocardiology: Structure-Based Function. *Compr Physiol*. 2016;6:1635-1653.
4. Shivkumar K, Ajijola OA, Anand I, Armour JA, Chen PS, Esler M, De Ferrari GM, Fishbein MC, Goldberger JJ, Harper RM, et al. Clinical neurocardiology defining the value of neuroscience-based cardiovascular therapeutics. *J Physiol*. 2016;594:3911-3954.
5. Florea VG, Cohn JN. The autonomic nervous system and heart failure. *Circ Res*. 2014;114:1815-1826.
6. McMurray JJ, Packer M, Desai AS, Gong J, Lefkowitz MP, Rizkala AR, Rouleau JL, Shi VC, Solomon SD, Swedberg K, et al. Angiotensin-neprilysin inhibition versus enalapril in heart failure. *N Engl J Med*. 2014;371:993-1004.
7. Vaseghi M, Gima J, Kanaan C, Ajijola OA, Marmureanu A, Mahajan A, Shivkumar K. Cardiac sympathetic denervation in patients with refractory ventricular arrhythmias or electrical storm: intermediate and long-term follow-up. *Heart Rhythm*. 2014;11:360-366.

8. Bourke T, Vaseghi M, Michowitz Y, Sankhla V, Shah M, Swapna N, Boyle NG, Mahajan A, Narasimhan C, Lokhandwala Y, et al. Neuraxial modulation for refractory ventricular arrhythmias: value of thoracic epidural anesthesia and surgical left cardiac sympathetic denervation. *Circulation*. 2010;121:2255-2262.
9. Sharma K, Premchand RK, Mittal S, Monteiro R, Libbus I, DiCarlo LA, Ardell JL, Amurthur B, KenKnight BH, Anand IS. Long-term follow-up of patients with heart failure and reduced ejection receiving autonomic regulation therapy in the ANTHEM-HF pilot study. *Int J Cardiol*. 2020.
10. Schwartz PJ, Priori SG, Cerrone M, Spazzolini C, Odero A, Napolitano C, Bloise R, De Ferrari GM, Klersy C, Moss AJ, et al. Left cardiac sympathetic denervation in the management of high-risk patients affected by the long-QT syndrome. *Circulation*. 2004;109:1826-1833.
11. Schwartz PJ, De Ferrari GM, Sanzo A, Landolina M, Rordorf R, Raineri C, Campana C, Revera M, Ajmone-Marsan N, Tavazzi L, et al. Long term vagal stimulation in patients with advanced heart failure: first experience in man. *Eur J Heart Fail*. 2008;10:884-891.
12. Wilde AA, Bhuiyan ZA, Crotti L, Facchini M, De Ferrari GM, Paul T, Ferrandi C, Koolbergen DR, Odero A, Schwartz PJ. Left cardiac sympathetic denervation for catecholaminergic polymorphic ventricular tachycardia. *N Engl J Med*. 2008;358:2024-2029.
13. Armour JA. Potential clinical relevance of the 'little brain' on the mammalian heart. *Exp Physiol*. 2008;93:165-176.

14. Palma JA, Benarroch EE. Neural control of the heart: recent concepts and clinical correlations. *Neurology*. 2014;83:261-271.

15. Jänig W. *The Integrative Action of the Autonomic Nervous System: Neurobiology of Homeostasis*. New York: Cambridge University Press; 2006.

16. Hill MR, Wallick DW, Martin PJ, Levy MN. Effects of repetitive vagal stimulation on heart rate and on cardiac vasoactive intestinal polypeptide efflux. *Am J Physiol*. 1995;268:H1939-1946.

17. Norris JE, Foreman RD, Wurster RK. Responses of the canine heart to stimulation of the first five ventral thoracic roots. *Am J Physiol*. 1974;227:9-12.

18. Norris JE, Lippincott D, Wurster RD. Responses of canine endocardium to stimulation of the upper thoracic roots. *Am J Physiol*. 1977;233:H655-659.

19. Herring N, Cranley J, Lokale MN, Li D, Shanks J, Alston EN, Girard BM, Carter E, Parsons RL, Habecker BA, et al. The cardiac sympathetic co-transmitter galanin reduces acetylcholine release and vagal bradycardia: implications for neural control of cardiac excitability. *J Mol Cell Cardiol*. 2012;52:667-676.

20. Hoang JD, Salavatian S, Yamaguchi N, Swid MA, Vaseghi M. Cardiac sympathetic activation circumvents high-dose beta blocker therapy in part through release of neuropeptide Y. *JCI insight*. 2020;5.

21. Armour JA, Ardell JL. *Basic and Clinical Neurocardiology*. New York: Oxford University Press; 2004.

22. Thompson GW, Horackova M, Armour JA. Chemotransduction properties of nodose ganglion cardiac afferent neurons in guinea pigs. *Am J Physiol Regul Integr Comp Physiol*. 2000;279:R433-439.

23. Fu LW, Longhurst JC. Regulation of cardiac afferent excitability in ischemia. *Handb Exp Pharmacol*. 2009:185-225.

24. Malliani A, Schwartz PJ, Zanchetti A. A sympathetic reflex elicited by experimental coronary occlusion. *Am J Physiol*. 1969;217:703-709.

25. Malliani A, Montano N. Emerging excitatory role of cardiovascular sympathetic afferents in pathophysiological conditions. *Hypertension*. 2002;39:63-68.

26. Billman GE. A comprehensive review and analysis of 25 years of data from an in vivo canine model of sudden cardiac death: implications for future anti-arrhythmic drug development. *Pharmacology & therapeutics*. 2006;111:808-835.

27. Malliani A, Recordati G, Schwartz PJ. Nervous activity of afferent cardiac sympathetic fibres with atrial and ventricular endings. *J Physiol*. 1973;229:457-469.

28. Cardinal R, Page P, Vermeulen M, Ardell JL, Armour JA. Spatially divergent cardiac responses to nicotinic stimulation of ganglionated plexus neurons in the canine heart. *Auton Neurosci*. 2009;145:55-62.

29. Rajendran PS, Nakamura K, Ajijola OA, Vaseghi M, Armour JA, Ardell JL, Shivkumar K. Myocardial infarction induces structural and functional remodelling of the intrinsic cardiac nervous system. *J Physiol*. 2016;594:321-341.

30. Beaumont E, Southerland EM, Hardwick JC, Wright GL, Ryan S, Li Y, KenKnight BH, Armour JA, Ardell JL. Vagus nerve stimulation mitigates intrinsic cardiac neuronal and adverse myocyte remodeling postmyocardial infarction. *Am J Physiol Heart Circ Physiol*. 2015;309:H1198-1206.

31. Hardwick JC, Southerland EM, Ardell JL. Chronic myocardial infarction induces phenotypic and functional remodeling in the guinea pig cardiac plexus. *Am J Physiol Regul Integr Comp Physiol*. 2008;295:R1926-1933.

32. Ajijola OA, Hoover DB, Simerly TM, Brown TC, Yanagawa J, Biniwale RM, Lee JM, Sadeghi A, Khanlou N, Ardell JL, et al. Inflammation, oxidative stress, and glial cell activation characterize stellate ganglia from humans with electrical storm. *JCI insight*. 2017;2.

33. Zucker IH, Patel KP, Schultz HD. Neurohumoral stimulation. *Heart Fail Clin*. 2012;8:87-99.

34. Wang HJ, Wang W, Cornish KG, Rozanski GJ, Zucker IH. Cardiac sympathetic afferent denervation attenuates cardiac remodeling and improves cardiovascular dysfunction in rats with heart failure. *Hypertension*. 2014;64:745-755.

35. Yoshie K, Rajendran PS, Massoud L, Mistry J, Swid MA, Wu X, Sallam T, Zhang R, Goldhaber JI, Salavatian S, et al. Cardiac TRPV1 afferent signaling promotes arrhythmogenic ventricular remodeling after myocardial infarction. *JCI insight*. 2020;5.

36. Levy MN, Schwartz PJ. *Vagal Control of the Heart: Experimental Basis and Clinical Implications*. Armonk, NY: Futura Pub. Co.; 1994.

37. Hanna P, Shivkumar K, Ardell JL. Calming the Nervous Heart: Autonomic Therapies in Heart Failure. *Card Fail Rev*. 2018;4:92-98.

38. Kuntz A, Morehouse A. Thoracic sympathetic cardiac nerves in man. *Arch Surg*. 1930;20:607-613.

39. Armour JA, Janes RD. Neuronal activity recorded extracellularly from in situ canine mediastinal ganglia. *Can J Physiol Pharmacol*. 1988;66:119-127.

40. Olshansky B, Sabbah HN, Hauptman PJ, Colucci WS. Parasympathetic nervous system and heart failure: pathophysiology and potential implications for therapy. *Circulation*. 2008;118:863-871.

41. Armour JA, Kember G. Cardiac sensory neurons. In: Armour JA, Ardell JL, eds. *Basic and Clinical Neurocardiology*. New York: Oxford University Press; 2004:79-117.

42. Tjen ALS, Bonham A, Longhurst J. Interactions between sympathetic and vagal cardiac afferents in nucleus tractus solitarii. *Am J Physiol*. 1997;272:H2843-2851.

43. Malliani A, Lombardi F, Pagani M, Recordati G, Schwartz PJ. Spinal cardiovascular reflexes. *Brain Res*. 1975;87:239-246.

44. Habecker BA, Anderson ME, Birren SJ, Fukuda K, Herring N, Hoover DB, Kanazawa H, Paterson DJ, Ripplinger CM. Molecular and cellular neurocardiology: development, and cellular and molecular adaptations to heart disease. *J Physiol*. 2016;594:3853-3875.

45. Ardell JL, Rajendran PS, Nier HA, KenKnight BH, Armour JA. Central-peripheral neural network interactions evoked by vagus nerve stimulation: functional consequences on control of cardiac function. *Am J Physiol Heart Circ Physiol*. 2015;309:H1740-1752.

46. Linz D, Ukena C, Mahfoud F, Neuberger HR, Bohm M. Atrial autonomic innervation: a target for interventional antiarrhythmic therapy? *J Am Coll Cardiol*. 2014;63:215-224.

47. Randall WC. Efferent Sympathetic Innervation of the Heart. In: Armour JA, Ardell JL, eds. *Neurocardiology*. New York: Oxford University Press; 1994:77-94.

48. Kawashima T. The autonomic nervous system of the human heart with special reference to its origin, course, and peripheral distribution. *Anat Embryol (Berl)*. 2005;209:425-438.

49. Hopkins DA, Armour JA. Localization of sympathetic postganglionic and parasympathetic preganglionic neurons which innervate different regions of the dog heart. *J Comp Neurol*. 1984;229:186-198.

50. Armour JA, Hopkins DA. Localization of sympathetic postganglionic neurons of physiologically identified cardiac nerves in the dog. J *Comp Neurol*. 1981;202:169-184.

51. Kawano H, Okada R, Yano K. Histological study on the distribution of autonomic nerves in the human heart. *Heart Vessels*. 2003;18:32-39.

52. Wharton J, Polak JM, Gordon L, Banner NR, Springall DR, Rose M, Khagani A, Wallwork J, Yacoub MH. Immunohistochemical demonstration of human cardiac innervation before and after transplantation. *Circ Res*. 1990;66:900-912.

53. Hoover DB, Isaacs ER, Jacques F, Hoard JL, Page P, Armour JA. Localization of multiple neurotransmitters in surgically derived specimens of human atrial ganglia. *Neuroscience*. 2009;164:1170-1179.

54. Lundberg JM, Franco-Cereceda A, Lacroix JS, Pernow J. Neuropeptide Y and sympathetic neurotransmission. *Ann N Y Acad Sci*. 1990;611:166-174.

55. Ajijola OA, Chatterjee NA, Gonzales MJ, Gornbein J, Liu K, Li D, Paterson DJ, Shivkumar K, Singh JP, Herring N. Coronary Sinus Neuropeptide Y Levels and

Adverse Outcomes in Patients With Stable Chronic Heart Failure. *JAMA Cardiol*. 2019.

56. Shanks J, Herring N. Peripheral cardiac sympathetic hyperactivity in cardiovascular disease: role of neuropeptides. *Am J Physiol Regul Integr Comp Physiol*. 2013;305:R1411-1420.

57. Bohlender J, Imboden H. Angiotensinergic neurotransmission in the peripheral autonomic nervous system. *Front Biosci*. 2012;17:2419-2432.

58. Burwash IG, Morgan DE, Koilpillai CJ, Blackmore GL, Johnstone DE, Armour JA. Sympathetic stimulation alters left ventricular relaxation and chamber size. *Am J Physiol*. 1993;264:R1-7.

59. Haws CW, Lux RL. Correlation between in vivo transmembrane action potential durations and activation-recovery intervals from electrograms. Effects of interventions that alter repolarization time. *Circulation*. 1990;81:281-288.

60. Vaseghi M, Yamakawa K, Sinha A, So EL, Zhou W, Ajijola OA, Lux RL, Laks M, Shivkumar K, Mahajan A. Modulation of regional dispersion of repolarization and T-peak to T-end interval by the right and left stellate ganglia. *Am J Physiol Heart Circ Physiol*. 2013;305:H1020-1030.

61. Vaseghi M, Zhou W, Shi J, Ajijola OA, Hadaya J, Shivkumar K, Mahajan A. Sympathetic innervation of the anterior left ventricular wall by the right and left stellate ganglia. *Heart Rhythm*. 2012;9:1303-1309.

62. Yanowitz F, Preston JB, Abildskov JA. Functional distribution of right and left stellate innervation to the ventricles. Production of neurogenic

electrocardiographic changes by unilateral alteration of sympathetic tone. *Circ Res*. 1966;18:416-428.

63. Ajijola OA, Vaseghi M, Zhou W, Yamakawa K, Benharash P, Hadaya J, Lux RL, Mahajan A, Shivkumar K. Functional differences between junctional and extrajunctional adrenergic receptor activation in mammalian ventricle. *Am J Physiol Heart Circ Physiol*. 2013;304:H579-588.

64. Zhou S, Chen LS, Miyauchi Y, Miyauchi M, Kar S, Kangavari S, Fishbein MC, Sharifi B, Chen PS. Mechanisms of cardiac nerve sprouting after myocardial infarction in dogs. *Circ Res*. 2004;95:76-83.

65. Cao JM, Chen LS, KenKnight BH, Ohara T, Lee MH, Tsai J, Lai WW, Karagueuzian HS, Wolf PL, Fishbein MC, et al. Nerve sprouting and sudden cardiac death. *Circ Res*. 2000;86:816-821.

66. Ajijola OA, Wisco JJ, Lambert HW, Mahajan A, Stark E, Fishbein MC, Shivkumar K. Extracardiac neural remodeling in humans with cardiomyopathy. *Circ Arrhythm Electrophysiol*. 2012;5:1010-1116.

67. Ajijola OA, Yagishita D, Reddy NK, Yamakawa K, Vaseghi M, Downs AM, Hoover DB, Ardell JL, Shivkumar K. Remodeling of stellate ganglion neurons after spatially targeted myocardial infarction: Neuropeptide and morphologic changes. *Heart Rhythm*. 2015;12:1027-1035.

68. Gardner RT, Wang L, Lang BT, Cregg JM, Dunbar CL, Woodward WR, Silver J, Ripplinger CM, Habecker BA. Targeting protein tyrosine phosphatase sigma after myocardial infarction restores cardiac sympathetic innervation and prevents arrhythmias. *Nat Commun*. 2015;6:6235.

69. Tapa S, Wang L, Francis Stuart SD, Wang Z, Jiang Y, Habecker BA, Ripplinger CM. Adrenergic supersensitivity and impaired neural control of cardiac electrophysiology following regional cardiac sympathetic nerve loss. *Sci Rep*. 2020;10:18801.

70. Dibner-Dunlap ME, Kinugawa T, Thames MD. Activation of cardiac sympathetic afferents: effects of exogenous adenosine and adenosine analogues. *Am J Physiol*. 1993;265:H395-400.

71. Minisi AJ, Thames MD. Distribution of left ventricular sympathetic afferents demonstrated by reflex responses to transmural myocardial ischemia and to intracoronary and epicardial bradykinin. *Circulation*. 1993;87:240-246.

72. Huang MH, Horackova M, Negoescu RM, Wolf S, Armour JA. Polysensory response characteristics of dorsal root ganglion neurones that may serve sensory functions during myocardial ischaemia. *Cardiovasc Res*. 1996;32:503-515.

73. Minisi AJ, Thames MD. Activation of cardiac sympathetic afferents during coronary occlusion. Evidence for reflex activation of sympathetic nervous system during transmural myocardial ischemia in the dog. *Circulation*. 1991;84:357-367.

74. Ardell JL, Foreman RD, Armour JA, Shivkumar K. Cardiac sympathectomy and spinal cord stimulation attenuate reflex-mediated norepinephrine release during ischemia preventing ventricular fibrillation. *JCI Insight*. 2019;4.

75. Schwartz PJ, La Rovere MT, Vanoli E. Autonomic nervous system and sudden cardiac death. Experimental basis and clinical observations for post-myocardial infarction risk stratification. *Circulation*. 1992;85:I77-91.

76. Han S, Kobayashi K, Joung B, Piccirillo G, Maruyama M, Vinters HV, March K, Lin SF, Shen C, Fishbein MC, et al. Electroanatomic remodeling of the left stellate ganglion after myocardial infarction. *J Am Coll Cardiol*. 2012;59:954-961.

77. Armour JA. Cardiac neuronal hierarchy in health and disease. *Am J Physiol Regul Integr Comp Physiol*. 2004;287:R262-271.

78. Mill JG, Stefanon I, dos Santos L, Baldo MP. Remodeling in the ischemic heart: the stepwise progression for heart failure. *Braz J Med Biol Res*. 2011;44:890-898.

79. Schwartz PJ, Foreman RD, Stone HL, Brown AM. Effect of dorsal root section on the arrhythmias associated with coronary occlusion. *Am J Physiol*. 1976;231:923-928.

80. Olivas A, Gardner RT, Wang L, Ripplinger CM, Woodward WR, Habecker BA. Myocardial Infarction Causes Transient Cholinergic Transdifferentiation of Cardiac Sympathetic Nerves via gp130. *J Neurosci*. 2016;36:479-488.

81. Wang L, Olivas A, Francis Stuart SD, Tapa S, Blake MR, Woodward WR, Habecker BA, Ripplinger CM. Cardiac sympathetic nerve transdifferentiation reduces action potential heterogeneity after myocardial infarction. *Am J Physiol Heart Circ Physiol*. 2020;318:H558-H565.

82. Triposkiadis F, Karayannis G, Giamouzis G, Skoularigis J, Louridas G, Butler J. The sympathetic nervous system in heart failure physiology, pathophysiology, and clinical implications. *J Am Coll Cardiol*. 2009;54:1747-1762.

83. Schwartz PJ. Cardiac sympathetic denervation to prevent life-threatening arrhythmias. *Nat Rev Cardiol*. 2014;11:346-353.

84. Buckley U, Chui RW, Rajendran PS, Vrabec T, Shivkumar K, Ardell JL. Bioelectronic neuromodulation of the paravertebral cardiac efferent sympathetic outflow and its effect on ventricular electrical indices. *Heart Rhythm*. 2017;14:1063-1070.

85. Chui RW, Buckley U, Rajendran PS, Vrabec T, Shivkumar K, Ardell JL. Bioelectronic block of paravertebral sympathetic nerves mitigates post-myocardial infarction ventricular arrhythmias. *Heart Rhythm*. 2017;14:1665-1672.

86. Hopkins DA, Bieger D, deVente J, Steinbusch WM. Vagal efferent projections: viscerotopy, neurochemistry and effects of vagotomy. *Prog Brain Res*. 1996;107:79-96.

87. Standish A, Enquist LW, Schwaber JS. Innervation of the heart and its central medullary origin defined by viral tracing. *Science*. 1994;263:232-234.

88. Pauza DH, Rysevaite-Kyguoliene K, Vismantaite J, Brack KE, Inokaitis H, Pauza AG, Rimasauskaite-Petraitiene V, Pauzaite JI, Pauziene N. A combined acetylcholinesterase and immunohistochemical method for precise anatomical analysis of intrinsic cardiac neural structures. *Ann Anat*. 2014;196:430-440.

89. Yuan BX, Ardell JL, Hopkins DA, Armour JA. Differential cardiac responses induced by nicotine sensitive canine atrial and ventricular neurones. *Cardiovasc Res*. 1993;27:760-769.

90. Armour JA, Collier K, Kember G, Ardell JL. Differential selectivity of cardiac neurons in separate intrathoracic autonomic ganglia. *Am J Physiol*. 1998;274:R939-949.

91. Petraitiene V, Pauza DH, Benetis R. Distribution of adrenergic and cholinergic nerve fibres within intrinsic nerves at the level of the human heart hilum. *Eur J Cardiothorac Surg*. 2014;45:1097-1105.

92. Hoover DB, Ganote CE, Ferguson SM, Blakely RD, Parsons RL. Localization of cholinergic innervation in guinea pig heart by immunohistochemistry for high-affinity choline transporters. *Cardiovasc Res*. 2004;62:112-121.

93. Schultz HD, Ustinova EE. Cardiac vagal afferent stimulation by free radicals during ischaemia and reperfusion. *Clin Exp Pharmacol Physiol*. 1996;23:700-708.

94. Schultz HD. Cardiac vagal chemosensory afferents. Function in pathophysiological states. *Ann N Y Acad Sci*. 2001;940:59-73.

95. Janes RD, Brandys JC, Hopkins DA, Johnstone DE, Murphy DA, Armour JA. Anatomy of human extrinsic cardiac nerves and ganglia. *Am J Cardiol*. 1986;57:299-309.

96. Kalia M, Mesulam MM. Brain stem projections of sensory and motor components of the vagus complex in the cat: I. The cervical vagus and nodose ganglion. *J Comp Neurol*. 1980;193:435-465.

97. Yoo PB, Lubock NB, Hincapie JG, Ruble SB, Hamann JJ, Grill WM. High-resolution measurement of electrically-evoked vagus nerve activity in the anesthetized dog. *J Neural Eng*. 2013;10:026003.

98. Hoover DB, Shepherd AV, Southerland EM, Armour JA, Ardell JL. Neurochemical diversity of afferent neurons that transduce sensory signals from dog ventricular myocardium. *Auton Neurosci.* 2008;141:38-45.

99. Prechtl JC, Powley TL. The fiber composition of the abdominal vagus of the rat. *Anat Embryol (Berl)*. 1990;181:101-115.

100. Paintal AS. Vagal sensory receptors and their reflex effects. *Physiol Rev*. 1973;53:159-227.

101. Paintal AS. Vagal Afferent Fibres. *Ergebnisse der Physiologie, biologischen Chemie und experimentellen Pharmakologie*. 1963;52:74-156.

102. Paintal AS. The conduction velocities of respiratory and cardiovascular afferent fibres in the vagus nerve. *J Physiol*. 1953;121:341-359.

103. Schultz HD, Marcus NJ, Del Rio R. Mechanisms of carotid body chemoreflex dysfunction during heart failure. *Exp Physiol*. 2015;100:124-129.

104. Berthoud HR, Neuhuber WL. Functional and chemical anatomy of the afferent vagal system. *Auton Neurosci*. 2000;85:1-17.

105. Thoren PN. Atrial receptors with nonmedullated vagal afferents in the cat. Discharge frequency and pattern in relation to atrial pressure. *Circ Res*. 1976;38:357-362.

106. Ardell JL, Randall WC. Selective vagal innervation of sinoatrial and atrioventricular nodes in canine heart. *Am J Physiol*. 1986;251:H764-773.

107. Armour JA, Randall WC, Sinha S. Localized myocardial responses to stimulation of small cardiac branches of the vagus. *Am J Physiol*. 1975;228:141-148.

108. Yamakawa K, So EL, Rajendran PS, Hoang JD, Makkar N, Mahajan A, Shivkumar K, Vaseghi M. Electrophysiological effects of right and left vagal nerve stimulation on the ventricular myocardium. *Am J Physiol Heart Circ Physiol*. 2014;307:H722-731.

109. Ardell JL, Nier H, Hammer M, Southerland EM, Ardell CL, Beaumont E, KenKnight BH, Armour JA. Defining the neural fulcrum for chronic vagus nerve stimulation: implications for integrated cardiac control. *J Physiol*. 2017;595:6887-6903.

110. Schwartz PJ, Pagani M, Lombardi F, Malliani A, Brown AM. A cardiocardiac sympathovagal reflex in the cat. *Circ Res*. 1973;32:215-220.

111. Boyden ES, Zhang F, Bamberg E, Nagel G, Deisseroth K. Millisecond-timescale, genetically targeted optical control of neural activity. *Nat Neurosci*. 2005;8:1263-1268.

112. Zemelman BV, Lee GA, Ng M, Miesenbock G. Selective photostimulation of genetically chARGed neurons. *Neuron*. 2002;33:15-22.

113. Wengrowski AM, Wang X, Tapa S, Posnack NG, Mendelowitz D, Kay MW. Optogenetic release of norepinephrine from cardiac sympathetic neurons alters mechanical and electrical function. *Cardiovasc Res*. 2015;105:143-150.

114. Moreno A, Endicott K, Skancke M, Dwyer MK, Brennan J, Efimov IR, Trachiotis G, Mendelowitz D, Kay MW. Sudden Heart Rate Reduction Upon Optogenetic Release of Acetylcholine From Cardiac Parasympathetic Neurons in Perfused Hearts. *Front Physiol*. 2019;10:16.

115. Sternson SM, Roth BL. Chemogenetic tools to interrogate brain functions. *Annu Rev Neurosci*. 2014;37:387-407.

116. Garrott K, Dyavanapalli J, Cauley E, Dwyer MK, Kuzmiak-Glancy S, Wang X, Mendelowitz D, Kay MW. Chronic activation of hypothalamic oxytocin neurons

improves cardiac function during left ventricular hypertrophy-induced heart failure. *Cardiovasc Res*. 2017;113:1318-1328.

117. Shivkumar K, Ardell JL. Cardiac autonomic control in health and disease. *J Physiol*. 2016;594:3851-3852.

118. Vaseghi M, Salavatian S, Rajendran PS, Yagishita D, Woodward WR, Hamon D, Yamakawa K, Irie T, Habecker BA, Shivkumar K. Parasympathetic dysfunction and antiarrhythmic effect of vagal nerve stimulation following myocardial infarction. *JCI Insight*. 2017;2.

119. Salavatian S, Yamaguchi N, Hamon D, Fishbein MC, Ardell JL, Shivkumar K, Vaseghi M. Myocardial Infarction Causes Both Structural and Functional Remodeling in Cardiac Neurons of the Inferior Vagal (Nodose) Ganglia: Implications for Mechanisms Behind Parasympathetic Withdrawal in Heart Disease (Abstract 17355). *Circulation*. 2017;136:A17355.

120. Salavatian S, Beaumont E, Gibbons D, Hammer M, Hoover DB, Armour JA, Ardell JL. Thoracic spinal cord and cervical vagosympathetic neuromodulation obtund nodose sensory transduction of myocardial ischemia. *Auton Neurosci*. 2017;208:57-65.

121. Southerland EM, Milhorn DM, Foreman RD, Linderoth B, DeJongste MJ, Armour JA, Subramanian V, Singh M, Singh K, Ardell JL. Preemptive, but not reactive, spinal cord stimulation mitigates transient ischemia-induced myocardial infarction via cardiac adrenergic neurons. *Am J Physiol Heart Circ Physiol*. 2007;292:H311-317.

122. McGuirt AS, Schmacht DC, Ardell JL. Autonomic interactions for control of atrial rate are maintained after SA nodal parasympathectomy. *Am J Physiol*. 1997;272:H2525-2533.

123. Salavatian S, Beaumont E, Longpre JP, Armour JA, Vinet A, Jacquemet V, Shivkumar K, Ardell JL. Vagal stimulation targets select populations of intrinsic cardiac neurons to control neurally induced atrial fibrillation. *Am J Physiol Heart Circ Physiol*. 2016;311:H1311-H1320.

124. Butler CK, Smith FM, Cardinal R, Murphy DA, Hopkins DA, Armour JA. Cardiac responses to electrical stimulation of discrete loci in canine atrial and ventricular ganglionated plexi. *Am J Physiol*. 1990;259:H1365-1373.

125. Armour JA, Yuan BX, Butler CK. Cardiac responses elicited by peptides administered to canine intrinsic cardiac neurons. *Peptides*. 1990;11:753-761.

126. Ardell JL, Butler CK, Smith FM, Hopkins DA, Armour JA. Activity of in vivo atrial and ventricular neurons in chronically decentralized canine hearts. *Am J Physiol*. 1991;260:H713-721.

127. Rysevaite K, Saburkina I, Pauziene N, Vaitkevicius R, Noujaim SF, Jalife J, Pauza DH. Immunohistochemical characterization of the intrinsic cardiac neural plexus in whole-mount mouse heart preparations. *Heart Rhythm*. 2011;8:731-738.

128. Rysevaite K, Saburkina I, Pauziene N, Noujaim SF, Jalife J, Pauza DH. Morphologic pattern of the intrinsic ganglionated nerve plexus in mouse heart. *Heart Rhythm*. 2011;8:448-454.

129. Ali IM, Butler CK, Armour JA, Murphy DA. Modification of supraventricular tachyarrhythmias by stimulating atrial neurons. *Ann Thorac Surg*. 1990;50:251-256.

130. Randall DC, Brown DR, McGuirt AS, Thompson GW, Armour JA, Ardell JL. Interactions within the intrinsic cardiac nervous system contribute to chronotropic regulation. *Am J Physiol Regul Integr Comp Physiol*. 2003;285:R1066-1075.

131. Ripplinger CM, Noujaim SF, Linz D. The nervous heart. *Prog Biophys Mol Biol*. 2016;120:199-209.

132. Liu Y, Scherlag BJ, Fan Y, Varma V, Male S, Chaudhry MA, Huang C, Po SS. Inducibility of atrial fibrillation after GP ablations and "autonomic blockade": evidence for the pathophysiological role of the nonadrenergic and noncholinergic neurotransmitters. *J Cardiovasc Electrophysiol*. 2013;24:188-195.

133. Nakagawa H, Scherlag BJ, Patterson E, Ikeda A, Lockwood D, Jackman WM. Pathophysiologic basis of autonomic ganglionated plexus ablation in patients with atrial fibrillation. *Heart Rhythm*. 2009;6:S26-34.

134. Armour JA, Murphy DA, Yuan BX, Macdonald S, Hopkins DA. Gross and microscopic anatomy of the human intrinsic cardiac nervous system. *Anat Rec*. 1997;247:289-298.

135. Lo LW, Scherlag BJ, Chang HY, Lin YJ, Chen SA, Po SS. Paradoxical long-term proarrhythmic effects after ablating the "head station" ganglionated plexi of the vagal innervation to the heart. *Heart Rhythm*. 2013;10:751-757.

136. Gibbons DD, Southerland EM, Hoover DB, Beaumont E, Armour JA, Ardell JL. Neuromodulation targets intrinsic cardiac neurons to attenuate neuronally

mediated atrial arrhythmias. *Am J Physiol Regul Integr Comp Physiol*. 2012;302:R357-364.

137. Beaumont E, Salavatian S, Southerland EM, Vinet A, Jacquemet V, Armour JA, Ardell JL. Network interactions within the canine intrinsic cardiac nervous system: implications for reflex control of regional cardiac function. *J Physiol*. 2013;591:4515-4533.

138. Buckley U, Shivkumar K, Ardell JL. Autonomic Regulation Therapy in Heart Failure. *Curr Heart Fail Rep*. 2015;12:284-293.

139. Schwartz PJ, La Rovere MT, De Ferrari GM, Mann DL. Autonomic modulation for the management of patients with chronic heart failure. *Circ Heart Fail*. 2015;8:619-628.

140. Li M, Zheng C, Sato T, Kawada T, Sugimachi M, Sunagawa K. Vagal nerve stimulation markedly improves long-term survival after chronic heart failure in rats. *Circulation*. 2004;109:120-124.

141. Zhang Y, Popovic ZB, Bibevski S, Fakhry I, Sica DA, Van Wagoner DR, Mazgalev TN. Chronic vagus nerve stimulation improves autonomic control and attenuates systemic inflammation and heart failure progression in a canine high-rate pacing model. *Circ Heart Fail*. 2009;2:692-699.

142. Beaumont E, Wright GL, Southerland EM, Li Y, Chui R, KenKnight BH, Armour JA, Ardell JL. Vagus nerve stimulation mitigates intrinsic cardiac neuronal remodeling and cardiac hypertrophy induced by chronic pressure overload in guinea pig. *Am J Physiol Heart Circ Physiol*. 2016;310:H1349-1359.

143. Zhao M, He X, Bi XY, Yu XJ, Gil Wier W, Zang WJ. Vagal stimulation triggers peripheral vascular protection through the cholinergic anti-inflammatory pathway in a rat model of myocardial ischemia/reperfusion. *Basic Res Cardiol*. 2013;108:345.

144. Corr PB, Gillis RA. Role of the vagus nerves in the cardiovascular changes induced by coronary occlusion. *Circulation*. 1974;49:86-97.

145. Billman GE, Schwartz PJ, Stone HL. Baroreceptor reflex control of heart rate: a predictor of sudden cardiac death. *Circulation*. 1982;66:874-880.

146. Billman GE, Schwartz PJ, Stone HL. The effects of daily exercise on susceptibility to sudden cardiac death. *Circulation*. 1984;69:1182-1189.

147. Vanoli E, De Ferrari GM, Stramba-Badiale M, Hull SS, Jr., Foreman RD, Schwartz PJ. Vagal stimulation and prevention of sudden death in conscious dogs with a healed myocardial infarction. *Circ Res*. 1991;68:1471-1481.

148. De Ferrari GM, Vanoli E, Stramba-Badiale M, Hull SS, Jr., Foreman RD, Schwartz PJ. Vagal reflexes and survival during acute myocardial ischemia in conscious dogs with healed myocardial infarction. *Am J Physiol*. 1991;261:H63-69.

149. Ando M, Katare RG, Kakinuma Y, Zhang D, Yamasaki F, Muramoto K, Sato T. Efferent vagal nerve stimulation protects heart against ischemia-induced arrhythmias by preserving connexin43 protein. *Circulation*. 2005;112:164-170.

150. Janig W. Neurocardiology: a neurobiologist's perspective. *J Physiol*. 2016;594:3955-3962.

151. De Ferrari GM. Vagal stimulation in heart failure. *J Cardiovasc Transl Res*. 2014;7:310-320.

152. Sabbah HN, Ilsar I, Zaretsky A, Rastogi S, Wang M, Gupta RC. Vagus nerve stimulation in experimental heart failure. *Heart Fail Rev*. 2011;16:171-178.

153. Winbury MM, Green DM. Studies on the nervous and humoral control of coronary circulation. *Am J Physiol*. 1952;170:555-563.

154. Schofield BM, Walker JM. Perfusion of the coronary arteries of the dog. *J Physiol*. 1953;122:489-497.

155. Feigl EO. Coronary physiology. *Physiol Rev*. 1983;63:1-205.

156. Feigl EO. Parasympathetic control of coronary blood flow in dogs. *Circ Res*. 1969;25:509-519.

157. Levy MN, Martin PJ. Neural control of the heart. In: Berne RM, ed. *Handbook of Physiology: Section 2: The Cardiovascular System, Volume 1: The Heart*. Bethesda: The American Physiological Society; 1979:581-620.

158. Tracey KJ. Physiology and immunology of the cholinergic antiinflammatory pathway. *J Clin Invest*. 2007;117:289-296.

159. Sabbah HN. Electrical vagus nerve stimulation for the treatment of chronic heart failure. *Cleve Clin J Med*. 2011;78 Suppl 1:S24-29.

160. Ruble SB, Hamann JJ, Gupta RC, Mishra S, Sabbah HN. Chronic vagus nerve stimulation impacts biomarkers of heart failure in canines. Paper/Poster presented at: J Am Coll Cardiol; 2010;

161. Calvillo L, Vanoli E, Andreoli E, Besana A, Omodeo E, Gnecchi M, Zerbi P, Vago G, Busca G, Schwartz PJ. Vagal stimulation, through its nicotinic action, limits

infarct size and the inflammatory response to myocardial ischemia and reperfusion. *J Cardiovasc Pharmacol*. 2011;58:500-507.

162. Virani SS, Alonso A, Benjamin EJ, Bittencourt MS, Callaway CW, Carson AP, Chamberlain AM, Chang AR, Cheng S, Delling FN, et al. Heart Disease and Stroke Statistics-2020 Update: A Report From the American Heart Association. *Circulation*. 2020;141:e139-e596.

163. Benjamin EJ, Muntner P, Alonso A, Bittencourt MS, Callaway CW, Carson AP, Chamberlain AM, Chang AR, Cheng S, Das SR, et al. Heart Disease and Stroke Statistics-2019 Update: A Report From the American Heart Association. *Circulation*. 2019;139:e56-e528.

164. Gloschat CR, Koppel AC, Aras KK, Brennan JA, Holzem KM, Efimov IR. Arrhythmogenic and metabolic remodelling of failing human heart. *J Physiol*. 2016;594:3963-3980.

165. La Rovere MT, Bigger JT, Jr., Marcus FI, Mortara A, Schwartz PJ. Baroreflex sensitivity and heart-rate variability in prediction of total cardiac mortality after myocardial infarction. ATRAMI (Autonomic Tone and Reflexes After Myocardial Infarction) Investigators. *Lancet*. 1998;351:478-484.

166. Yancy CW, Jessup M, Bozkurt B, Butler J, Casey DE, Jr., Drazner MH, Fonarow GC, Geraci SA, Horwich T, Januzzi JL, et al. 2013 ACCF/AHA guideline for the management of heart failure: a report of the American College of Cardiology Foundation/American Heart Association Task Force on Practice Guidelines. *J Am Coll Cardiol*. 2013;62:e147-239.

167. Dargie HJ. Effect of carvedilol on outcome after myocardial infarction in patients with left-ventricular dysfunction: the CAPRICORN randomised trial. *Lancet*. 2001;357:1385-1390.

168. Vantrimpont P, Rouleau JL, Wun CC, Ciampi A, Klein M, Sussex B, Arnold JM, Moye L, Pfeffer M. Additive beneficial effects of beta-blockers to angiotensin-converting enzyme inhibitors in the Survival and Ventricular Enlargement (SAVE) Study. SAVE Investigators. *J Am Coll Cardiol*. 1997;29:229-236.

169. Pfeffer MA, Braunwald E, Moye LA, Basta L, Brown EJ, Cuddy TE, Davis BR, Geltman EM, Goldman S, Flaker GC, et al. Effect of Captopril on Mortality and Morbidity in Patients with Left-Ventricular Dysfunction after Myocardial-Infarction - Results of the Survival and Ventricular Enlargement Trial. *New Engl J Med*. 1992;327:669-677.

170. Verdecchia P, Sleight P, Mancia G, Fagard R, Trimarco B, Schmieder RE, Kim JH, Jennings G, Jansky P, Chen JH, et al. Effects of Telmisartan, Ramipril, and Their Combination on Left Ventricular Hypertrophy in Individuals at High Vascular Risk in the Ongoing Telmisartan Alone and in Combination With Ramipril Global End Point Trial and the Telmisartan Randomized Assessment Study in ACE Intolerant Subjects With Cardiovascular Disease. *Circulation*. 2009;120:1380-1389.

171. Aaronson ST, Carpenter LL, Conway CR, Reimherr FW, Lisanby SH, Schwartz TL, Moreno FA, Dunner DL, Lesem MD, Thompson PM, et al. Vagus nerve stimulation therapy randomized to different amounts of electrical charge for

treatment-resistant depression: acute and chronic effects. *Brain Stimul*. 2013;6:631-640.

172. Arle JE, Carlson KW, Mei L. Investigation of mechanisms of vagus nerve stimulation for seizure using finite element modeling. *Epilepsy Res*. 2016;126:109-118.

173. Ben-Menachem E, Revesz D, Simon BJ, Silberstein S. Surgically implanted and non-invasive vagus nerve stimulation: a review of efficacy, safety and tolerability. *European journal of neurology*. 2015;22:1260-1268.

174. Anand IS, Konstam MA, Ardell JL, Libbus I, Dicarlo L, Mann DL. Neuromodulation for drug-refractory epilepsy and chronic heart failure: Targets, delivery, composition and titration. *Int J Neurol and Neurother*. 2019;6.

175. Gold MR, Van Veldhuisen DJ, Hauptman PJ, Borggrefe M, Kubo SH, Lieberman RA, Milasinovic G, Berman BJ, Djordjevic S, Neelagaru S, et al. Vagus Nerve Stimulation for the Treatment of Heart Failure: The INOVATE-HF Trial. *J Am Coll Cardiol*. 2016;68:149-158.

176. De Ferrari GM, Stolen C, Tuinenburg AE, Wright DJ, Brugada J, Butter C, Klein H, Neuzil P, Botman C, Castel MA, et al. Long-term vagal stimulation for heart failure: Eighteen month results from the NEural Cardiac TherApy foR Heart Failure (NECTAR-HF) trial. *Int J Cardiol*. 2017;244:229-234.

177. De Ferrari GM, Crijns HJ, Borggrefe M, Milasinovic G, Smid J, Zabel M, Gavazzi A, Sanzo A, Dennert R, Kuschyk J, et al. Chronic vagus nerve stimulation: a new and promising therapeutic approach for chronic heart failure. *Eur Heart J*. 2011;32:847-855.

178. Premchand RK, Sharma K, Mittal S, Monteiro R, Dixit S, Libbus I, DiCarlo LA, Ardell JL, Rector TS, Amurthur B, et al. Autonomic Regulation Therapy via Left or Right Cervical Vagus Nerve Stimulation in Patients with Chronic Heart Failure: Results of the ANTHEM-HF Trial. *J Card Fail*. 2014;20:808-816.

179. Anand IS, Konstam MA, Klein HU, Mann DL, Ardell JL, Gregory DD, Massaro JM, Libbus I, DiCarlo LA, Udelson JJE, et al. Comparison of symptomatic and functional responses to vagus nerve stimulation in ANTHEM-HF, INOVATE-HF, and NECTAR-HF. *ESC Heart Fail*. 2020;7:75-83.

180. Konstam MA, Udelson JE, Butler J, Klein HU, Parker JD, Teerlink JR, Wedge PM, Saville BR, Ardell JL, Libbus I, et al. Impact of Autonomic Regulation Therapy in Patients with Heart Failure: ANTHEM-HFrEF Pivotal Study Design. *Circ Heart Fail*. 2019;12:e005879.

181. DiCarlo LA, Libbus I, Kumar HU, Mittal S, Premchand RK, Amurthur B, KenKnight BH, Ardell JL, Anand IS. Autonomic regulation therapy to enhance myocardial function in heart failure patients: the ANTHEM-HFpEF study. *ESC Heart Fail*. 2018;5:95-100.

182. Premchand RK, Sharma K, Mittal S, Monteiro R, Dixit S, Libbus I, DiCarlo LA, Ardell JL, Rector TS, Amurthur B, et al. Extended Follow-Up of Patients With Heart Failure Receiving Autonomic Regulation Therapy in the ANTHEM-HF Study. *J Card Fail*. 2016;22:639-642.

183. Zannad F, De Ferrari GM, Tuinenburg AE, Wright D, Brugada J, Butter C, Klein H, Stolen C, Meyer S, Stein KM, et al. Chronic vagal stimulation for the treatment of low ejection fraction heart failure: results of the NEural Cardiac TherApy foR

Heart Failure (NECTAR-HF) randomized controlled trial. *Eur Heart J*. 2015;36:425-433.

184. Anand IS, Konstam MA, Klein HU, Mann DL, Ardell JL, Gregory DD, Massaro JM, Libbus I, DiCarlo LA, Udelson JJE, et al. Comparison of symptomatic and functional responses to vagus nerve stimulation in ANTHEM-HF, INOVATE-HF, and NECTAR-HF. *ESC Heart Fail*. 2020.

185. De Ferrari GM, Dusi V, Spazzolini C, Bos JM, Abrams DJ, Berul CI, Crotti L, Davis AM, Eldar M, Kharlap M, et al. Clinical Management of Catecholaminergic Polymorphic Ventricular Tachycardia: The Role of Left Cardiac Sympathetic Denervation. *Circulation*. 2015;131:2185-2193.

CHAPTER 2

Scalable and reversible axonal neuromodulation of the sympathetic chain for cardiac control

Introduction

Sudden cardiac death (SCD), the leading cause of mortality in the United States, is linked to elevated sympathetic activity acting on abnormal cardiac substrates, leading to increased potential for life-threatening ventricular arrhythmias.[1,2] Maladaptation of the autonomic nervous system has been implicated in various cardiovascular disorders including SCD, congestive heart failure (CHF), and hypertension.[3,4] In both humans and animal models of disease, remodeling of the sympathetic nervous system, including changes in sympathetic nerve density, excitability of the ventricular myocardium, and changes in peripheral ganglia have been described.[5-8] Current medical practice to treat cardiovascular diseases focuses on treating the symptoms associated with the disease process, often with pharmacological agents targeted to end-effectors, device therapy (e.g. pacemakers), surgery or focal ablations.[9] While effective in most cases, some pathologies such as refractory ventricular tachycardia, rely on reactive implantable cardioverter defibrillator (ICD) devices to sustain the patients, treating the symptom, not a root cause of the disease process.[3,9] A number of neuromodulatory approaches have shown efficacy in the management of refractory ventricular tachycardia (VT), although each bears significant limitations.[10,11] While surgical sympathectomy is efficacious, sympathetic denervation is permanent and associated with several side effects including hyperhidrosis and hyperalgesia.[12] Moreover, bilateral therapy, rather than left sided alone, is commonly necessary for improved freedom from ICD-shocks, heart transplantation, or death.[11] Sympathetic blockade using thoracic epidural anesthesia or stellate ganglia block has also been used in the management of VT storm with minimal morbidity, but it is temporary and often a bridge to more definitive therapy.[13,14] Targeted

bioelectric neuromodulation allows for an alternative path for control of sympathetic projections to the heart that is available on-demand and reversible.

Electrical stimulation of peripheral nerves has been a growing avenue to target maladaptive operation of the nervous system, offering non-pharmacological, scalable, reversible, on-demand therapeutic alternatives facilitated by advances in low-power, smart, miniaturized bioelectronic implants.[4,15] Although the use of electrical stimulation is well-recognized and has multiple clinical applications, the use of bioelectronic approaches to selectively block the conduction of action potentials is a more recent discovery.[16-19] This blocking mechanism can be achieved with charge-balanced kilohertz frequency alternating current (KHFAC) with zero net charge delivery, charge balanced direct current carousel (CBDCC), or a hybrid wave form involving both.[20,21] Mechanistically, conduction block mediated through such axonal modulation therapy (AMT) occurs by producing a region whereby action potentials cannot pass, with several studies suggesting a memory effect whereby nerve conduction is depressed for a period of time after current delivery.[19,22,23] In porcine models, we have previously demonstrated short-term efficacy of KHFAC in reducing evoked cardiac sympathetic responses when applied to the paravertebral chain.[24] Importantly, using CBDCC in swine with chronic myocardial infarction, we found that transient nerve block resulted in reduced ventricular arrhythmia inducibility by programmed ventricular stimulation.[25] We, and others, have further identified critical components of the paravertebral chain as primary inputs for afferent and efferent neurotransmission to the heart, including the stellate and proximal thoracic paravertebral ganglia.[26,27]

In the current work, we aimed to characterize KHFAC block and evaluate its efficacy in two sets of mechanistic experiments (Figure 12). First, we studied several features of KHFAC block such as scalability (i.e., relationship between amplitude and block), sustainability/plasticity, and memory (Figure 12B, Protocol 1). We anticipated the presence of a reproducible, dose-response relationship between amplitude and block and the persistence of a partial KHFAC block following cessation of current. Given the increasing clinical relevance of neuromodulation of the bilateral sympathetic chain, in a second set of experiments, we evaluated the efficacy of KHFAC block in the setting of unilateral sympathectomy, and its impact on sympathetic nerve stimulation induced myocardial neurotransmitter release (Figure 12C, Protocol 2). The primary hypothesis is that KHFAC mitigates sympathoexcitation in a scalable fashion and that KHFAC AMT continues to mitigate sympathoexcitation in the setting of unilateral sympathectomy.

Methods

Study Approval

The study protocol was approved by the Institutional Animal Care and Use Committee (IACUC) at the University of California, Los Angeles (Protocol 16-085), and is in accordance with the National Institutes of Health's Guide for the Care and Use of Laboratory Animals. At the end of experiments, animals were euthanized in concordance with IACUC guidelines.

Surgical Preparation

A total of 14 Yorkshire pigs (*Sus scrofa*, S&S Farms, California) of both sexes (9 males and 5 females), aged 3 ± 1 months, weighing 36 ± 3 kg, were used for these studies (Figure 12A). Animals were housed using standard 12-hour light and 12-hour dark cycles; pigs were fasted overnight except for water prior to experiments.

Yorkshire pigs were sedated with tiletamine-zolazepam (5-6 mg/kg, intramuscular) and isoflurane (3-5%, inhaled). Following endotracheal intubation, animals were mechanically ventilated (tidal volume 300-450mL, rate 10-12 breaths per minute) and anesthesia maintained with isoflurane (1-4%, inhaled). Fentanyl (20-30 μg/kg) was administered for analgesia during surgical preparation. The femoral arteries and veins were cannulated using the modified Seldinger technique, and carotid artery cannulated directly through surgical cutdown, and vascular access sheaths placed. Systemic arterial blood pressure was monitored through the side-port of a sheath in the femoral artery, and normal saline (4-6 mL/kg/hr) was infused through the femoral vein to replenish insensible fluid losses. Temperature was monitored (rectal or esophageal), and maintained through forced-air warming blankets. Three-lead electrocardiogram and end-tidal carbon dioxide were used to ensure acceptable physiologic status for experiments. Arterial blood gas contents were assessed on an hourly basis and adjustments to tidal volume, rate, fraction of inspired oxygen, or administration of sodium bicarbonate were performed as appropriate to maintain physiologic levels.

A median sternotomy was performed and the bilateral pleural cavities were entered. The parietal pleura was divided posteriorly, and the right and left paravertebral chain from the stellate (cervicothoracic) ganglia to T3 ganglia were exposed. The pericardium was opened and pericardial cradle created to support the heart. For studies

examining catecholamine release, a catheter was advanced into the coronary sinus via the right external jugular vein for blood sampling. Following completion of surgical preparation, anesthesia was transitioned from isoflurane to alpha-chloralose (50 mg/kg over 1 hour, followed by 25-50 mg/kg/h; intravenous) to minimize the cardio-depressive effects of inhaled anesthetics. For Protocol 1, pre-treatment with atropine (1 mg/kg intravenous) or bilateral vagus nerve transection was performed to remove competing effects of parasympathetic efferent responses. Surgical preparation time ranged from 2 to 4 hours, and total duration of anesthesia ranged from 8 to 12 hours. Pigs were allowed to stabilize for 30 minutes after completion of alpha-chloralose bolus and maintenance of stable infusion before experimental protocols were initiated.

Hemodynamic and Electrophysiologic Measurements

A solid-state pressure catheter (Mikro-Tip Model SPR-350, Millar Instruments, Houston, Texas) was guided to the left ventricle through the femoral or carotid artery, and used to continuously measure left ventricular pressure, rate of change of left ventricular pressure (LV dP/dt), and heart rate (HR). These data, as well as a lead II electrocardiogram, were acquired through a Cambridge Electronics Design (Cambridge, United Kingdom) acquisition system and computed using Cambridge Electronics Design Spike2 Data Acquisition & Analysis Package (Cambridge, United Kingdom).

For the first set of experiments (Figure 12B, Protocol 1), electrophysiologic data was acquired using a custom 56-electrode epicardial sock placed over the right and left ventricles. Unipolar local electrograms were recorded at 1000Hz using a Prucka CardioLab Acquisition System (GE Healthcare, Fairfield, Connecticut). For the second set of experiments (Figure 12C, Protocol 2), high-density electrophysiologic recordings

were acquired using a custom 128-electrode epicardial array (NeuroNexus, Ann Arbor, Michigan) placed over the anterior left ventricle, with sampling rate at 1360Hz through an AlphaLab SnR acquisition system (Alpha Omega, Alpharetta, Georgia). For both approaches, data were analyzed using ScalDyn 5 (University of Utah, Salt Lake City, Utah). Activation recovery intervals (ARI) were calculated on a beat-by-beat basis by subtracting activation time (the time of minimum dV/dt during depolarization) from recovery time (the time of maximum dV/dt during repolarization) as previously described.[24,25] ARI serves as a strong surrogate of ventricular action potential duration at 90% repolarization.[28]

Assessment of Myocardial and Systemic Catecholamine Levels

Myocardial interstitial catecholamine levels were assessed using fast scanning cyclic voltammetry (FSCV), an electrochemical approach that leverages detection of oxidation and reduction of norepinephrine (NE) through a small-diameter platinum electrode under voltage clamp, as previously described.[29] Briefly, perfluoroalkoxy coated platinum wires were prepared by soldering an approximately 5mm portion of bare wire to a gold-plated pin connector. Following completion of surgical preparation, six to eight probes were placed directly into the anterior left ventricular myocardium through 23-gauge needles. Ground and reference electrodes were placed into the intercostal muscle. Probes were connected to a custom amplifier (NPI Electronics, Tamm, Germany); data were acquired and analyzed for mean relative myocardial NE levels using Igor Pro 7.08 (WaveMetrics, Lake Oswego, Oregon) as previously described.[29]

Blood from the coronary sinus and femoral artery were collected prior to nerve stimulation and at peak-nerve stimulation effect to measure plasma NE concentrations

in the intact state. Blood samples were collected in EDTA collection tubes (Becton, Dickinson and Company, Franklin Lakes, New Jersey), followed by centrifugation for 15 minutes at 1500 *g* for separation of plasma. Plasma was snap frozen in liquid nitrogen and stored at -80 °C. Enzyme-linked immunosorbent assay was used to assay plasma NE levels following the manufacturer's instructions (Rocky Mountain Diagnostics, Colorado Springs, Colorado).

Instrumentation and Implementation of KHFAC Block

Separate platinum bipolar electrodes were placed around the right T1-T2 paravertebral chain and right T2-T3 paravertebral chain. When this configuration was not anatomically possible (n=6, Protocol 1), one set of electrodes was placed above the right stellate ganglia (a fusion of the inferior cervical ganglia and T1) and the second at T1-T2. The proximal electrode was connected to a voltage-controlled, constant-current waveform function generator (Stanford Research Systems, Sunnyvale, California) with a capacitor (2.2 μF) in series to prevent application of direct current, and used for KHFAC block. For Protocol 1, KHFAC block was performed at varying frequency and current (15-30kHz, 2-20mA peak to peak) and for Protocol 2 at fixed parameters: 15kHz and 15mA peak to peak. The distal set of electrodes was used for right sympathetic stimulation (RSS) using a Grass S88 stimulator, interfaced through a PSIU6 constant current photoelectric stimulus isolation unit (Grass Instruments, Warwick, Rhode Island). RSS was selected as it would also allow for completion of left sympathectomy for Protocol 2 without disruption of electrodes. RSS was performed using 4ms square pulse waves at 4Hz, as these settings produce moderate increases in cardiac indices. For Protocol 1, current was titrated to identify a stimulus threshold that resulted in a 20% increase in heart rate,

and subsequent stimulations were performed at 2 times threshold for 30-second periods. For Protocol 2, threshold was set at 10% increase in heart rate, with subsequent stimulations performed at 1.5 times threshold for 30-second periods.

Study Protocols

Protocol 1 (Figure 12B) included assessment of scalability, plasticity, and memory. For scalability studies, KHFAC was applied at a variety of currents (2-20mA, randomized sweep) at a fixed frequency for each animal (15-30kHz) dependent on the electrode-nerve interface. The initial frequency tested for each animal was 30kHz. If 30kHz did not produce a reduction in RSS-evoked responses, 20kHz was assessed, followed by 15kHz. To allow for return of hemodynamic and electrophysiologic parameters to baseline, there was a minimum waiting period of 5 minutes between assessments. For plasticity assessments, KHFAC was applied for 20 minutes at the previously identified optimal blocking frequency and current amplitude for each animal. RSS was performed prior to KHFAC, and repeated at 1 minute, 10 minutes, and 20 minutes after initiation of KHFAC. For memory assessments, RSS was repeated at 5, 10, and 20 minutes after cessation of KHFAC, or until baseline RSS-evoked response returned. For each stimulation, comparisons were made between RSS-evoked changes with application of KHFAC, relative to RSS-evoked changes in the absence of KHFAC, to calculate a percentage block in terms of cardiac indices HR, LV dP/dt_{max}, and ARI. Onset response duration and amplitude were simultaneously evaluated with scalability studies, and similarly quantified as duration and percentage evoked change in cardiac indices.

Protocol 2 (Figure 12C) utilized a fixed KHFAC frequency (15kHz) across all animals to evaluate KHFAC in the setting of an intact cardiac neuraxis and after

sympathectomy. RSS was performed in the absence of KHFAC, followed by application of KHFAC to produce a stable block, and 30 seconds of RSS to evaluate evoked changes in the presence of KHFAC. To confirm restoration of RSS-evoked changes, RSS was repeated after cessation of KHFAC. Assessments were spaced by a minimum of 10 minutes to allow cardiac indices and catecholamines to return to baseline. Following assessment of KHFAC in the intact state, the left paravertebral chain was excised (stellate to T3 ganglia) and assessment repeated. The right paravertebral chain was subsequently excised (stellate to T3 ganglia), stimulating electrodes placed directly caudal to the excised T3 ganglia on the paravertebral chain, and assessment repeated.

Statistics

For both sets of studies, HR, LVP, LV dP/dt_{max}, and global ventricular ARI were assessed at baseline, during RSS in the absence of KHFAC, and during RSS with KHFAC applied. Percent block of sympathetic response was calculated by dividing the difference of RSS-evoked changes without KHFAC and RSS-evoked changes with KHFAC, by RSS-evoked changes with KHFAC, multiplied by 100. Normalization was performed due to variation in physiologic parameters across animals and during the course of an experiment. Statistical analysis was performed using Prism 9 (GraphPad Software, San Diego, California). Normality was assessed using the Shapiro-Wilk test. For normally distributed data, 1-way repeated analysis of variance and Fisher's least significant difference test were used to compare evoked changes in cardiac indices with and without KHFAC block. For non-normally distributed data, Friedman test and Dunn’s test were used. Data are presented as mean with standard error. Effect size was assessed using Cohen’s *d*, with $d > 0.8$, $d > 0.5$, and $d > 0.2$ suggesting strong,

moderate, and weak effect sizes, respectively.[30] Pearson correlation coefficients, *r*, with 95% confidence intervals (CI) were calculated to examine correlation between block parameters and evoked changes in cardiac indices. Statistical significance was set at $p < 0.05$.

Results

KHFAC Block Reduces Sympathetic Stimulation Evoked Hemodynamic Changes

To characterize the effect of preemptive KHFAC block on evoked sympathetic responses, we performed RSS at baseline, and with a preemptive KHFAC block. A representative set of stimulations in the presence and absence of KHFAC is depicted in Figure 13A. Isolated RSS resulted in an increase in HR, LV dP/dt_{max}, and left ventricular systolic pressure. With application of preemptive KHFAC block, RSS-evoked increases in HR, LV dP/dt_{max}, and left ventricular systolic pressure were mitigated, corresponding to an 89% block for HR and 75% block for LV dP/dt_{max}. Notably, within 5 minutes of cessation of block, RSS-evoked changes were restored similar to baseline. Axonal block induced by KHFAC application was evident across all animals at varying current levels (Figure 14A). Comparison of RSS-evoked hemodynamic responses prior to KHFAC block and following cessation of block demonstrated no significant difference in evoked changes in heart rate or dP/dt_{max} in both the intact state and following left sympathectomy, indicating restored nerve conduction and lack of physiologic injury (Figure 13B-C).

KHFAC is Scalable across Cardiac Mechanical and Electrical Indices

Across a total of six animals, KHFAC current amplitude was varied from 2mA to 20mA at a set frequency to study the relationship between block amplitude and efficacy. For each animal studied, increasing KHFAC current resulted in a greater block of RSS-induced increases in HR (Figure 14A) and LV dP/dt_{max} (Figure 14B). Likewise, mitigation of RSS-induced shortening of ventricular activation recovery intervals (ARI, a surrogate for action potential duration) was more pronounced at greater KHFAC currents (Figure 14C). We found strong correlation between current amplitude and mean response for HR (r=0.94, 95% CI 0.84-0.98, p<0.001), LV dP/dt_{max} (0.96, 95% CI 0.89-0.98, p<0.001), and ventricular ARI (0.83, 95% CI 0.60-0.93, p<0.001). When examined at the animal level, which accounts for the unique electrode-nerve interface for each subject, strong correlations between block of cardiac indices and current amplitude were evident (Table 1).

With most block parameters, KHFAC resulted in a self-limited onset response for both HR and LV dP/dt_{max}. Onset responses were of low magnitude (28.0% for HR and 34.4% for LV dP/dt_{max}), and lasted a mean of 32.0±5.0 seconds and 71.3±6.6 seconds for HR and LV dP/dt_{max} respectively (Table 2), although variability was observed.

KHFAC is Efficacious over Time with a Short and Limited Memory Period

We examined the plasticity of KHFAC in mitigating RSS-evoked changes by applying a long term (20 minute) block and superimposing RSS stimulation at fixed time periods (1, 10, and 20 minutes). Most animals displayed similar block efficacy at each time point studied, although the block efficacy ranged for each animal (Figure 15). We found a similar temporal relationship for block efficacy across the three studied cardiac indices: HR, LV dP/dt_{max}, and ARI. We further examined whether a memory response persisted

following KHFAC block by applying intermittent RSS at fixed time periods after cessation of block. The majority of animals had restored evoked changes within five minutes of cessation of block, while a residual block was evident in a limited number (3) of animals for 20 minutes after block (Figure 15).

KHFAC Block Reduces Sympathoactivation in Setting of Unilateral Sympathectomy (Stellate to T3 Ganglia)

To study the utility of KHFAC in the setting of graded sympathectomy, RSS was performed with and without KHFAC block, prior to left sympathectomy, following left sympathectomy, and following bilateral sympathectomy. Sympathectomy was performed targeting the primary cardiac input to the heart, with excision from the stellate ganglia to the T3 ganglia, and placement of stimulating electrodes directly below the excised T3 ganglia on the right paravertebral chain.[26] Given the relevance of NE as a mediator of sympathoexcitation and its role in SCD, we also measured interstitial catecholamines using fast scanning cyclic voltammetry (FSCV) and trans-cardiac NE release profiles using concurrent coronary sinus and systemic arterial blood sampling. Figure 16 illustrates representative changes in hemodynamics and continuous myocardial catecholamines during RSS without (panel A) and with (panel B) preemptive KHFAC block. At these parameters, a minimal onset response was evident, with subsequent reduction in evoked changes in heart rate and contractility, and with a corresponding KHFAC mitigation of NE release during RSS.

Figures 6 and 7 summarize changes in cardiac indices and corresponding NE release profiles to RSS as mitigated by preemptive KHFAC in intact versus decentralized states across 5 animals. In the intact state, RSS resulted in a 22.9% ±

3.6% increase in HR, which was reduced by preemptive KHFAC block (8.7% ± 4.4%, p=0.046, *d*=1.9, strong effect size, Figure 17A). Following left sympathectomy, RSS similarly increased HR (27.4% ± 5.4%), which was mitigated by preemptive application of KHFAC block (12.0% ± 4.1%, p=0.0455, *d*=1.9, strong effect size). Similarly, KHFAC block mitigated RSS-evoked increases in dP/dt_{max} from 70.7% ± 7.7% to 26.0% ± 10.5% (p=0.004, *d*=2.7, strong effect size, Figure 17B) in the intact state and following left sympathectomy (86.1% ± 21.8% vs 26.0% ± 9.9%, p<0.001, *d*=0.5, moderate effect size). Following bilateral sympathectomy, T3 stimulation had no significant impact on dP/dt_{max} (-0.1% ± 1.0%). Non-normalized and absolute changes are also presented in Table 3 with consistent findings.

Consistent with hemodynamic findings, RSS shortened ventricular ARI by 72.3ms ± 7.0ms, which was mitigated by preemptive KHFAC block (-6.6ms ± 5.5ms, p=0.001, *d*=5.7, strong effect size, Figure 17C). Following left sympathectomy, RSS continued to shorten ventricular ARI, which was similarly mitigated by application of KHFAC (-69.1ms ± 3.9ms vs -20.4ms ± 10.2ms, p=0.039, *d*=1.9, strong effect size). After bilateral sympathectomy, T3 stimulation evoked no significant changes in ventricular ARI (∆ARI 4.8ms ± 2.9ms).

Local myocardial catecholamine levels in the left ventricle, assessed using FSCV, increased by 55.8nM ± 14.6nM from baseline with RSS, which was reduced by preemptive KHFAC block (1.0nM ± 3.8nM, p=0.030, *d*=2.8, strong effect size, Figure 18A). Similar findings were evident following left sympathectomy (43.2nM ± 10.2nM vs 4.3nM ± 5.4nM, p=0.016, *d*=2.6, strong effect size), suggesting efficacy of KHFAC following left sympathectomy. After removal of bilateral sympathetic chains, T3

stimulation led to no significant change in myocardial NE compared to baseline (ΔNE=0.3nM ± 0.9nM), consistent with hemodynamic and electrophysiologic findings. Consistent with changes in hemodynamics and ARI, KHFAC induced a transient, low-level release of myocardial NE in the intact state and following left sympathectomy, which was transient and lower in magnitude compared to RSS alone (Table 4). Coronary sinus NE content increased from baseline with RSS (*d*=2.8, strong effect size), but was unchanged from baseline when preemptive KHFAC was applied (Figure 18B), while systemic NE levels unchanged (arterial NE, *d*=0.2, weak effect size, Figure 18C).

Discussion

In the present study, we build upon prior proof-of-concept work and assessed several important properties of KHFAC block when applied to the paravertebral chain.[24,25] We found that KHFAC can reproducibly induce high degrees of sympathetic efferent block following a scalable dose-response. Intermediate-duration KHFAC produced a short-lived memory effect, whereby conduction block persisted for a brief period of time following cessation of block. Importantly, KHFAC remained efficacious in the setting of unilateral sympathectomy and directly reduced myocardial catecholamine levels and their end effect on the heart.

Prior studies have examined KHFAC in the vagus nerve, peripheral nerves, and spinal cord to generate a reproducible conduction block.[22,31-33] Notably, a recent study demonstrated the feasibility of KHFAC in blocking chemo-afferent mediated signals

through the carotid sinus nerve in a porcine model.[34] Our prior work demonstrated proof-of-concept of KHFAC in the paravertebral chain, with reduction of sympathetic stimulation evoked changes with KHFAC.[24] In the present work, we provide data supporting the short-term scalability of KHFAC at a fixed frequency with increasing current. While animal-to-animal variability between electrode and cardio-neural interface was evident, a linear relationship between current and efficacy was present. We further found evidence of short-term memory in subset of animals, such that reduction of efferent evoked responses persisted for 5 to 20 minutes beyond termination of KHFAC, consistent with studies in peripheral nerves.[35] These findings suggest that a transient period of block may induce reorganization and adaptation within the nervous system, perhaps by altering neuronal recruitment within a network, leading to memory. This mirrors evidence from spinal cord stimulation (SCS) in the setting of myocardial ischemia, whereby SCS-mediated suppression of intrinsic cardiac neuronal activity lasted for a period of at least 20 minutes after cessation of transient SCS and coronary artery occlusion.[36] Although KHFAC was effective in mitigating sympathoexcitation, transient onset responses to KHFAC were present. These may be mitigated by application of a combined direct current and KHFAC block, which has been efficacious in motor neurons.[21] Importantly, as this study focused on short-term evaluation of KHFAC under anesthesia, studies examining the effects of KHFAC in healthy animals and models of chronic disease are necessary to define therapeutic potential, the presence of tolerance, and the presence of long-term memory. In a rat model of early type 2 diabetes mellitus, chronic KHFAC targeted at the carotid sinus nerve improved insulin sensitivity and glucose tolerance over a 9 week period compared to sham,

suggesting feasibility of chronic nerve block technology in the conscious state.[37] Nonetheless, further preclinical studies of KHFAC block properties, as well as an improved understanding of the cardiac neuraxis, is necessary to augment the translation of bioelectric therapies.

Although mechanisms of KHFAC are incompletely understood, its effects have been attributed to a regional block of conduction.[19,22] Consistent with this notion, we found significant reductions in RSS-induced changes in various cardiac indices after application of KHFAC as compared to the basal state. These findings are best explained by block of efferent sympathetic fibers. As the heart has significant overlap between innervation patterns derived from the right and left paravertebral chain, evidenced through functional and histologic studies[3,38,39], we further evaluated the efficacy of KHFAC after partial cardiac denervation. These innervation patterns are clinically relevant as left and bilateral cardiac sympathetic denervation, a form of permanent neuromodulation, has been increasingly adopted for refractory VT.[9] After removal of clinically-relevant portions of the left paravertebral chain, we found persistent RSS-induced chronotropic and inotropic effects, which were mitigated by KHFAC, simulating a transient and reversible state of bilateral sympathectomy. Importantly, we found that these physiologic changes at the end-organ level are mirrored by reductions in local catecholamine release, confirming that at least one putative mechanism of KHFAC results in blunted neurotransmitter release at the end-organ.

This study has several limitations inherent to its design, as experiments were performed under general anesthesia in the absence of structural heart disease. For the first set of studies, atropine was administered to mitigate competing autonomic input

and allow for focused study of efferent activity. The second set of studies was conducted without denervation or pharmacological blockade with complementary findings, demonstrating the feasibility of KHFAC in a mixed neural population. Further study of KHFAC onset properties and approaches to mitigate onset responses will facilitate more effective nerve block and clinical translation. Moreover, due to the anesthetized preparation, studies were limited to relatively short-term assessments of KHFAC, and data regarding memory beyond 10 minutes were limited to less than 50% of the sample. A sham KHFAC group was not included in the present study, and it is possible that spontaneous responses to nerve stimulation decreased over time. In the absence of structural heart disease and presence of general anesthesia, our animals had low sympathetic tone and low baseline levels of catecholamines; as such, we tested sympathetic block in response to electrical stimulation of the sympathetic chain, rather than spontaneous sympathoexcitation. Further work to evaluate KHFAC, and other nerve block technologies, in response to spontaneous sympathoexcitation is warranted. As one potential application of KHFAC is a reactionary mode in response to a perceived cardioneural stressor, future efforts will focus on a closed loop system whereby KHFAC is applied in response to a sensed stressor. In addition, studies in ambulatory healthy and chronic heart failure or myocardial infarction models using implantable devices will shed light on optimal parameters and long-term effects of KHFAC, particularly plasticity and memory. This study serves as a logical first-step prior to application of KHFAC in disease models, and will guide further iterative work.

Autonomic neuromodulation for cardiovascular disease is a rapidly evolving field with substantial growth in the last decade. Restoration of parasympathetic function in

disease states has been emphasized through several trials evaluating cervical vagal nerve stimulation, using implantable pulse generators, for congestive heart failure, demonstrating an improvement in ventricular function and quality of life.[40-42] Excess sympathoexcitation in the setting of myocardial infarction and refractory ventricular arrythmias has been clinically treated using reversible and irreversible approaches targeting the paravertebral chain, as well as with catheter-based approaches to renal denervation.[9,10] Cardiac sympathetic denervation, a procedure that entails resection of the lower third of the stellate (cervicothoracic) ganglia through T4 of the paravertebral chain, has been increasingly utilized for the management of VT.[10,11] While initial studies focused on left sided cardiac sympathetic denervation, recent retrospective data suggests greater shock-free survival with bilateral denervation for those with refractory VT or VT storm.[11,43] An alternative, bioelectronic based approach that may produce similar changes to sympathectomy is blockade of axonal conduction using KHFAC or alternate technologies. These approaches my function in a closed-loop system whereby a biological parameter would be detected, and therapy delivered using an implantable pulse generator, or in an open-loop system utilizing intermittent block with duty cycles as is performed with chronic vagus nerve stimulation in humans. Such an approach may complement existing therapies, including left sympathectomy, for which proof-of-concept is demonstrated in this study. With further maturation of the field of neuromodulation, an on-demand, reactionary system that provides reversible axonal modulation may be an avenue for therapeutic development.

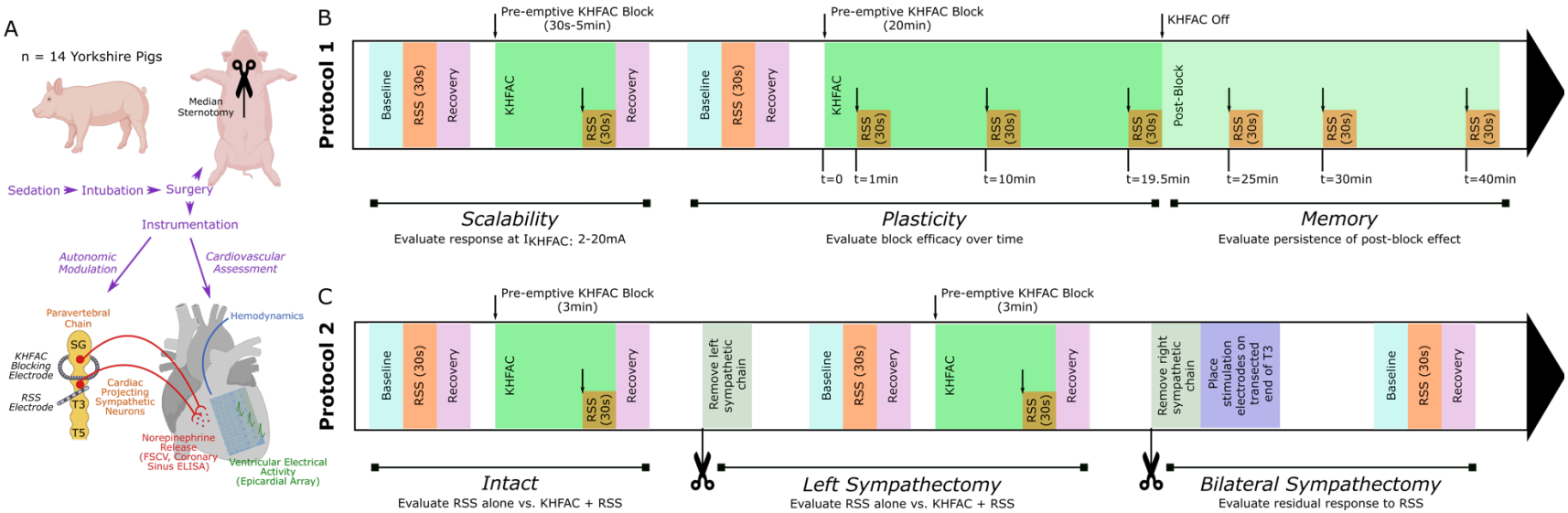
A
n = 14 Yorkshire Pigs
Median Sternotomy
Sedation
Intubation
Surgery
Instrumentation
Autonomic Modulation
Cardiovascular Assessment
Paravertebral Chain
SG
T3
T5
KHFAC Blocking Electrode
RSS Electrode
Cardiac Projecting Sympathetic Neurons
Hemodynamics
Norepinephrine Release (FSCV, Coronary Sinus ELISA)
Ventricular Electrical Activity (Epicardial Array)
B
Protocol 1
Pre-emptive KHFAC Block (30s-5min)
Pre-emptive KHFAC Block (20min)
KHFAC Off
Baseline
RSS (30s)
Recovery
KHFAC
Post-Block
t=0
t=1min
t=10min
t=19.5min
t=25min
t=30min
t=40min
Scalability
Evaluate response at I_KHFAC: 2-20mA
Plasticity
Evaluate block efficacy over time
Memory
Evaluate persistence of post-block effect
C
Protocol 2
Pre-emptive KHFAC Block (3min)
Remove left sympathetic chain
Remove right sympathetic chain
Place stimulation electrodes on transected end of T3
Intact
Evaluate RSS alone vs. KHFAC + RSS
Left Sympathectomy
Evaluate RSS alone vs. KHFAC + RSS
Bilateral Sympathectomy
Evaluate residual response to RSS

Figure 12. Study design and methods. (A) Schematic of autonomic modulation using KHFAC targeted at the right paravertebral chain. KHFAC was applied at the right proximal paravertebral chain to block activation of cardiac-projecting sympathetic neurons, and the right sympathetic chain was stimulated distally using bipolar stimulating electrodes. Cardiac mechanical function, regional cardiac electrical activity, and catecholamine release were evaluated in response to activation of the sympathetic chain using the stimulating electrode, and, subsequently, during combined KHFAC block and sympathetic chain stimulation. (B) Protocol 1 evaluated scalability of KHFAC by applying KHFAC at varying currents (2-20mA) during a short KHFAC block. Subsequently, plasticity and memory were evaluated using a 20-minute KHFAC block with intermittent RSS. (C) Protocol 2 evaluated the impact of KHFAC in the intact state and following left and bilateral sympathectomy. FSCV, fast scanning cyclic voltammetry; ELISA, enzyme-linked immunosorbent assay; KHFAC, kilohertz frequency alternating current; RSS, right sympathetic chain stimulation; SG, stellate ganglia; T3 and T5, third and fifth sympathetic chain ganglia.

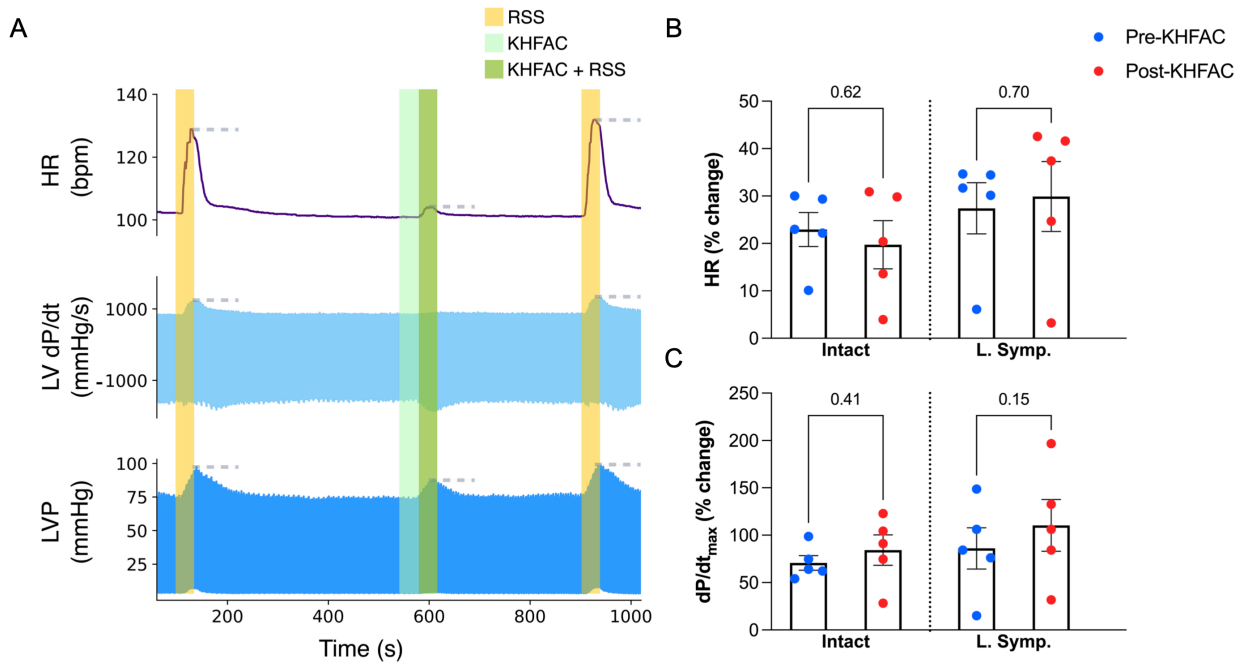

Figure 13. Fully reversible KHFAC block reduces sympathetic stimulation-evoked hemodynamic changes. (A) The first stimulation demonstrates baseline responses to RSS, with significant increases in HR, LV dP/dt_{max} (contractility), and LVP. The second stimulation demonstrates mitigation of these sympathetically-induced responses with low-intensity preemptive KHFAC block. Note that these responses were readily reversible following cessation of KHFAC block and repeat RSS. (B, C) In both the intact state and following left sympathectomy, no significant difference between evoked responses prior to and following cessation of KHFAC, indicating restored conduction. n=5 animals; HR and LV dP/dt_{max} evaluated with 1-way repeated analysis of variance and Fisher's least significant difference test. HR, heart rate; KHFAC, kilohertz frequency alternating current; L. Symp., left sympathectomy; LV dP/dt, rate of change of left ventricular pressure; LV dP/dt_{max}, maximum rate of change of left ventricular pressure; LVP, left ventricular pressure; RSS, right sympathetic chain stimulation.

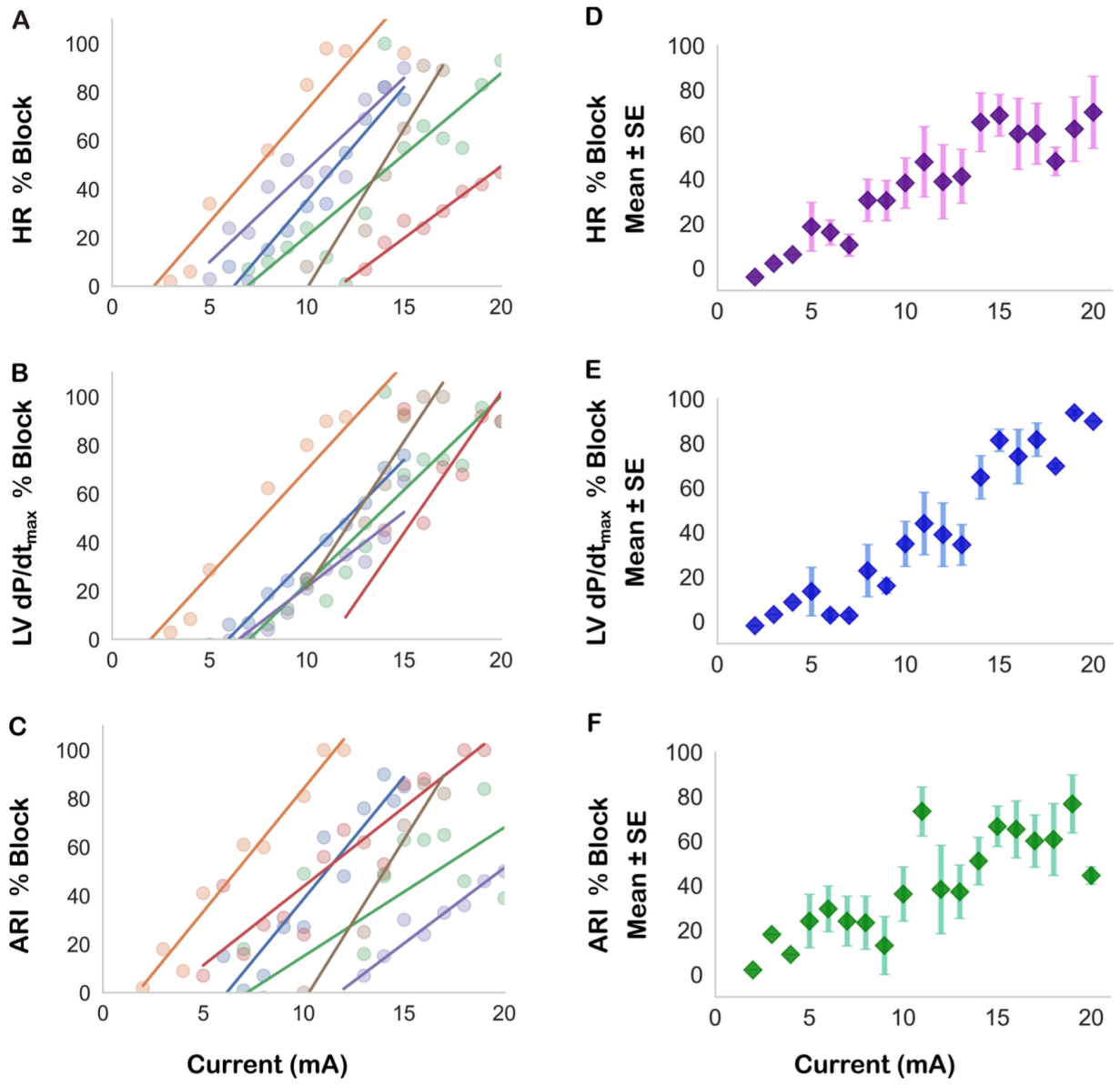

Figure 14. Scalability and efficacy of KHFAC block. KHFAC mitigated RSS-induced increases in HR, LV dP/dt_{max}, and shortening of ARI. The left panels (A-C) demonstrate current-block relationships plotted individually for each animal in a separate color, and are summarized on the right (D-F) as mean and standard error of the mean of n=6 animals. For each cardiac index, a clear, positive correlation between current amplitude and block efficacy was evident. ARI, activation recovery interval; HR, heart rate;

KHFAC, kilohertz frequency alternating current; LV dP/dt_{max}, maximum rate of change of left ventricular pressure; LVP, left ventricular pressure; RSS, right sympathetic chain stimulation.

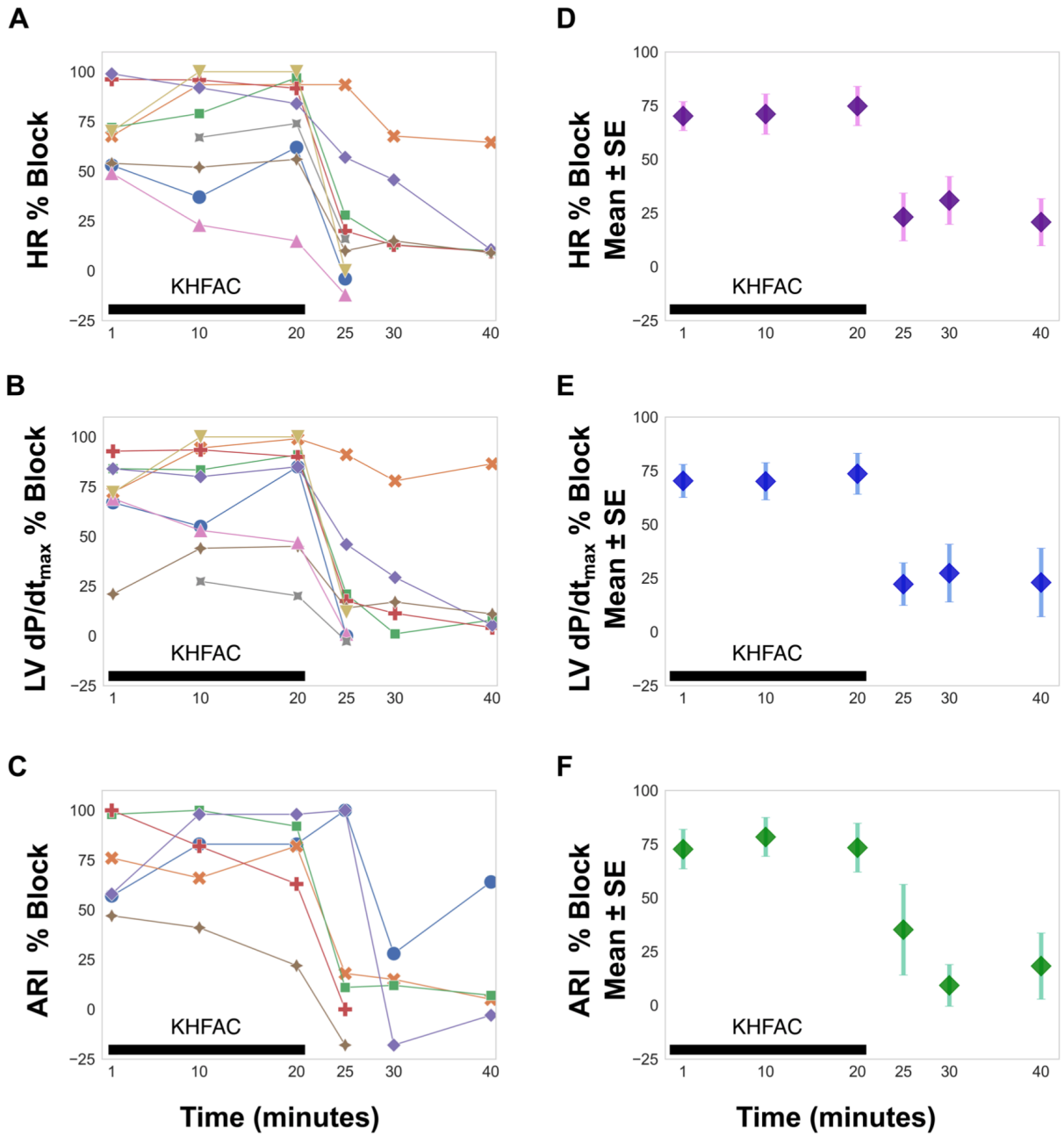

Figure 15. Evaluation of plasticity and memory properties. KHFAC-mitigation of changes in HR, LV dP/dt_{max}, and ventricular ARI were studied at six time points. The left panels (A-C) report responses for each animal, which are summarized on the right (D-F) as mean and standard error of the mean. RSS was performed at 1, 10, and 20 minutes of KHFAC block, and block efficacy for HR, LV dp/dt_{max}, and ARI were assessed,

whereby a block efficacy of 100% indicates complete block and 0% indicates an ineffective block. Block efficacy was comparable at 1, 10, and 20 minutes of KHFAC block. For some animals, RSS following cessation of KHFAC produced a brief memory response at 5, 10, and 20 minutes post-block, whereby sympathetic-stimulation induced changes were temporarily blunted. Note that for the majority of animals, responses were restored to near baseline evoked-changes within 10 minutes of cessation of block. n=9 animals for HR and LV dP/dt_{max}, n=6 animals for ARI. ARI, activation recovery interval; HR, heart rate; KHFAC, kilohertz frequency alternating current; LV dP/dt_{max}, maximum rate of change of left ventricular pressure; LVP, left ventricular pressure; RSS, right sympathetic chain stimulation.

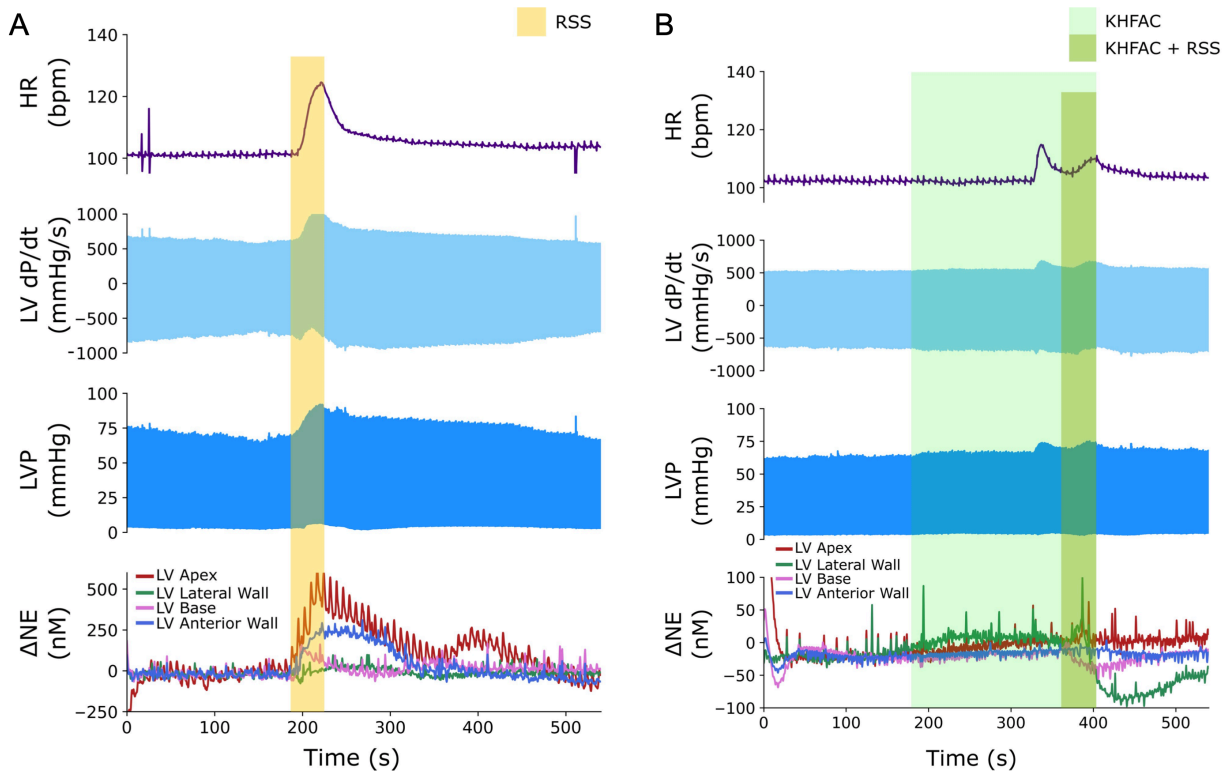

Figure 16. KHFAC blocks catecholamine release in the myocardium. In the intact state, substantial increases in cardiovascular indices in response to 30 seconds of RSS were evident, with significant increases in norepinephrine levels detected by fast scanning cyclic voltammetry (A). These responses were reduced with preemptive application of KHFAC block prior to RSS (B); a delayed onset response was noted with this stimulation. HR, heart rate; KHFAC, kilohertz frequency alternating current; LV, left ventricle; LV dP/dt, rate of change of left ventricular pressure; LVP, left ventricular pressure; NE, norepinephrine; RSS, right sympathetic chain stimulation.

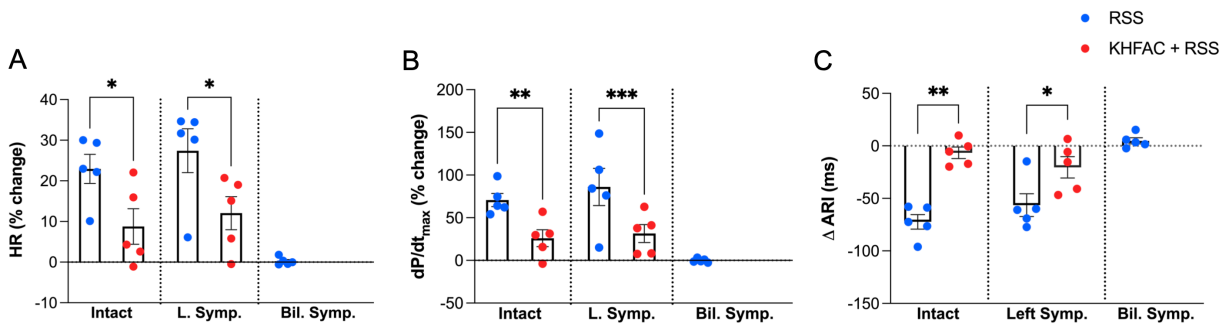

Figure 17. KHFAC mitigates sympathetic stimulation-induced changes in hemodynamic and electrophysiologic parameters. RSS produced significant increases in HR (A) and LV dP/dt_{max} (B) with shortening of ventricular ARI (C) when applied in the intact state. These changes were significantly reduced with application of preemptive KHFAC prior to RSS. Similar findings were noted following left sympathectomy (middle). Notably, after bilateral sympathectomy and stimulation of distal end of T3, no significant changes in HR, LV dP/dt_{max}, or ARI from baseline were noted. n=5 animals; HR evaluated with Friedman and Dunn's tests, and LV dP/dt_{max} and ARI with 1-way repeated analysis of variance and Fisher's least significant difference test. LV dP/dt_{max}, maximum rate of change of left ventricular pressure; L. Symp., left sympathectomy; RSS, right sympathetic chain stimulation. *p<0.05, **p<0.01, *** p<0.001.

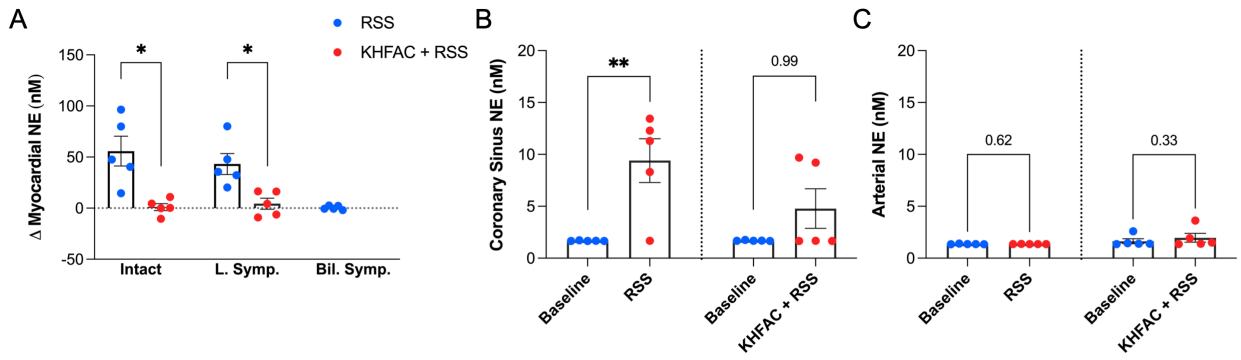

Figure 18. KHFAC mitigates sympathetic stimulation-induced increases in myocardial NE. (A) RSS produced significant increases in intramyocardial NE release in the intact state and following left sympathectomy. With application of KHFAC, RSS-evoked increases in NE were significantly reduced. Note that following bilateral sympathectomy, stimulation of the distal end of T3 produced minimal changes in NE. Coronary sinus NE content (B) increased during RSS from baseline, but was unchanged with preemptive KHFAC. Note that systemic (arterial) NE levels remained unchanged during RSS (C), indicating cardiac projecting neurons as the primary source of NE. Baseline plasma samples were at the lower limit of detection of the assay for CS and arterial plasma evaluations. n=5 animals; arterial and CS NE evaluated with Friedman and Dunn's tests, and myocardial NE with 1-way repeated analysis of variance and Fisher's least significant difference test. Bil. Symp., bilateral sympathectomy; KHFAC, kilohertz frequency alternating current; L. Symp., left sympathectomy; NE, norepinephrine; RSS, right sympathetic chain stimulation; *p<0.05.

Subject	HR	LV dP/dt_{max}	ARI
1	0.97 (0.89-0.99)‡	0.99 (0.94-0.99)‡	0.94 (0.76-0.99)‡
2	0.96 (0.82-0.99)‡	0.97 (0.84-0.99)‡	0.98 (0.91-0.99)‡
3	0.83 (0.53-0.94)‡	0.90 (0.71-0.97)‡	0.68 (0.21-0.90)*
4	0.97 (0.87-0.99)‡	0.82 (0.34-0.96)†	0.93 (0.78-0.98)‡
5	0.94 (0.79-0.99)‡	0.96 (0.85-0.99)‡	0.97 (0.87-0.99)‡
6	0.95 (0.63-0.99)†	0.97 (0.72-0.99)†	0.97 (0.75-0.99)†

Table 1. Correlation between current amplitude and block efficacy for cardiac indices. Pearson correlation coefficient and 95% confidence interval calculated on a per-animal basis for each variable studied. ARI, activation recovery interval; HR, heart rate; LV dP/dt_{max}, maximum rate of change of left ventricular pressure. *$p<0.05$, †$p<0.01$, ‡$p<0.001$.

Parameter	Onset Magnitude (%)	Time to Onset (s)	Onset Duration (s)
Heart Rate	28.0 ± 12.7	9.7 ± 1.0	32.0 ± 5.0
LV dP/dt_{max}	34.4 ± 9.1	9.9 ± 1.2	71.3 ± 6.6

Table 2. Transient onset response properties with kilohertz frequency alternating current. Heart rate onset magnitude represents percent change from baseline, while time to onset and onset duration represent respective time (seconds). Data reported as mean and standard error for n=6 animals.

		Heart Rate (bpm)	dP/dt_{max} (mmHg/s)	Activation Recovery Interval (ms)
Intact, RSS without KHFAC	Pre	91.4 ± 7.7	1303.3 ± 195.8	360.4 ± 21.9
	RSS	111.6 ± 7.9*	2214.2 ± 335.8*	288.1 ± 18.0*
	Δ	20.2 ± 2.6†	910.9 ± 166.8†	-72.3 ± 7.0†
Intact, KHFAC + RSS	Pre	105.0 ± 6.3	1532.3 ± 264.3	310.5 ± 10.5
	RSS	113.7 ± 6.9	1997.1 ± 445.3	304.0 ± 6.3
	Δ	8.7 ± 4.2†	464.8 ± 210.4†	-6.6 ± 5.5†
L. Symp., RSS without KHFAC	Pre	112.2 ± 5.0	1094.1 ± 76.8	325.7 ± 10.4
	RSS	140.3 ± 6.1*	2170.5 ± 274.9*	256.6 ± 13.3*
	Δ	28.1 ± 5.7	1076.4 ± 270.4†	-69.1 ± 3.9†
L. Symp., KHFAC + RSS	Pre	121.8 ± 7.5	1281.2 ± 164.2	301.1 ± 12.2
	RSS	141.3 ± 10.3	1892.2 ± 298.1	280.7 ± 8.8
	Δ	19.5 ± 7.8	611.0 ± 270.0†	-20.4 ± 10.2†
Bil. Symp., RSS without KHFAC	Pre	104.9 ± 2.5	889.1 ± 180.4	320.6 ± 7.7
	RSS	105.1 ± 2.3	1158.0 ± 345.3	325.4 ± 7.7
	Δ	0.2 ± 0.4	268.8 ± 265.8	4.8 ± 2.9

Table 3. KHFAC mitigates the degree of sympathetic stimulation-induced changes in hemodynamics and activation recovery interval. In the intact state and following left sympathectomy, RSS increased heart rate and dP/dt_{max} and shortened ventricular activation recovery interval, while KHFAC + RSS evoked no significant changes. The degree of absolute change was greater for RSS compared to KHFAC + RSS for most parameters. Data reported as mean and standard error for n=5 animals using paired t-test or Wilcoxon matched-pairs signed rank test. *$p<0.05$ for RSS vs Pre-stimulation for

each parameter and stimulation. *p<0.05 for RSS vs Pre-stimulation for each parameter and stimulation. †p<0.05 for ΔRSS vs ΔKHFAC + RSS for each condition (intact, L. Symp., Bil. Symp.) and parameter. Bil. Symp., bilateral sympathectomy; KHFAC, Kilohertz frequency alternating current; L. Symp., left sympathectomy; RSS, right sympathetic chain stimulation.

	Intact	L. Symp.	Bil. Symp.
RSS	55.8 ± 14.6*	43.2 ± 10.2*	0.3 ± 0.9
KHFAC	10.1 ± 2.1	8.3 ± 3.4	-
KHFAC + RSS	1.0 ± 3.8†	4.3 ± 5.4†	-

Table 4. Transient onset properties of KHFAC in the intact state and following sympathectomy. KHFAC demonstrated transient, low-level release of NE in the intact state and following left sympathectomy. Onset changes in NE were transient and to a lesser degree than RSS alone (*$p<0.05$ for KHFAC + RSS vs RSS) and, after block stabilization, RSS resulted in minimal change in NE compared to RSS without KHFAC (†$p<0.05$ for KHFAC + RSS vs RSS). Change in NE reported as mean and standard error for n=5 animals using 1-way repeated analysis of variance and Fisher's least significant difference test. Bil. Symp., bilateral sympathectomy; KHFAC, kilohertz frequency alternating current; L. Symp., left sympathectomy; NE, norepinephrine; RSS, right sympathetic chain stimulation.

References

1. Benjamin EJ, Virani SS, Callaway CW, Chamberlain AM, Chang AR, Cheng S, Chiuve SE, Cushman M, Delling FN, Deo R, et al. Heart Disease and Stroke Statistics-2018 Update: A Report From the American Heart Association. *Circulation*. 2018;137:e67-e492.
2. Fukuda K, Kanazawa H, Aizawa Y, Ardell JL, Shivkumar K. Cardiac innervation and sudden cardiac death. *Circ Res*. 2015;116:2005-2019.
3. Ardell JL, Andresen MC, Armour JA, Billman GE, Chen PS, Foreman RD, Herring N, O'Leary DS, Sabbah HN, Schultz HD, et al. Translational neurocardiology: preclinical models and cardioneural integrative aspects. *J Physiol*. 2016;594:3877-3909.
4. Hadaya J, Ardell JL. Autonomic Modulation for Cardiovascular Disease. *Front Physiol*. 2020;11:617459.
5. Ajijola OA, Hoover DB, Simerly TM, Brown TC, Yanagawa J, Biniwale RM, Lee JM, Sadeghi A, Khanlou N, Ardell JL, et al. Inflammation, oxidative stress, and glial cell activation characterize stellate ganglia from humans with electrical storm. *JCI Insight*. 2017;2.
6. Ajijola OA, Wisco JJ, Lambert HW, Mahajan A, Stark E, Fishbein MC, Shivkumar K. Extracardiac neural remodeling in humans with cardiomyopathy. *Circ Arrhythm Electrophysiol*. 2012;5:1010-1116.
7. Belevych AE, Terentyev D, Terentyeva R, Ho HT, Gyorke I, Bonilla IM, Carnes CA, Billman GE, Gyorke S. Shortened Ca2+ signaling refractoriness underlies

cellular arrhythmogenesis in a postinfarction model of sudden cardiac death. *Circ Res*. 2012;110:569-577.

8. Billman GE. Cardiac autonomic neural remodeling and susceptibility to sudden cardiac death: effect of endurance exercise training. *Am J Physiol Heart Circ Physiol*. 2009;297:H1171-1193.

9. Shivkumar K, Ajijola OA, Anand I, Armour JA, Chen PS, Esler M, De Ferrari GM, Fishbein MC, Goldberger JJ, Harper RM, et al. Clinical neurocardiology defining the value of neuroscience-based cardiovascular therapeutics. *J Physiol*. 2016;594:3911-3954.

10. Bourke T, Vaseghi M, Michowitz Y, Sankhla V, Shah M, Swapna N, Boyle NG, Mahajan A, Narasimhan C, Lokhandwala Y, et al. Neuraxial modulation for refractory ventricular arrhythmias: value of thoracic epidural anesthesia and surgical left cardiac sympathetic denervation. *Circulation*. 2010;121:2255-2262.

11. Vaseghi M, Barwad P, Malavassi Corrales FJ, Tandri H, Mathuria N, Shah R, Sorg JM, Gima J, Mandal K, Saenz Morales LC, et al. Cardiac Sympathetic Denervation for Refractory Ventricular Arrhythmias. *J Am Coll Cardiol*. 2017;69:3070-3080.

12. Gossot D, Kabiri H, Caliandro R, Debrosse D, Girard P, Grunenwald D. Early complications of thoracic endoscopic sympathectomy: a prospective study of 940 procedures. *Ann Thorac Surg*. 2001;71:1116-1119.

13. Mahajan A, Moore J, Cesario DA, Shivkumar K. Use of thoracic epidural anesthesia for management of electrical storm: a case report. *Heart Rhythm*. 2005;2:1359-1362.

14. Do DH, Bradfield J, Ajijola OA, Vaseghi M, Le J, Rahman S, Mahajan A, Nogami A, Boyle NG, Shivkumar K. Thoracic Epidural Anesthesia Can Be Effective for the Short-Term Management of Ventricular Tachycardia Storm. *J Am Heart Assoc*. 2017;6.

15. Goroszeniuk T, Pang D. Peripheral neuromodulation: a review. *Curr Pain Headache Rep*. 2014;18:412.

16. Cuellar JM, Alataris K, Walker A, Yeomans DC, Antognini JF. Effect of high-frequency alternating current on spinal afferent nociceptive transmission. *Neuromodulation.* 2013;16:318-327; discussion 327.

17. Kilgore KL, Bhadra N. Reversible nerve conduction block using kilohertz frequency alternating current. *Neuromodulation.* 2014;17:242-254; discussion 254-245.

18. Vrabec T, Bhadra N, Acker G, Bhadra N, Kilgore K. Continuous Direct Current Nerve Block Using Multi Contact High Capacitance Electrodes. *IEEE Trans Neural Syst Rehabil Eng*. 2016.

19. Waataja JJ, Tweden KS, Honda CN. Effects of high-frequency alternating current on axonal conduction through the vagus nerve. *J Neural Eng*. 2011;8:056013.

20. Ackermann DM, Jr., Bhadra N, Foldes EL, Kilgore KL. Conduction block of whole nerve without onset firing using combined high frequency and direct current. *Med Biol Eng Comput*. 2011;49:241-251.

21. Franke M, Vrabec T, Wainright J, Bhadra N, Bhadra N, Kilgore K. Combined KHFAC + DC nerve block without onset or reduced nerve conductivity after block. *J Neural Eng*. 2014;11:056012.

22. Bhadra N, Kilgore KL. Direct current electrical conduction block of peripheral nerve. *IEEE Trans Neural Syst Rehabil Eng*. 2004;12:313-324.

23. Bhadra N, Kilgore KL. Chapter 10 - Fundamentals of Kilohertz Frequency Alternating Current Nerve Conduction Block of the Peripheral Nervous System. In: Krames ES, Peckham PH, Rezai AR, eds. *Neuromodulation (Second Edition)*. Academic Press; 2018:111-120.

24. Buckley U, Chui RW, Rajendran PS, Vrabec T, Shivkumar K, Ardell JL. Bioelectronic neuromodulation of the paravertebral cardiac efferent sympathetic outflow and its effect on ventricular electrical indices. *Heart Rhythm*. 2017;14:1063-1070.

25. Chui RW, Buckley U, Rajendran PS, Vrabec T, Shivkumar K, Ardell JL. Bioelectronic block of paravertebral sympathetic nerves mitigates post-myocardial infarction ventricular arrhythmias. *Heart Rhythm*. 2017;14:1665-1672.

26. Buckley U, Yamakawa K, Takamiya T, Andrew Armour J, Shivkumar K, Ardell JL. Targeted stellate decentralization: Implications for sympathetic control of ventricular electrophysiology. *Heart Rhythm*. 2016;13:282-288.

27. Norris JE, Foreman RD, Wurster RK. Responses of the canine heart to stimulation of the first five ventral thoracic roots. *Am J Physiol*. 1974;227:9-12.

28. Millar CK, Kralios FA, Lux RL. Correlation between refractory periods and activation-recovery intervals from electrograms: effects of rate and adrenergic interventions. *Circulation*. 1985;72:1372-1379.

29. Chan SA, Vaseghi M, Kluge N, Shivkumar K, Ardell JL, Smith C. Fast in vivo detection of myocardial norepinephrine levels in the beating porcine heart. *Am J Physiol Heart Circ Physiol*. 2020;318:H1091-H1099.

30. Wilcox RR, Tian TS. Measuring effect size: a robust heteroscedastic approach for two or more groups. *J Appl Stat*. 2011;38:1359-1368.

31. Patel YA, Saxena T, Bellamkonda RV, Butera RJ. Kilohertz frequency nerve block enhances anti-inflammatory effects of vagus nerve stimulation. *Sci Rep*. 2017;7:39810.

32. Shechter R, Yang F, Xu Q, Cheong YK, He SQ, Sdrulla A, Carteret AF, Wacnik PW, Dong X, Meyer RA, et al. Conventional and kilohertz-frequency spinal cord stimulation produces intensity- and frequency-dependent inhibition of mechanical hypersensitivity in a rat model of neuropathic pain. *Anesthesiology*. 2013;119:422-432.

33. Tanner JA. Reversible blocking of nerve conduction by alternating-current excitation. *Nature*. 1962;195:712-713.

34. Fjordbakk CT, Miranda JA, Sokal D, Donega M, Viscasillas J, Stathopoulou TR, Chew DJ, Perkins JD. Feasibility of kilohertz frequency alternating current neuromodulation of carotid sinus nerve activity in the pig. *Sci Rep*. 2019;9:18136.

35. Bhadra N, Foldes E, Vrabec T, Kilgore K, Bhadra N. Temporary persistence of conduction block after prolonged kilohertz frequency alternating current on rat sciatic nerve. *J Neural Eng*. 2018;15:016012.

36. Armour JA, Linderoth B, Arora RC, DeJongste MJ, Ardell JL, Kingma JG, Jr., Hill M, Foreman RD. Long-term modulation of the intrinsic cardiac nervous system by

spinal cord neurons in normal and ischaemic hearts. *Auton Neurosci.* 2002;95:71-79.

37. Sacramento JF, Chew DJ, Melo BF, Donega M, Dopson W, Guarino MP, Robinson A, Prieto-Lloret J, Patel S, Holinski BJ, et al. Bioelectronic modulation of carotid sinus nerve activity in the rat: a potential therapeutic approach for type 2 diabetes. *Diabetologia*. 2018;61:700-710.

38. Vaseghi M, Zhou W, Shi J, Ajijola OA, Hadaya J, Shivkumar K, Mahajan A. Sympathetic innervation of the anterior left ventricular wall by the right and left stellate ganglia. *Heart Rhythm*. 2012;9:1303-1309.

39. Yanowitz F, Preston JB, Abildskov JA. Functional distribution of right and left stellate innervation to the ventricles. Production of neurogenic electrocardiographic changes by unilateral alteration of sympathetic tone. *Circ Res*. 1966;18:416-428.

40. Anand IS, Konstam MA, Klein HU, Mann DL, Ardell JL, Gregory DD, Massaro JM, Libbus I, DiCarlo LA, Udelson JJE, et al. Comparison of symptomatic and functional responses to vagus nerve stimulation in ANTHEM-HF, INOVATE-HF, and NECTAR-HF. *ESC Heart Fail*. 2020;7:75-83.

41. Schwartz PJ, De Ferrari GM, Sanzo A, Landolina M, Rordorf R, Raineri C, Campana C, Revera M, Ajmone-Marsan N, Tavazzi L, et al. Long term vagal stimulation in patients with advanced heart failure: first experience in man. *Eur J Heart Fail*. 2008;10:884-891.

42. Sharma K, Premchand RK, Mittal S, Monteiro R, Libbus I, DiCarlo LA, Ardell JL, Amurthur B, KenKnight BH, Anand IS. Long-term follow-up of patients with heart

failure and reduced ejection receiving autonomic regulation therapy in the ANTHEM-HF pilot study. *Int J Cardiol*. 2020.

43. Assis FR, Sharma A, Shah R, Akhtar T, Adari S, Calkins H, Ha JS, Mandal K, Tandri H. Long-Term Outcomes of Bilateral Cardiac Sympathetic Denervation for Refractory Ventricular Tachycardia. *JACC Clin Electrophysiol*. 2021;7:463-470.

CHAPTER 3

Chronic vagal nerve stimulation reduces ventricular arrhythmias and prevents adverse remodeling post-myocardial infarction

Introduction

Myocardial infarction (MI) and sudden cardiac death (SCD) are the leading cause of mortality worldwide.[1,2] Neurohormonal remodeling following MI is characterized by chronic sympathoexcitation, which, while initially helping to maintain cardiac output, ultimately becomes maladaptive and contributes to the risk of death.[3,4] Coronary reperfusion, antiadrenergic therapy, and neurohormonal blockade have drastically reduced mortality after MI, but such therapies remain inadequate in preventing neurally-mediated disease progression and SCD.[5,6]

Parasympathetic dysfunction has been increasingly recognized as a causal driver of adverse cardiac remodeling and ventricular arrhythmias following MI.[7-10] Clinically, interest in the antiarrhythmic actions of the parasympathetic nervous system dates back to 1977, whereby increased vagal drive was demonstrated to terminate ventricular tachycardia.[11] In animal models, chronic vagal nerve stimulation (VNS) reduces myocardial injury and improves cardiac function in small mammals, but has not been reproducibly evaluated in higher-level organisms, limiting its applicability.[12-16] Moreover, the translatability of chronic VNS for cardiovascular disease has been hampered by a lack of knowledge regarding cardiac reflexes, cardiac and extracardiac remodeling that occurs during disease, and appropriate delivery of VNS therapy. In fact, the three major existing clinical trials for chronic VNS for heart failure each targeted different neural substrates and delivered therapy at vastly different stimulation parameters, with only one trial reporting improvements in left ventricular function and quality of life.[17-20]

Efficacy of bioelectric interventions depend upon the site of delivery, the stimulation protocol utilized and the substrate upon which the neuromodulation is acting, both neural and end-organ target.[21] Our laboratory has previously characterized the neural fulcrum, a balance point for delivery of VNS whereby both afferent and efferent arms of the parasympathetic system are engaged, producing a null heart rate response.[22] In a guinea pig model of pressure overload, we have previously found that chronic VNS, delivered at the neural fulcrum, improved left ventricular function by reducing myocyte apoptosis and hypertrophy.[23] Similarly, in a guinea pig model of MI, chronic VNS improved left ventricular systolic function by stabilizing myocardial metabolism and intrinsic cardiac neuronal function.[13] Although prior work identifies several cardioprotective mechanisms of chronic VNS, studies in large mammals are imperative to evaluate the translational potential of chronic VNS in the treatment of cardiac dysfunction after acute MI. Moreover, the antiarrhythmic actions of chronic VNS post MI remain unknown.

Herein, we studied how chronic VNS mitigates myocardial structural and neural remodeling as well as ventricular arrhythmogenesis following MI (Figure 19A). We utilized a clinically-relevant model, the Yucatan minipig, that recapitulates many features of human ischemic cardiomyopathy including sudden cardiac death. We delivered VNS therapy in a neuroscience-guided manner, targeting the neural fulcrum using telemetry in the conscious state. We evaluated minipigs in three groups: control, untreated MI (a subset of which received sham VNS therapy), and chronic VNS (cVNS) + MI.

Methods

Study Overview and Approval

Animal experiments were approved by the UCLA Institutional Animal Care and Use Committee (IACUC) and performed in accordance with the National Institutes of Health's Guide for the Care and Use of Laboratory Animals. A total of 42 Yucatan minipigs (*Sus scrofa*, S&S Farms, California) of both sexes, weighing 50-60 kilograms at terminal experiment, were used for the present study. Six animals died within 48 hours of MI from SCD, and were not included in final analysis. Surviving animals comprised three experimental groups: control (n=10), MI (n=12 without sham VNS, n=4 with sham VNS), and MI + cVNS (n=10). Animals were housed using standard 12-hour light and 12-hour dark cycles; pigs were fasted overnight except for water prior to experiments. At the end of terminal experiments, animals were euthanized in concordance with IACUC guidelines.

Implantation of Vagal Nerve Stimulators

Following sedation with midazolam (1 mg/kg, intramuscular) and ketamine (10 mg/kg, intramuscular), animals were endotracheally intubated and mechanically ventilated (tidal volume 300-450mL, rate 10-12 breaths per minute). Anesthesia was maintained with isoflurane (1-4%, inhaled), and carprofen (4.4 mg/kg, intramuscular) and buprenorphine (0.02 mg/kg, intramuscular) were administered for analgesia. Ceftiofur (4 mg/kg, intravenous) and cefazolin (1 mg) were administered once perioperatively for antibiotic prophylaxis. Ear veins and the right or left femoral artery or tail artery were cannulated for medication administration and invasive blood pressure monitoring. Three-lead electrocardiogram, oxygen saturation, and end-tidal carbon dioxide were monitored. Body temperature was maintained using a forced-air normothermia system, and 0.9%

NaCl (5-6 mL/kg/hr) was administered to replenish insensible fluid loses. The intended incision site over the right ventral neck was anesthetized with a 1:1 mixture of lidocaine (1 mg/kg) and bupivacaine (1 mg/kg). The right external jugular vein and right vagus nerve were exposed. A wireless telemetry device (M01-F1, Data Sciences International, St. Paul, Minnesota) was implanted with one lead fluoroscopically guided to the cavoatrial junction through the right external jugular vein, and the second lead tunneled to a pocket in the lateral neck (Figure 19B-C). A bipolar VNS cuff (PerenniaFLEX Model 304, LivaNova, Houston, Texas) was placed around the right cervical vagus nerve and attached to a VNS pulse generator (Vitaria Model 7103, LivaNova, Houston, Texas). VNS devices were tested intraoperatively for evoked bradycardia to confirm device placement. Devices and leads were secured with 4-0 polypropylene sutures to the adjacent fascia, and the fascia overlying the vagus nerve and external jugular vein were each closed separately with absorbable suture. The device pockets and incision were then closed with 4 layers of absorbable suture, and the animals were extubated and recovered. Carprofen (4.4 mg/kg, per os, once daily) was administered for three days for postoperative analgesia. Pigs were evaluated twice daily for 10 days, and daily thereafter.

Titration of VNS Therapy

To achieve therapeutic levels of VNS, stimulation settings were systematically titrated to those that produced a null heart rate change at 5 Hz frequency and 250 μs pulse width during the on phase of VNS (14 s on, 66 s off) as shown in Figure 20A. To accomplish this, titration was began at 5 Hz, 130 μs, and 0.25 mA. At each titration session, current was increased in 0.25 mA increments until side effects (cough, gastrointestinal upset)

were elicited; current was then decreased by 0.25 mA and the pig rested for >1 day at these settings. Once a current of 3 mA was achieved, pulse width was stepped up to 250 μs and a similar process was repeated. Neural fulcrum was defined as a null change in heart rate, and titration discontinued once fulcrum was achieved. Two days following myocardial infarction, VNS was restarted and maintained at 5 Hz, 250 μs, and 17.5% duty cycle (14 s on, 66 s off), with intensity as previously determined individually to achieve neural fulcrum.

Myocardial Infarction

For induction of myocardial infarction, the same anesthesia, analgesia, and monitoring protocol described above was performed. The right or left femoral artery was accessed using the modified Seldinger technique and a vascular access sheath was placed. Ventricular arrhythmia prophylaxis consisted of amiodarone (1.5 mg/kg, intramuscular) and lidocaine (2 mg/kg, intravenous), while periprocedural anticoagulation was maintained with heparin (5000 units, intravenous). Under fluoroscopic guidance, an AL1.0 guide catheter (Medtronic) and 0.014” guidewire (Balance Middleweight Universal, Abbott) were used to cannulate the left coronary artery. An angioplasty balloon catheter was advanced over the guidewire to the mid-left anterior descending coronary artery to the level of the second diagonal branch and inflated. A suspension (2.25mL diluted to 6mL with 0.9% NaCl) of polysterene microspheres (Polysciences Inc., Warrington, Pennsylvania) was used to embolize the distal left anterior descending coronary artery (Figure 19D). Hyperacute T waves, T wave inversion, or ST segment elevation were evident on surface electrocardiogram. External cardioversion and standard cardiopulmonary resuscitation were performed if the animal developed

unstable ventricular tachycardia or ventricular fibrillation. For animals requiring cardiopulmonary resuscitation, epinephrine (0.01 mg/kg, intravenous) was administered every 3 to 5 minutes, and amiodarone (1.5 mg/kg, intravenous) and lidocaine (2 mg/kg, intravenous) were redosed. Animals were extubated and recovered as described above. All pigs received carprofen (4.4 mg/kg, per os) daily for two days and, if defibrillation was required, buprenorphine (0.02 mg/kg, intravenous) was administered twice daily for two days. After MI, the pigs receiving cVNS gained 1.8 ± 0.5 kg per week, while those not receiving cVNS gained 1.9 ± 0.5 kg ($p=0.62$).

Surgical Preparation at Terminal Study

Pigs were sedated, intubated, mechanically ventilated, maintained on isoflurane, and monitored as described above. Tiletamine-zolazepam (4-6 mg/kg, intramuscular) was used for induction rather than ketamine and midazolam and fentanyl citrate (20 mg/kg, intravenous) was administered for analgesia. Vascular access sheaths were placed in bilateral femoral arteries and veins for administration of fluids, monitoring, and placement of intracardiac catheters. Arterial blood gas contents were also evaluated hourly and ventilation parameters adjusted or sodium bicarbonate administered as needed to ensure physiologic parameters for experimental studies. The thorax and heart were exposed through a median sternotomy. A pericardial cradle was created to support the heart. The parietal pleural was divided posteriorly and the sympathetic chain isolated at the level of the stellate ganglia. The left vagus was dissected as described above, and the right vagus lead disconnected from the pulse generator. Following completion of surgical procedures, anesthesia was transitioned from isoflurane to alpha-chloralose (25-50 mg/kg/hour, intravenous), an anesthetic that does not depress cardiac

and autonomic reflexes. Surgical preparation time ranged from 2 to 4 hours, and total duration of anesthesia ranged from 9 to 12 hours. Pigs were allowed to stabilize for 30 minutes after completion of alpha-chloralose bolus and maintenance of stable infusion before experimental protocols were initiated.

Nerve Stimulation

Bipolar platinum nerve cuffs (Microprobes, Gaithersburg, Maryland) were placed around the right and left sympathetic chain at the level of the stellate ganglia. A bipolar VNS cuff was placed around the left vagus as described above. Nerve stimulation was performed using a Grass S88 stimulator, interfaced through a PSIU6 photoelectric constant-current isolation unit (Grass Instruments, Warwick, Rhode Island). For sympathetic chain stimulation, threshold was defined as the current required to elicit a 10% increase in heart rate or left ventricular end-systolic pressure at a fixed frequency and pulse width (4 Hz, 4 ms). For left vagal nerve stimulation, stimulus threshold was defined as the current required to elicit a 10% change in heart rate at a fixed frequency and pulse width (10 Hz and 1 ms). Bilateral sympathetic chain stimulation was performed at 1.5 times threshold at moderate (4 Hz) and high (10 Hz) intensity to evaluate evoked sympathetic responses. To test whether acute VNS influenced induction of VT or VF, acute bilateral VNS was performed in conjunction with ventricular arrhythmia inducibility at 1.5 times fulcrum (right) or threshold (left).

Echocardiography

Echocardiography was performed as previously described.[24] Left ventricular ejection fraction was calculated using the modified Simpson method. Left ventricular wall thicknesses were measured in diastole.

Hemodynamic and Electrophysiologic Data Acquisition and Analysis

A solid-state pressure catheter (Mikro-Tip Model SPR-350, Millar Instruments, Houston, Texas) was placed in the left ventricle through the femoral artery and used to measure rate of change of left ventricular pressure (dP/dt) and heart rate. A lead II electrocardiogram and bipolar electrocardiograms were measured with surface electrodes and quadripolar or duodecapolar electrode catheters (Boston Scientific). These data were acquired, digitized, and analyzed offline using a data acquisition system (Cambridge Electronics Design Power1401 and Spike2, Cambridge, United Kingdom). Left ventricular contractility or systolic function was evaluated with the maximum rate of change of left ventricular pressure (LV dP/dt_{max}) while lusitropy was evaluated using the minimum rate of change of left ventricular pressure (LV dP/dt_{min}).

A custom, 128-electrode thin film array (NeuroNexus, Ann Arbor, Michigan) was placed over the left ventricle scar-border zone (or equivalent area in controls) to acquire unipolar epicardial electrograms. Data was sampled using an AlphaLab SnR acquisition system (Alpha Omega, Alpharetta, Georgia). Activation recovery intervals (ARI) were analyzed from each epicardial electrogram using Scaldyn (University of Utah, Salt Lake City, Utah) as previously described. Maps were plotted using Fiji with identical scaling and bilinear interpolation for the three experimental groups simultaneously. Activation time was identified as the time from the beginning to the minimum dV/dt in the activation wavefront and repolarization time by the maximum dV/dt of the repolarization wavefront.

Activation delay was defined as the maximum minus minimum activation time, while activation dispersion was assessed as the variance of activation times. Repolarization gradients were defined as the 95th percentile minus the 5th percentile of local repolarization times divided by the geometric distance between corresponding electrodes as previously described.[25] ARI was calculated as the difference between repolarization time and activation time, ARI dispersion as the variance in ARI. ARI serves as a strong *in vivo* surrogate for local action potential duration.[26]

Arrhythmia Inducibility

Ventricular arrhythmia inducibility was performed using programmed electrical stimulation (PES) using a Micropace EPS 320 cardiac stimulator (Micropace EP, Santa Ana, California) interfaced with a Prucka CardioLab System (GE Healthcare, Chicago, Illinois). PES was performed at a stimulus drain train (S1) 20% above the resting heart rate followed by an S2 extrastimulus with a 10ms decrement until 200 ms or until effective refractory period (ERP) was reached. If the first extrastimulus did not induce sustained VT or VF, a second (S3) extrastimulus was added and the decrement process repeated. This was performed through a third (S4) extrastimulus. For animals receiving chronic VNS therapy, PES was performed twice: without acute VNS, and with bilateral acute VNS for 30 minutes prior to and during PES. Animals that did not experience sustained VT or VF for greater than 30 seconds with three extrastimuli were considered non-inducible. Non-sustained VT was defined as at least three or more ventricular beats at a rate of >120 bpm that terminated within 30 seconds. Animals were classified as non-inducible, induced for NSVT, or induced for sustained VT/VF. An arrhythmogenicity index was calculated to quantify the ease of VT/VF inducibility based

on the stimulus drive train and number of extrastimuli as previously described.[24] Higher values indicate greater ease of inducibility.

Tissue Collection and Processing

The left ventricular anterior myocardium adjacent to the left anterior descending coronary artery (consisting of scar, border, and remote regions), right stellate ganglia, and first thoracic dorsal root ganglia were collected and rinsed in cold phosphate buffered saline (PBS). Myocardial samples were fixed in 10% formalin (Sigma-Aldrich, Burlington, Massachusetts) at room temperature for 72 hours, washed with PBS 4 times for 1 hour each, and preserved in 70% ethanol. Stellate and dorsal root ganglia were fixed in 4% paraformaldehyde (Electron Microscopy Sciences, Hatfield, Pennsylvania) at 4 °C for 24 hours, washed with PBS 4 times for 1 hour each, and preserved in PBS with 0.02% sodium azide.

Masson's trichrome staining was performed on left ventricular samples spanning the scar-border zone, just adjacent to the LAD, and evaluated for structural abnormalities. Abnormalities included increased myocytolysis, decreased staining for muscle bands, reactive hypertrophy, and presence of dysmorphic myocytes. The following arbitrary scale was used: 3 = very abundant, 2 = moderate, 1 = low, 0 = none or rare. Three to four sections were evaluated per animal, and values were recorded for subepicardium, midwall, and subendocardium. These were added on the first pass and an average value for each animal was calculated.

Stellate ganglia sections were stained using a 2-day protocol with the following combinations: 1) PGP9.5, TH, VAChT; 2) PGP9.5, TH, NPY; and 3) PGP9.5, GFAP,

S100B. The right stellate ganglia were paraffin embedded to acquire 5 μm sections of the craniomedial portion along the long-axis of the ganglia. Slides with paraffin-embedded sections underwent two consecutive, 10-minute baths in xylene. Slides were then placed in ethanol baths of varying concentrations (100% for 10 minutes, followed by 95% for 5 minutes, followed by 70% for 5 minutes). Finally, slides were placed in dH_2O for five minutes. Slides were placed an antigen unmasking solution, made by diluting 2.5 mL of antigen retrieval buffer in 250 ml of dH_2O and boiling to 90 °C, for 25 minutes, then cooled for 1 hour. Slides were then placed in a soaking buffer solution (PBS with 0.4% TX-100) for thirty minutes at 4 °C. Tissue wells were created on slides using a PAP pen and 50-100 μL PBS was added to each well depending on tissue size. The slides were placed in a humidified chamber and agitated for 5 minutes. PBS was then replaced with blocking buffer solution (PBS + 10% donkey serum with 0.1% TX-100) for 1 hour. Primary antibody solution was then made by adding primary antibodies (Table 5) to the blocking buffer solution, which replaced the blocking solution in the wells. Slides were agitated overnight at 4 °C. Slides were then warmed to room temperature and washed with PBS with 0.2% TX-100 three times. Secondary antibody solution was then made by adding secondary antibodies (Table 6) to the blocking buffer solution, which then replaced the primary antibody solution in each well. Slides were agitated gently for 1 hour at room temperature then washed 3 times with PBS. PBS was then replaced with refractive index matching solution that covered each section entirely and cover slips were placed directly after to secure the tissue. Slides were imaged using confocal microscopy.

Dorsal root ganglia were stained using a 7-day protocol with the following combinations: 1) PGP9.5, CGRP, nNOS and 2) PGP9.5, GFAP, S100B. The right first thoracic DRG from each subject was embedded in agarose to acquire 100 μm sections along the long-axis of the ganglia. Each section was placed in 1 mL of blocking solution containing 10% donkey serum, 0.2% Triton X-100, and PBS for overnight incubation with slight agitation. A primary antibody solution was made using blocking solution and primary antibodies (Table 5). After 3 nights of incubation with slight agitation, the sections were washed with PBS every hour for at least 6 washes. A secondary antibody solution made with blocking solution and secondary antibodies (Table 6). Sections were incubated for 3 nights with slight agitation. Sections were then washed with PBS every hour for at least 6 washes. Sections were mounted on slides and refractive index matching solution was added in drops until the sections were covered entirely, and a coverslip was placed to secure the tissue. Slides were imaged using confocal microscopy.

Confocal imaging was performed using a Zeiss LSM-880 confocal laser microscope (Zeiss, Oberkochen, Germany). The following lasers were used: 488 nm, 562 nm, 647 nm. Imaging was done at 10x and stitched together using the tile scan feature. Maximum intensity projections (MIP) for a representative Z-stack were subsequently used for analysis. Pseudo-colors (red 562 nm, blue 647 nm, green 488 nm) were assigned to each channel to allow for adequate contrast in merged images; assigned colors for each antibody are reported in each confocal image.

Three representative 500 by 500 μm regions of interest (ROI) were selected for each stellate section on Zen Black (Zeiss, Oberkochen, Germany). 16-bit full-resolution

images were exported and analyzed on ImageJ Software (NIH, USA). The PGP9.5, TH, and VAChT combination was analyzed for cholinergic transdifferentiation by using the cell counter feature in ImageJ to obtain a total neuron count using the PGP9.5 channel and a count of neurons double-labeled for TH and VAChT. The PGP9.5, TH, and NPY combination was similarly analyzed for NPY expression. This corresponded to a mean of 362.5 PGP9.5-positive neurons per animal to study cholinergic transdifferentiation and 359.0 for neuropeptide Y expression. Glial analysis was performed by selecting 15 satellite glial cells (5 cells per ROI) from each animal for individual analysis. The length and area of each satellite glial cell was measured on ImageJ using the GFAP stain. The immunoreactive area (μm^2) per cell for each ROI was calculated by converting the GFAP channels to binary images. The thresholding tool in ImageJ was then used to calculate the total GFAP stain area in each ROI. A ratio of total GFAP area to total cell count based on the PGP9.5 channel was then calculated for each ROI and averaged for each animal.

One representative 500 by 500 μm ROI was selected for each DRG section. 16-bit full-resolution images were exported and analyzed on ImageJ Software. The PGP9.5, CGRP, and nNOS staining combination was analyzed for cells labeled for nNOS or CGRP and PGP9.5. To evaluate glial activation, the immunoreactive area (μm^2) per cell for each ROI was similarly calculated by converting the GFAP channels to binary images. The thresholding tool was then used to calculate the total GFAP stain area in each ROI. A ratio of total GFAP area to total cell count based on the PGP9.5 channel was then calculated for each animal.

Statistical Analysis

Data is presented as mean with standard error (SE). Normality was assessed using the Shapiro-Wilk test. For normally distributed variables, differences in standard deviation were tested using the Brown-Forsythe test. For normally distributed variables, comparisons were made using standard analysis of variance (ANOVA) if standard deviations were not significantly different, Welch's ANOVA if standard deviations differed. For non-normally distributed variables, the Friedman test was used. Pairwise comparisons were subsequently performed using the two-stage step-up method method of Benjamini, Krieger and Yekuteili to control for multiple comparisons. Statistical analysis was conducted using Prism 9 (GraphPad Software, San Diego, California).

Results

Implementation of chronic vagal nerve stimulation in Yucatan minipigs

To study the effects of cVNS on MI, we developed a strategy for cVNS delivery at the neural fulcrum. Our preliminary studies suggested that titration to therapeutic VNS parameters required approximately 30 days due to side effects in pigs. As the majority of myocardial remodeling occurs within the first month following MI, we implanted right vagus nerve cuffs, pulse generators and telemetry units and titrated to therapeutic settings prior to MI (Figure 20A-B). This strategy allowed us to begin therapeutic VNS on-demand following MI. Both MI + cVNS pigs and MI + sham cVNS pigs underwent VNS implantable pulse generator and lead implantation, followed by titration to VNS fulcrum (range 3-6 weeks). Once VNS fulcrum was achieved (5 Hz, 250 μs, mean current 1.8 ± 0.2 mA), therapy was discontinued and pigs underwent MI at least 1 day

after cessation of therapy to ensure no memory effect from VNS titration.[27] MI was induced in MI, MI + sham cVNS, and MI + cVNS pigs by percutaneous embolization of the left anterior descending (LAD) coronary artery, and infarcts were allowed to mature for 6-8 weeks prior to terminal study. VNS therapy was restarted 2 days following MI in the MI + cVNS group. Among all animals undergoing MI induction, six experienced sudden cardiac death within 2 days of MI, confirming the adequacy of this model (Figure 19E). A sensitivity analysis, reported below, found no significant difference in sympathetic function, electrophysiologic parameters, cardiac structural remodeling, or arrhythmia inducibility in MI compared to MI + sham cVNS groups. As such, these were considered as one group for the primary analysis reported in this study. Age- and weight-matched controls that had not undergone any interventions were utilized for comparison.

Chronic vagal nerve stimulation rescues cardiac mechanical function following MI

To determine whether chronic VNS influences basal left ventricular contractile function following MI, we performed echocardiography in control, MI, and MI + cVNS animals (Figure 21A-B, Figure 22). MI animals had significant impairment in left ventricular systolic function compared to controls, with left ventricular (LV) ejection fraction (EF) of 40.6 ± 1.2% compared to 71.6 ± 0.4%% ($p<0.001$). Chronic VNS therapy rescued changes in EF to 67.4 ± 1.3%, though this remained significantly different from controls (Figure 21B). Similarly, MI resulted in greater LV end-systolic volumes (LVESV) and LV internal diameter in diastole (LVIDd), which was significantly improved in MI + cVNS animals. Wall thickness in the anterior wall, the LV region primarily perfused by the left anterior descending, significantly decreased in MI vs control animals (0.82 ± 0.02 cm vs

0.57 ± 0.04 cm, p<0.001), which was partially attenuated with cVNS therapy to 0.65 ± 0.01 cm (Figure 21B). The myocardial regions not perfused by the LAD remained unaffected (Figure 22B). To evaluate functional sympathetic control of the heart, we performed bilateral sympathetic stimulation (BSS) and tested whether MI or MI + cVNS influenced changes in inotropy or lusitropy. Baseline hemodynamics and thresholds used for sympathetic nerve stimulation are reported in Table 7 and Table 8. MI resulted in dysfunctional inotropic and lusitropic responses to BSS, which were restored to levels similar to control in MI pigs receiving cVNS therapy (Figure 21C). This was evident with both moderate- and high-intensity stimulation (Figure 21C, right), suggesting that cVNS ameliorated reduced cardiac sympathetic reserve evident in MI animals.

Chronic vagal nerve stimulation reduces the susceptibility to ventricular arrhythmias following MI

MI and its associated structural abnormalities in the border zone are known to increase the risk of life-threatening ventricular arrhythmias (VAs). To evaluate whether cVNS reduces VAs following MI, we performed programmed electrical stimulation using extrastimulus pacing in MI and MI + cVNS pigs. A representative recording of VT induction is shown in Figure 23A; as noted, the MI animal was induced with 2 extrastimuli, while the MI + cVNS subject remained non-inducible despite 3 extrastimuli. Ventricular tachycardia (VT) or ventricular fibrillation (VF) was induced in 92% of MI pigs, while the remaining animal experienced non-sustained VT (NSVT). In MI + cVNS subjects, 11% were inducible for VT/VF at baseline (p<0.001 vs MI), while the remaining were non-inducible (Figure 23B). When active VNS was reestablished in MI + cVNS pigs for 30 minutes prior to and during the extrastimulus protocol, 0% were inducible for

VT/VF and 11% experienced NSVT ($p<0.001$ vs MI). The ease of inducibility, quantified based on the rate of the drive train and number of extrastimuli required to induce VT/VF, was significantly greater in MI compared to MI + cVNS subjects (4.4 vs 0.4, $p<0.001$) but similar regardless of whether active VNS therapy was applied (Figure 23C). Full results of the pacing protocol for each animal are reported in Figure 24.

High-density electrophysiologic mapping reveals abnormal impulse propagation following MI, which is improved with cVNS

To evaluate the substrate-level mechanisms by which chronic VNS ameliorated VAs, we performed high-resolution electrical mapping of the left ventricular scar-border zone in MI and MI + cVNS animals, and the corresponding anatomic region in controls (Figure 25A). Heterogeneous areas of myocardial scars contribute to ventricular arrhythmogenesis by facilitating slow conduction and reentry. These regions, as well as subsets with late tissue activation, are the clinical targets of catheter ablation, the current standard of care for reentrant ventricular arrhythmias. Figure 25A demonstrates representative activation maps for control, MI, and MI + cVNS animals. As quantified in Figure 25B, MI animals displayed substantial conduction block (i.e., no increase in proportion of LV tissue activated relative to time) compared to controls, which was drastically improved with cVNS therapy. Consistent with prior work, we found that MI quantitatively resulted in greater mean ventricular activation time, activation dispersion (variance of activation time), activation delay, and maximal activation time (Figure 25C-F). Chronic VNS therapy normalized the majority of these measures to levels comparable to controls, including mean activation time, delay, and maximal activation time, while activation dispersion, a sensitive measure for scar, was improved relative to

MI (17.6 ± 1.5 ms^2 vs 28.5 ± 2.9 ms^2, $p<0.01$) but remained greater than control (17.6 ± 1.5 ms^2 vs 10.0 ± 1.4 ms^2, $p<0.01$, Figure 25D). These findings suggest that cVNS substantially remodels myocardial scars and ameliorates the majority of the conduction abnormalities observed after MI.

Chronic vagal nerve stimulation normalizes steep repolarization gradients and repolarization heterogeneities that occur following MI

Abnormal myocardial repolarization properties, particularly heterogeneity, have been implicated in arrhythmias following MI. To study the influence of chronic VNS on repolarization properties following MI, we first examined repolarization maps and tissue repolarization curves across the border zone, and found qualitatively less repolarization heterogeneities in MI + cVNS animals compared to MI alone (Figure 26A-B). We next evaluated left ventricular activation recovery intervals (ARI), a surrogate measure for APD_{90} that can be readily measured in vivo without causing myocardial injury.[26] Interestingly, we found no significant difference in mean ARI across the border zone, or equivalent region, in control compared to MI and MI + cVNS animals (Figure 26C). To quantify heterogeneity in ARI, we examined ARI dispersion, and found that MI induced substantial increases in ARI dispersion (399 ± 75 ms^2 vs 63 ± 22 ms^2, $p<0.01$), which were normalized by cVNS therapy (110 ± 32 ms^2, Figure 25D). Steep repolarization gradients (RG) have recently been associated with the development or maintenance of reentrant arrhythmias.[6,28,29] As anticipated, MI pigs had steep RG compared to controls (3.7 ± 0.6 ms/mm vs 1.6 ± 0.1 ms/mm, $p<0.01$), which was similarly improved with cVNS therapy (2.0 ± 0.4 ms/mm, Figure 26B, 26E). Taken together, these findings strongly suggest that cVNS not only improves conduction across the infarcted

myocardium, but improves the repolarization properties of myocytes themselves in vivo, protecting the heart against VAs.

Chronic vagal nerve stimulation exerts its antiarrhythmic effect partly by reducing aberrant remodeling of the myocardial substrate

Given the observed improvement in mechanical and electrophysiologic properties of cVNS in infarcted hearts, we evaluated structural changes in the scar-border zone. We performed Masson's trichrome staining on left ventricular sections spanning the scar-border zone, just adjacent to the site of LAD embolization. Compared to MI animals, we qualitatively observed less myocytolysis, improved staining of muscle bands, and less reactive hypertrophy in cVNS + MI pigs (Figure 27). These specific findings, particularly a reduction in myocytolysis (Figure 27B, arrows), is consistent with reduced potential for VT/VF. Quantification revealed a marked reduction in border zone abnormality among MI + cVNS compared to MI animals (1.8±0.2 vs 0.6±0.2, p=0.001, Figure 27E).

Myocardial infarction alters neural and glial phenotypes in the peripheral nervous system, which are partly attenuated with cVNS

In both humans and animal models, myocardial injury leads to extracardiac neural remodeling, which may drive sympathoexcitation after MI.[30,31] Stellate ganglia surgically removed from patients with recurrent VT showed evidence of oxidative stress, glial activation, and changes in neuronal phenotypes.[31] To evaluate for changes in neuronal phenotypes in our porcine models, we co-labeled neurons in the stellate ganglia for 1) protein gene product 9.5 (PGP9.5, a pan-neuronal marker), tyrosine hydroxylase (TH) and vesicular acetylcholine transporter (VAChT), and 2) PGP9.5 and neuropeptide Y

(NPY). We found a significant increase in TH+/VAChT+ neurons after MI, which was unchanged with cVNS therapy (Figure 28A). Similarly, the proportion of NPY+ neurons significantly increased following MI, a change that trended toward normalization with cVNS but did not reach statistical significance (Figure 28B). To evaluate for glial activation, stellate ganglia were co-labeled with S100 Calcium Binding Protein B (S100B), glial fibrillary acidic protein (GFAP), and PGP9.5. MI resulted in a substantial increase in glial activation, as evaluated by glial area normalized to neurons per section, which was reversed to control levels with cVNS treatment (Figure 28C). Similar findings were evident upon evaluation of length, width, and thickness of glial cells in the stellate ganglia (Figure 29). Representative confocal images of each channel by study group are presented in Figure 30 (cholinergic transdifferentiation), Figure 31 (neuropeptide Y expression), and Figure 32 (glial activation).

We similarly evaluated changes in afferent neuronal phenotypes and glial activation in the first thoracic dorsal root ganglia (DRG), the primary source of general visceral afferent fibers that innervate the heart. Neuronal nitric oxide synthase (nNOS) expression significantly increased following MI, which was mitigated by cVNS (Figure 33A). The expression of calcitonin gene-related peptide (CGRP) was similar in the three study groups (Figure 33B). Consistent with the stellate, MI led to significantly increased glial activation in the DRG, which was ameliorated by cVNS (Figure 33C). There was no significant difference in overall neuron size, nNOS+ neuron size, or CGRP+ neuron size by study group (Figure 34). Representative confocal images of each channel by study group are presented in Figure 35 (nNOS and CGRP expression) and Figure 36 (glial activation).

Sensitivity analysis examining sham VNS + MI animals compared to MI alone

To test whether the observed cardioprotective effects of cVNS were attributable to VNS during the titration period prior to MI, we studied a group of 4 animals, termed sham VNS + MI, that were similarly titrated to neural fulcrum, underwent MI, but received no reactive VNS therapy after MI. These sham VNS + MI animals were compared to pigs undergoing MI alone (with no titration to neural fulcrum). We found no significant difference in BSS-evoked changes in contractility (Figure 37A), electrophysiologic parameters (Figure 37B-E), or structural remodeling at the border zone (Figure 37F). Moreover, all 4 sham VNS + MI animals were inducible for sustained VT or VF.

Discussion

In this work, we demonstrate a substantial improvement in cardiac mechanical function and dramatic reduction in ventricular arrhythmias in MI + cVNS pigs compared to MI pigs. We establish that cVNS stabilizes MI-induced electrical heterogeneity in the scar-border zone, reduces anisotropic electrical propagation and conduction block, and normalizes myocardial repolarization—key drivers of ventricular arrhythmias in vivo. We demonstrate that chronic VNS reduces aberrant structural remodeling of the scar-border zone and principal sympathetic efferent and afferent ganglia (stellate and T1 dorsal root ganglia). Finally, cVNS preserved sympathetic control of the heart following MI.

While acute VNS has been well studied in the setting of acute ischemia or MI, there is a paucity of studies evaluating the impact of chronic VNS on cardiac function, arrhythmias, and remodeling after MI, particularly in large mammals. Among canine with

healed anterior MI, acute VNS initiated within 15 seconds of coronary occlusion reduced ventricular arrhythmias, though these effects were partly attenuated by atrial pacing to control for a 75bpm bradycardia.[32] Similarly, the antiarrhythmic effects of acute VNS in ischemia-reperfusion injury in porcine were mitigated by administration of atropine and were not evident when VNS was initiated during reperfusion, suggesting that the acute cardioprotective effects are mediated by muscarinic receptors.[33,34] In the present study, we found that chronic VNS, initiated two days post MI at the neural fulcrum, resulted in favorable myocardial and neural remodeling that prevented the induction of VT or VF. This antiarrhythmic effect was evident even in the absence of acute VNS, suggesting that its effects are not mediated solely by acute activation of muscarinic receptors. In guinea pigs, our group has previously found that chronic VNS, started 10 days following MI, significantly improved myocardial contractile function.[13] In the present study, we similarly found that chronic VNS improved left ventricular systolic function, with near normalization of ejection fraction to controls. Interestingly, we found that control and MI + VNS animals had greater sympathetic reserve using electrical stimulation of the sympathetic chain, as these groups of animals were able to more effectively mount inotropic and lusitropic responses compared to MI pigs. These specific findings indicate that chronic VNS may ameliorate abnormal calcium handling and inefficient excitation-contraction coupling that occurs in MI and heart failure. Structurally, chronic VNS reduced thinning of the anterior wall of the left ventricle, the primary location of MI in this model. Consistent with its anti-arrhythmic effect, VNS reduced the degree of myocytolysis and dysmorphic myocytes in the scar-border zone, and qualitatively resulted in more homogeneous scars, which clinically are known to be less

arrhythmogenic.[35,36] To our knowledge, this represents the first systematic evaluation of reactive VNS therapy on cardiac mechanical function, structural remodeling, and arrhythmias in large mammals, and is a logical step to translation of VNS therapy to clinical applications.

MI results in formation of areas of slow activation or conduction, and transient or permanent unidirectional block, such that steep APD differences manifest over relatively short distances. Moreover, in our model, we found that MI alters basic electrophysiologic properties of the border zone at the tissue level. These aberrant activation and repolarization phenomenon act in concert to promote ventricular arrhythmia risk. This risk was particularly elevated in our model, as all but one of the MI animals were induced for sustained monomorphic VT or VF at terminal study, and six died acutely after MI. Although prior work suggests that acute vagal nerve stimulation reduces ischemia-induced arrhythmias in canine, limited data exists regarding the impact of chronic VNS on induction of ventricular arrhythmias and mechanisms of arrhythmogenesis.[32,37] Notably, MI + cVNS animals were equally protected from VT or VF when inducibility was evaluated with or without active VNS therapy, suggesting that the observed cardioprotective effects are likely mediated by changes in the myocardial and neural substrates. We found that chronic VNS improves conduction across the scar-border zone, which is consistent with studies demonstrating that VNS preserves connexin-43 expression in the setting of acute ischemia in small mammals.[12] The effects of VNS were not limited to electrical propagation, since VNS also positively influenced myocardial activation and repolarization properties. Scar-border zone myocardium from MI + cVNS pigs had significantly less myocytolysis, a highly

arrhythmogenic component of infarcted human myocardium.[36] Moreover, in vivo, MI + cVNS animals demonstrated less ARI dispersion and more shallow repolarization gradients across the scar-border zone. To our knowledge, this represents the first integrative assessment of the impact of chronic VNS on myocardial excitability, impulse propagation, and repolarization following MI.

Acute myocardial injury leads to abnormal cardiac afferent signaling to both the stellate ganglia and high thoracic dorsal root ganglia, ultimately resulting in amplified sympathetic drive.[7,38,39] Consistent with this notion, stellate ganglia from humans with ischemic cardiomyopathy, as well as in animal models, are characterized by oxidative stress, glial activation, and changes in neuronal phenotypes.[30,31,40] In the present work, stellate ganglia neuronal and non-neuronal cells displayed marked changes after MI, including glial activation and cholinergic transdifferentiation. Cholinergic transdifferentiation, a process whereby cardiac sympathetic neurons transition to an acetylcholine-producing phenotype in the setting of heart failure or after MI, has been shown to reduce APD heterogeneity in small mammals and may be an adaptive physiological response to injury.[41-43] As one central premise of neuromodulation is to stabilize imbalance among the cardiac nervous system, we evaluated whether these changes were altered with chronic VNS therapy. We found that cholinergic transdifferentiation remained prominent and unchanged after chronic VNS therapy, while glial cell activation substantially decreased compared to MI animals. This finding underscores the importance of non-neuronal populations in extracardiac ganglia as potential avenues for further study and therapeutic targets. These non-neuronal populations are heterogeneous, and modify neuronal function through purinergic

signaling and intercellular communication via gap junctions, particularly in disease states such as MI.[44-46] While the stellate ganglia serves as the primary efferent sympathetic outflow to the heart, its integrative and processing functions have been increasingly recognized.[47,48] For example, extracellular recordings of stellate ganglia activity identifies greater network entropy and reduced neural specificity or synchrony with the cardiac cycle in porcine with heart failure compared to controls.[47] In the present work, MI impaired sympathetically-evoked changes in inotropy and lusitropy, which were rescued by chronic VNS, suggesting that chronic VNS may stabilize sympathetic function in disease states. Consistent with this, low level VNS in healthy canines increased stellate ganglia expression of small conductance calcium-activated potassium channels known to mediate afterhyperpolarizations, suggesting that chronic VNS may influence sympathetic nerve activity.[49] Myocardial ischemia also results in profound activation of spinal afferents in the high thoracic dorsal root ganglia, the principal general visceral fibers innervating the heart.[50,51] Chronic activation of these afferents, partly mediated through transient receptor potential cation subfamily V member 1 (TRPV1) channels, contributes to exaggerated sympathoactivation and adverse cardiac remodeling while epicardial depletion of TRPV1 fibers attenuates remodeling after MI and improves cardiac function.[24,52] Using extracellular recording, Koji et al. found that depletion of these afferent fibers reduced sympathetic dysfunction after MI, suggesting interaction between spinal afferents and the stellate ganglia.[24] Similarly, we found chronic VNS to reduce glial activation following MI in the DRG, which itself may explain in part the improved sympathetic function seen in MI + cVNS pigs compared to MI alone. Further work to understand spatiotemporal changes in sympathetic neuronal

activity, as well as to elucidate primary versus secondary challenges in the stellate ganglia, is warranted.

A mechanistic and rationale basis of VNS therapy is imperative to appropriate clinical application in the setting of MI and heart failure.[10,21] While low intensity acute VNS can reduce the propensity for arrhythmias during experimentally-induced coronary ischemia, high intensity stimulation causing marked bradycardia can lead to ventricular tachycardia or fibrillation.[32,53] Similarly, the efficacy of chronic VNS therapy in experimental models is also strongly influenced by stimulation parameters.[22] For example, Radcliffe et al. found no effect of chronic VNS therapy on pacing-induced cardiomyopathy in ovine when delivered at settings leading to a 30% bradycardia[16], while Zhang et al. targeted a 10% bradycardia in a similar canine model and found attenuation of heart failure development, though VNS therapy was began earlier in their study.[54] As demonstrated by our VNS titration protocol, increasing intensity of VNS initially evokes tachycardia followed by bradycardia; such an effect is consistent in dogs, pigs, and humans.[20,22,55] As such, dosing and delivery of VNS therapy, analogous to medications, has substantial impact on its efficacy and unintended off-target effects. Considerable differences in neural targets and stimulation parameters were evident in the three major trials of chronic VNS for heart failure.[17] The Autonomic Regulation Therapy to Enhance Myocardial Function in Heart Failure (ANTHEM-HF) operated at VNS parameters consistent with the neural fulcrum and led to improvements in both left ventricular function and quality of life, with a larger trial currently underway.[56,57] On the other hand, the VNS delivery modality and stimulation parameters for the two other major trials suffered from an inability to reach target VNS parameters due to side

effects, which may partly explain the lack of clinical efficacy observed.[17-19,58] Furthermore, a post hoc analysis of the Neural Cardiac Therapy For Heart Failure (NECTAR-HF) trial, which found no improvement in left ventricular function with chronic VNS, demonstrated poor engagement of the autonomic nervous system among patients (12%) randomized to VNS therapy.[58] The present work provides definitive evidence that chronic VNS exerts significant antiarrhythmic effects and mitigates aberrant cardiac and neural remodeling in large mammals when delivered in a rational, neuroscience-guided manner. Such factors must be considered in further clinical trials of VNS or other device-based therapy.

The present study has several limitations inherent to its design and defined objectives. We solely evaluated efficacy of right-sided VNS, which is the more commonly utilized modality in the clinical setting. Pigs were titrated to neural fulcrum prior to MI. To demonstrate that our findings were mediated by chronic VNS after MI rather than VNS-induced cardioprotection evolving from the titration phase, VNS was turned off before MI induction and not restarted until 2 days following MI. Furthermore, a group of animals, termed sham VNS + MI, were similarly titrated to neural fulcrum, underwent MI, but received no reactive VNS therapy after MI. Our sensitivity analysis clearly demonstrates that these animals were identical to MI alone with regards to myocardial performance, ventricular activation and repolarization properties, arrhythmia inducibility, and scar-border zone histologic characteristics. In addition, our evaluation of cardiac mechanical function was performed in the sedated state, as echocardiography was not feasible in the conscious state in pigs. Among our cohort, six animals died within 48 hours following myocardial infarction due to sudden cardiac death despite

standard cardiopulmonary resuscitation. These animals were likely more susceptible to malignant ventricular arrhythmias, and may have derived more substantial benefit from chronic VNS, as prior studies have found greater impairment in parasympathetic function in animals susceptible to ischemia-induced arrhythmias compared to those resistant.[59,60] Further work is necessary to delineate the specific mechanisms by which chronic VNS imparts its cardioprotective effects.

In summary, our data highlights that chronic VNS ameliorates myocardial structural and extracardiac neural remodeling that occurs early after MI, preventing heart failure. Chronic VNS stabilizes the left ventricular scar-border zone by reducing heterogeneity in activation and repolarization in vivo, drastically reducing the potential for lethal ventricular arrhythmias. Chronic VNS likewise improves sympathetic control of the heart post-MI, an effect that should result in a more robust reflex response to everyday cardiovascular stressors and translate into improved quality of life. Moreover, chronic VNS substantially reduced extracardiac neural remodeling following MI, particularly glial activation in the stellate and dorsal root ganglia. This data suggests that restoration of parasympathetic function, whether pharmacologically or through neuromodulation, is an attractive therapeutic strategy for MI.

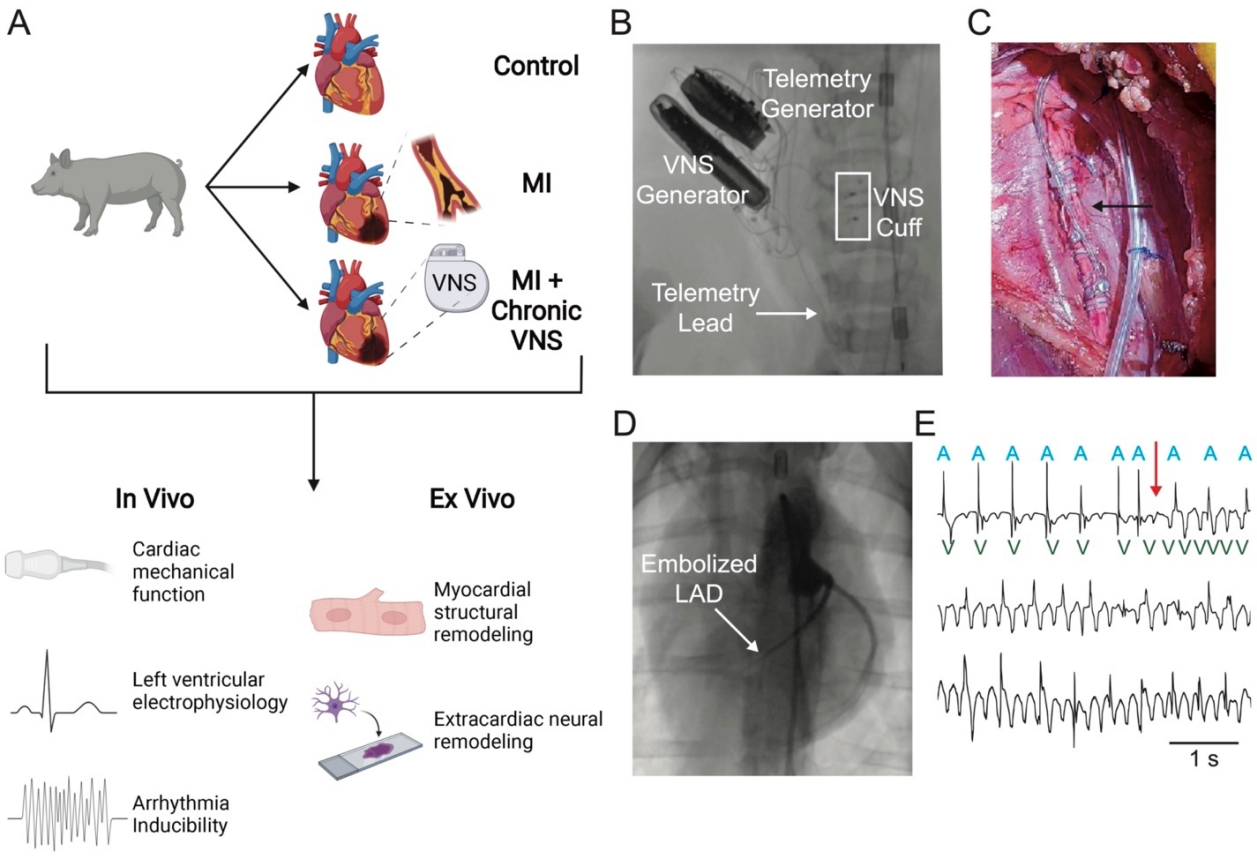

Figure 19. Overview of study design. (A) Control, MI, and MI + chronic VNS Yucatan minipigs underwent in vivo evaluation of cardiac mechanical and electrophysiologic function, as well as ex vivo myocardial and extracardiac neural remodeling. Representative x-ray (B) and image of implanted VNS generator and cuff to the right vagus nerve. (D) Left coronary angiogram after microsphere embolization of the mid left anterior descending coronary artery. (E) Spontaneous ventricular tachycardia in an ambulatory pig observed two days following MI, which led to sudden death. Atrial activation is noted with A, while ventricular noted with V. LAD, left anterior descending coronary artery; MI, myocardial infarction; VNS, vagal nerve stimulation. Portions of this figure were created with BioRender.com.

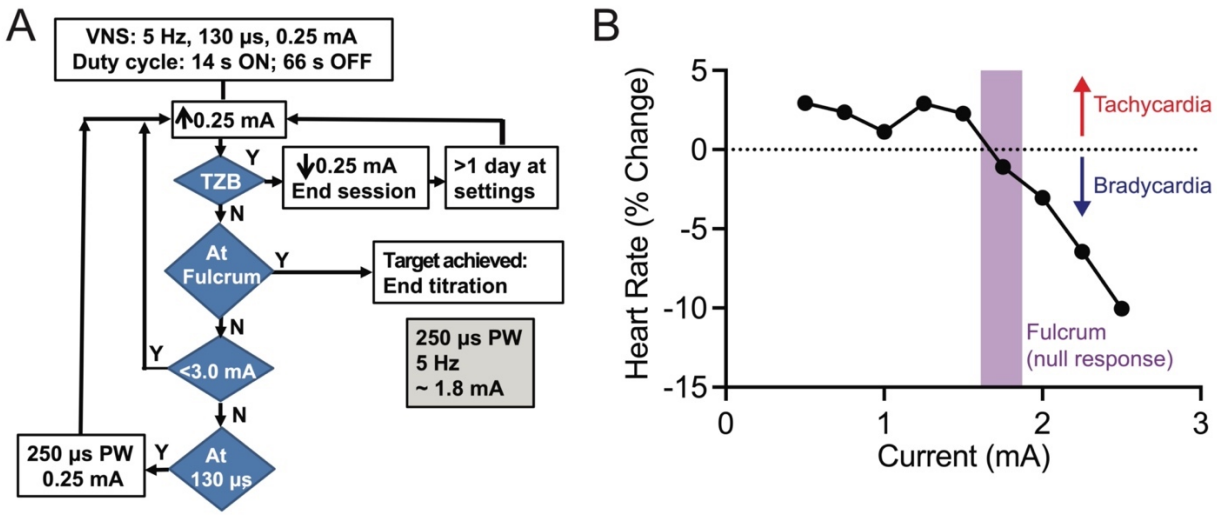

Figure 20. Implementation of chronic vagal nerve stimulation. (A) Diagram of VNS titration protocol to deliver therapeutic VNS at the neural fulcrum. (B) Representative titration curve in conscious minipig demonstrating evoked tachycardia at low-intensity stimulation, followed by bradycardia. VNS therapy was delivered at the neural fulcrum, the point of balanced activation of vagal afferent and efferent fibers, manifested by a null heart rate response (purple). PW, pulse width; TZB, tolerance zone boundary (current level at which side effects elicited); VNS, vagal nerve stimulation.

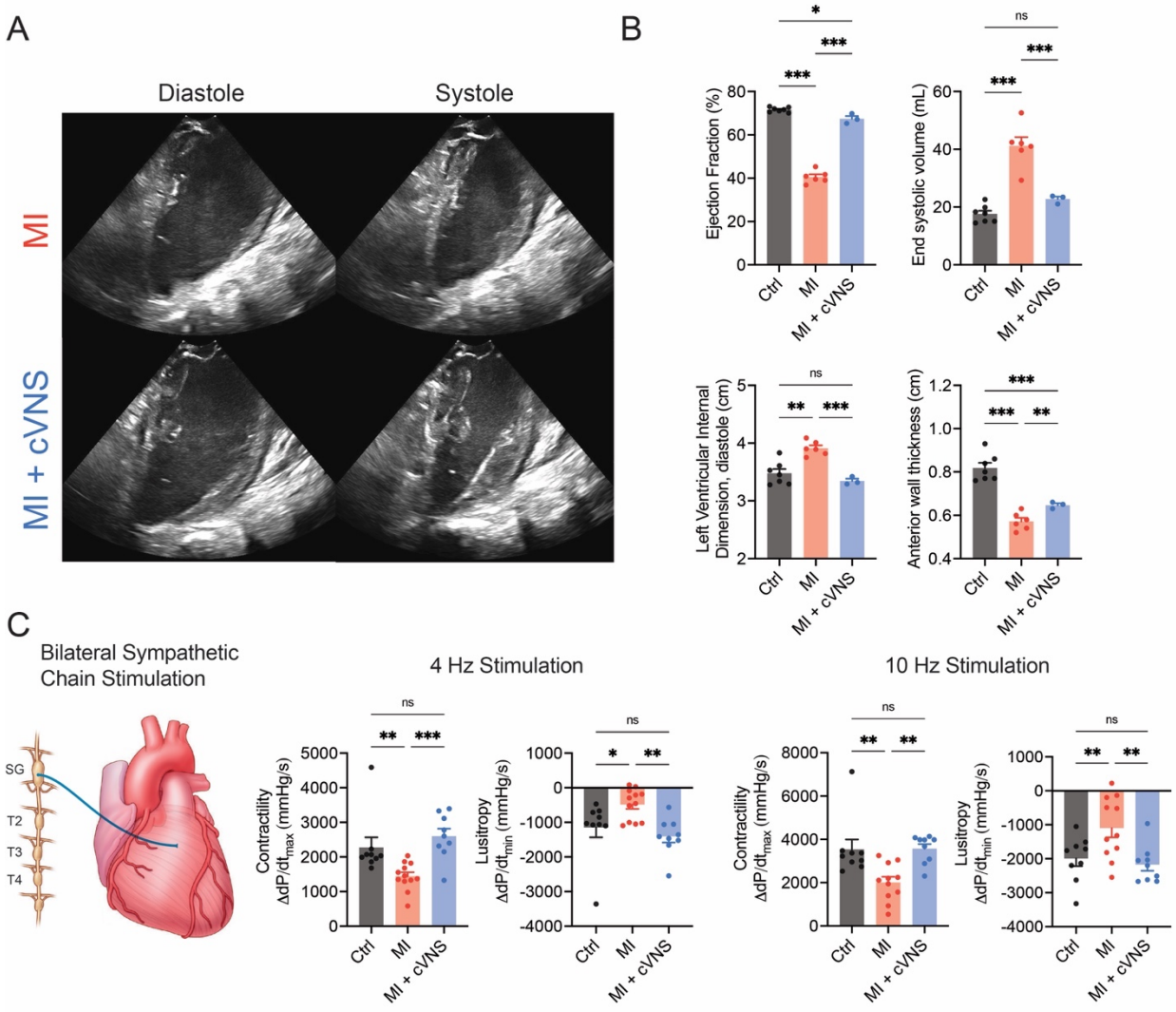

Figure 21. Chronic vagal nerve stimulation improves cardiac mechanical performance and contributes to greater cardiac sympathetic reserve post myocardial infarction. (A) Representative long-axis echocardiograms of MI and MI + cVNS animals. Note the degree of chamber dilation and high end-systolic volume in MI compared to MI + cVNS. (B) MI resulted in a significant reduction in left ventricular systolic function, with lower ejection fraction and higher left ventricular internal dimension in diastole, which was ameliorated by cVNS. (C) MI animals had impaired inotropic (dP/dt_{max}) and lusitropic (dP/dt_{min}) sympathetic responses to both 4 Hz and 10

Hz bilateral sympathetic chain stimulation, which was rescued by cVNS. Ctrl, control; cVNS, chronic vagal nerve stimulation; MI, myocardial infarction. *p<0.05, **p<0.01, ***p<0.001.

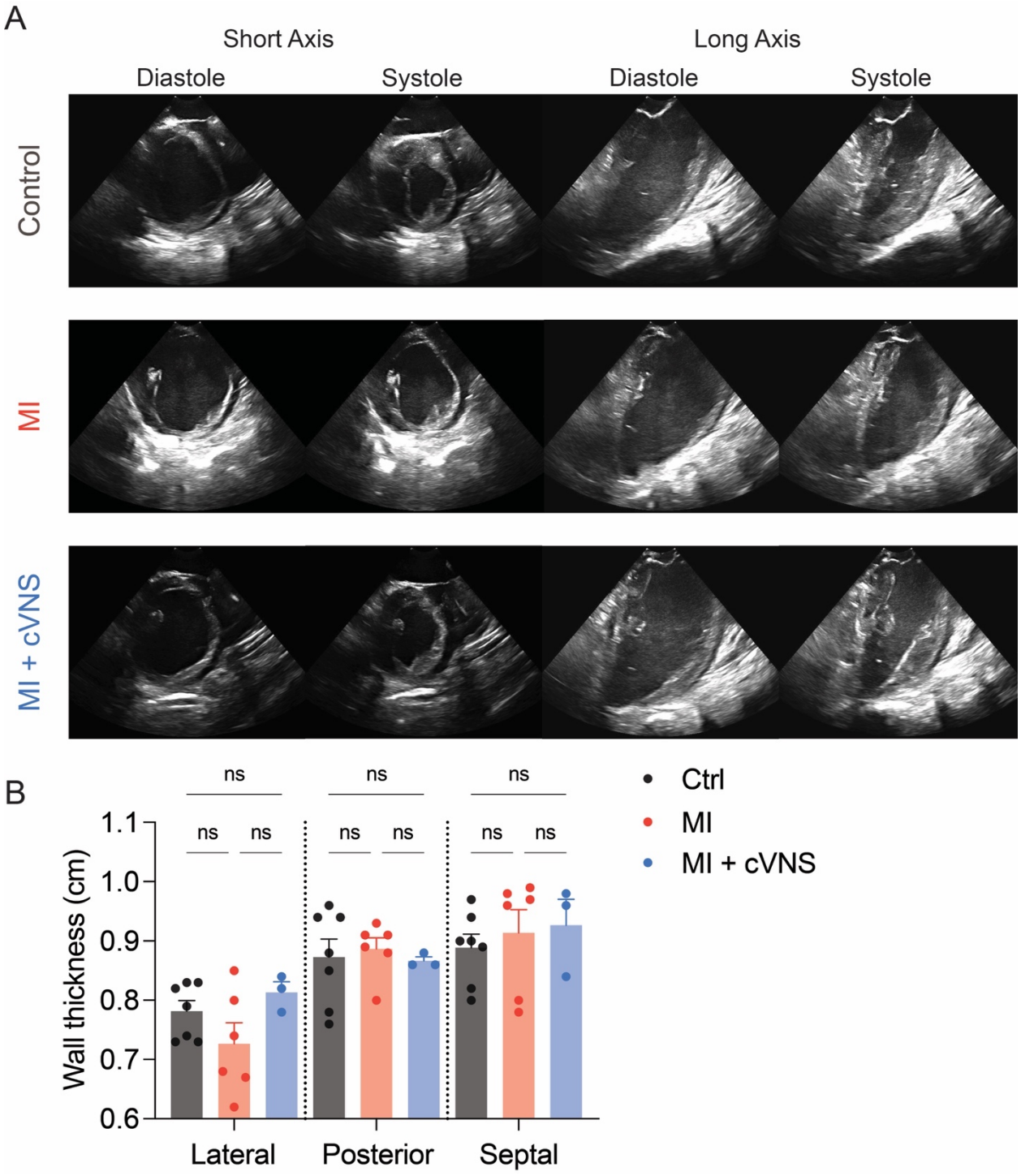

Figure 22. Full echocardiographic analysis for control, MI, and MI + cVNS animals. (A) Representative long-axis and short-axis views in systole and diastole for each study group. (B) No difference in wall thickness of the lateral, posterior, and septal wall was

evident following MI or with cVNS relative to controls. LVIDs, left ventricular internal dimension in systole.

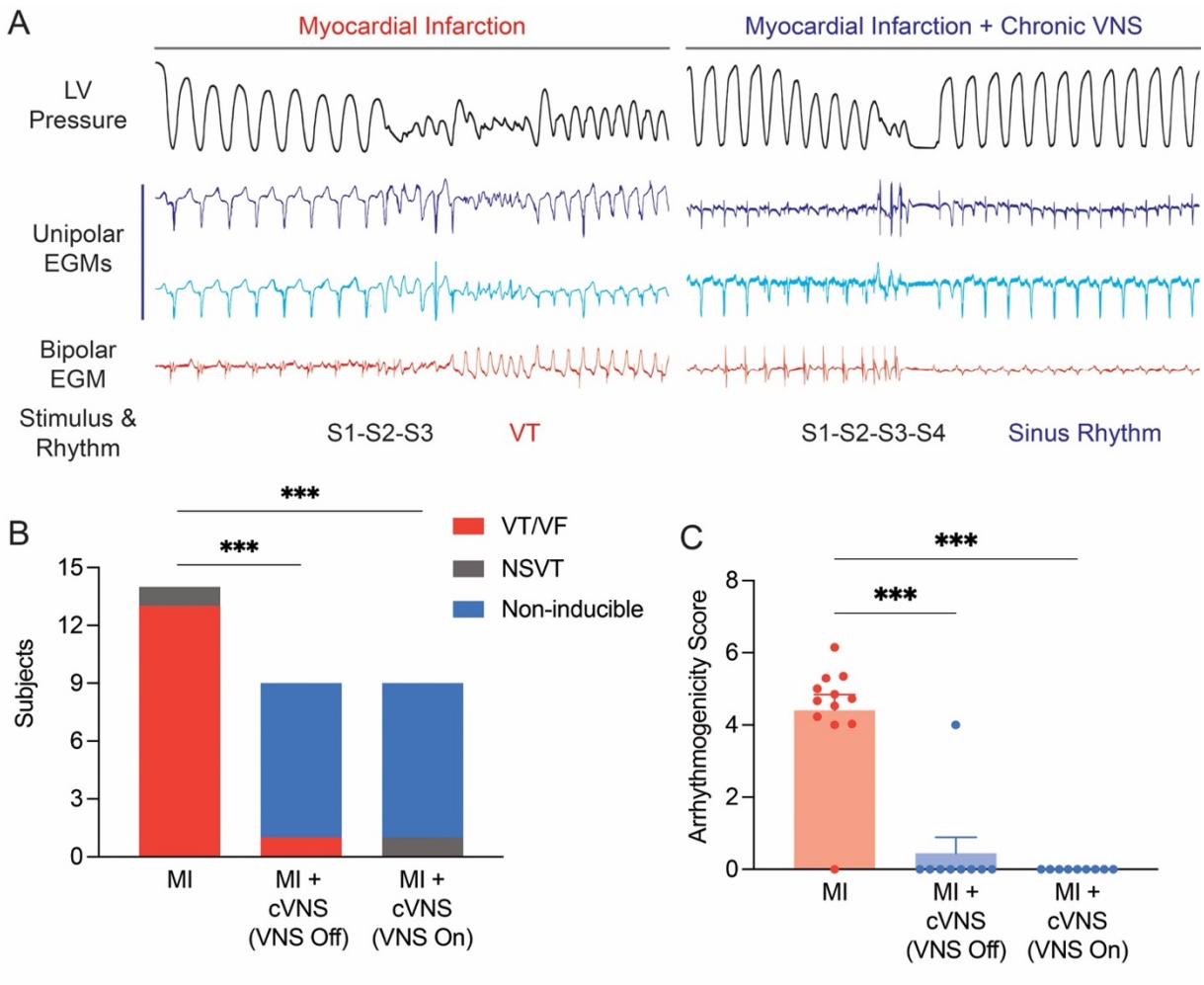

Figure 23. Antiarrhythmic effects of chronic vagal nerve stimulation. (A) Representative left ventricular pressure tracing, and unipolar and bipolar electrograms during programmed electrical stimulation in MI and MI + cVNS animal. (B) Chronic VNS significantly reduced the inducibility of sustained VT or VF regardless of whether PES was performed with or without active VNS. (C) MI animals demonstrated significantly greater ease of VT/VF induction compared to MI + cVNS pigs. Ctrl, control; cVNS, chronic vagal nerve stimulation; EGM; electrogram; LV, left ventricular; MI, myocardial infarction; NSVT, non-sustained ventricular tachycardia; PES, programmed electrical stimulation; VF, ventricular fibrillation; VT, ventricular tachycardia. ***p<0.001.

Myocardial Infarction

	S1	S2	S3	S4	VT or VF
Subject 1	Spontaneous				Yes
Subject 2	550	370	260	240	Yes
Subject 3	520	300	250		Yes
Subject 4	460	260	250		Yes
Subject 5	500	310	280	270	Yes
Subject 6	Spontaneous				Yes
Subject 7	450	300	220	240	Yes
Subject 8	450	320	220	210	Yes
Subject 9	500	240	280	250	Yes
Subject 10	450	320	270	200	NSVT
Subject 11	650	330	220	200	Yes
Subject 12	500	280	220		Yes
Subject 13	580	280	200		Yes
Subject 14	600	370	260		Yes

Myocardial Infarction + Chronic VNS (VNS Off)

	S1	S2	S3	S4	VT or VF
Subject 1	500	290	200	210	Yes
Subject 2	430	240	220	200	No
Subject 3	350	200	200	200	No
Subject 4	510	280	220	200	No
Subject 5	440	230	220	200	No
Subject 6	540	280	220	200	No
Subject 7	400	220	220	200	No
Subject 8	420	250	220	200	No
Subject 9	380	220	220	200	No

Myocardial Infarction + Chronic VNS (VNS On)

	S1	S2	S3	S4	VT or VF
Subject 1	575	340	280	220	No
Subject 2	480	380	300	260	No
Subject 3	420	250	220	200	No
Subject 4	545	300	240	220	No
Subject 5	500	270	220	200	No
Subject 6	620	290	220	200	No
Subject 7	440	240	220	200	No
Subject 8	550	280	220	200	NSVT
Subject 9	450	220	220	200	No

Figure 24. Full arrhythmia inducibility data at terminal experiments. Values represent paced cycle length for programmed electrical stimulation. Note that two MI animals experienced spontaneous VT/VF during terminal study and could not be resuscitated despite internal cardioversion, which did not occur with any MI + cVNS animals. cVNS, chronic vagal nerve stimulation; MI, myocardial infarction; NSVT, non-sustained ventricular tachycardia; VF, ventricular fibrillation; VT, ventricular tachycardia.

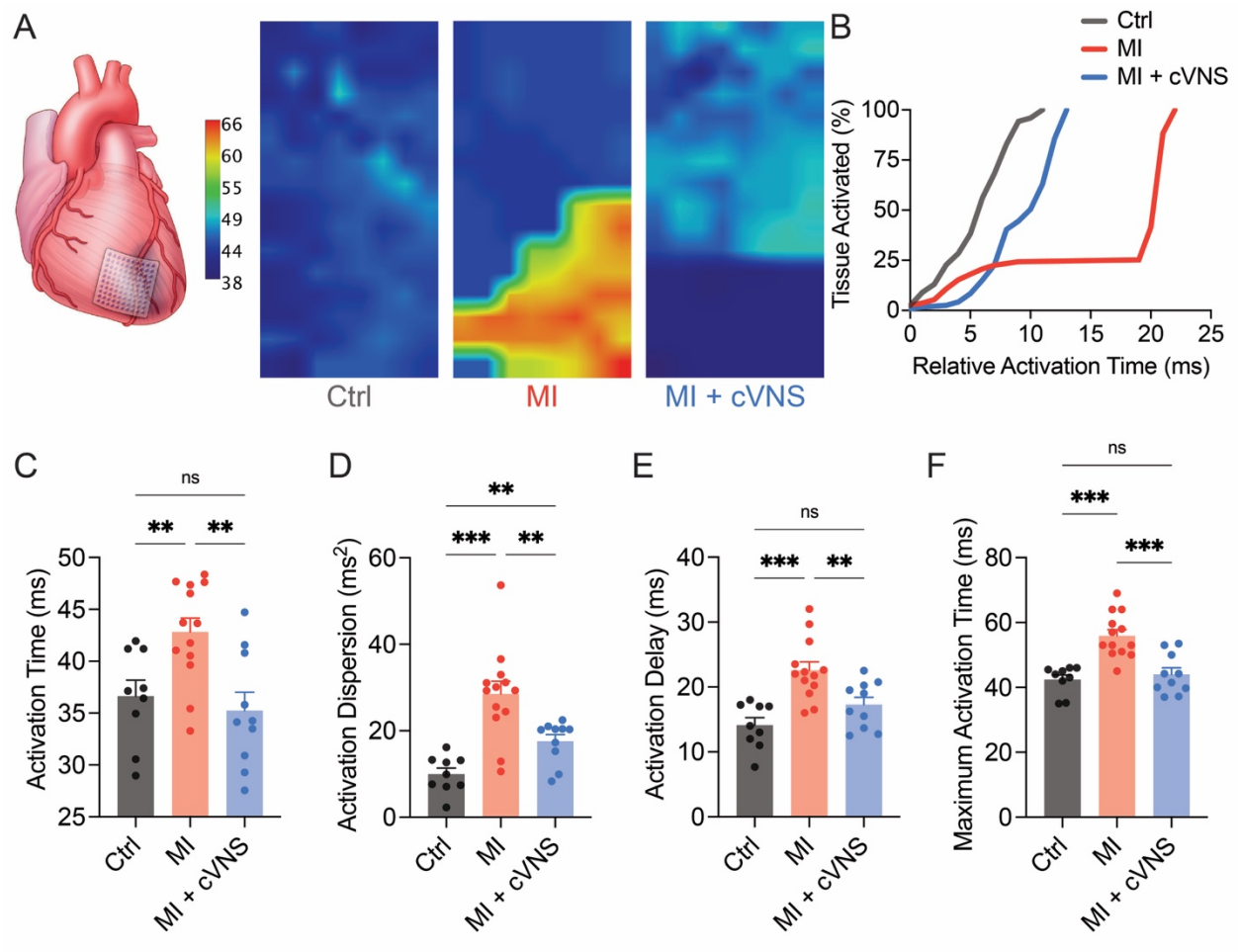

Figure 25. Chronic vagal nerve stimulation stabilizes electrical activation across the infarcted left ventricle, mitigates conduction block, and promotes homogeneous activation in sinus rhythm. (A) High-density electrophysiologic mapping was performed across the left ventricular scar-border zone (and equivalent region in control), representative activation maps for control, MI and MI + cVNS displayed. (B) Representative tissue activation curve demonstrating isotropic conduction in control animals compared to anisotropic conduction with block in MI, which was qualitatively improved with cVNS. (C-F) MI animals displayed significantly worse activation properties in sinus rhythm including greater activation time, dispersion, delay, and maximum activation time. These were all normalized in MI + cVNS animals, except

activation dispersion (D). Ctrl, control; cVNS, chronic vagal nerve stimulation; MI, myocardial infarction. **p<0.01, ***p<0.001.

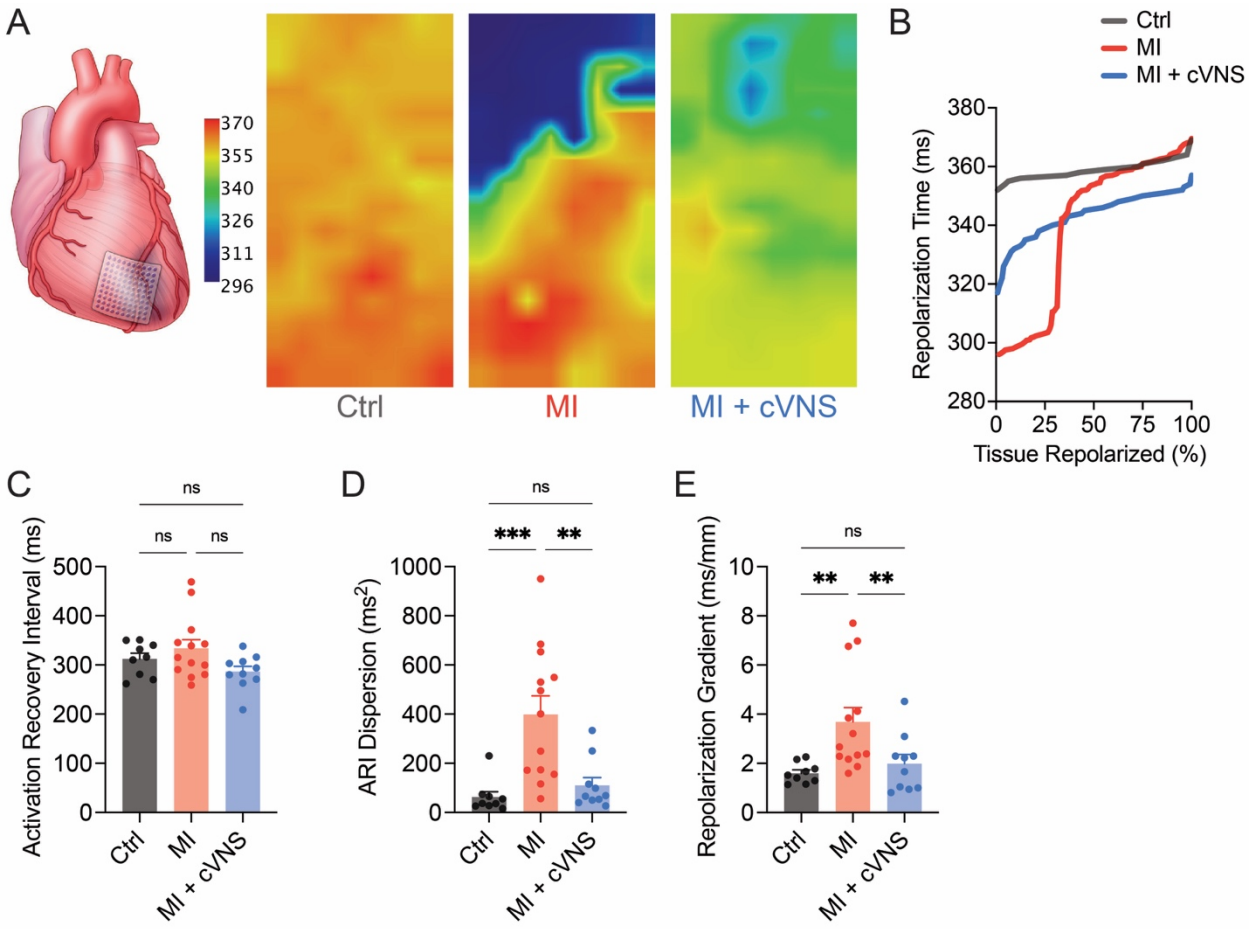

Figure 26. Chronic vagal nerve stimulation reduces repolarization heterogeneity and leads to more shallow repolarization gradients. (A) Representative repolarization maps for control, MI and MI + cVNS demonstrating very steep and heterogeneous repolarization across the scar-border zone in MI animals, which was qualitatively improved in MI + cVNS. (B) Representative tissue repolarization curve demonstrating regions of rapid changes in repolarization time in an MI animal. (C) No significant difference in left ventricular ARI was evident in the studied groups, while MI resulted in greater ARI heterogeneity, which was partially improved with cVNS (D). Repolarization gradients (E) were significantly greater in MI animals, and normalized

with cVNS. ARI, activation recovery interval; Ctrl, control; cVNS, chronic vagal nerve stimulation; MI, myocardial infarction. **p<0.01, ***p<0.001.

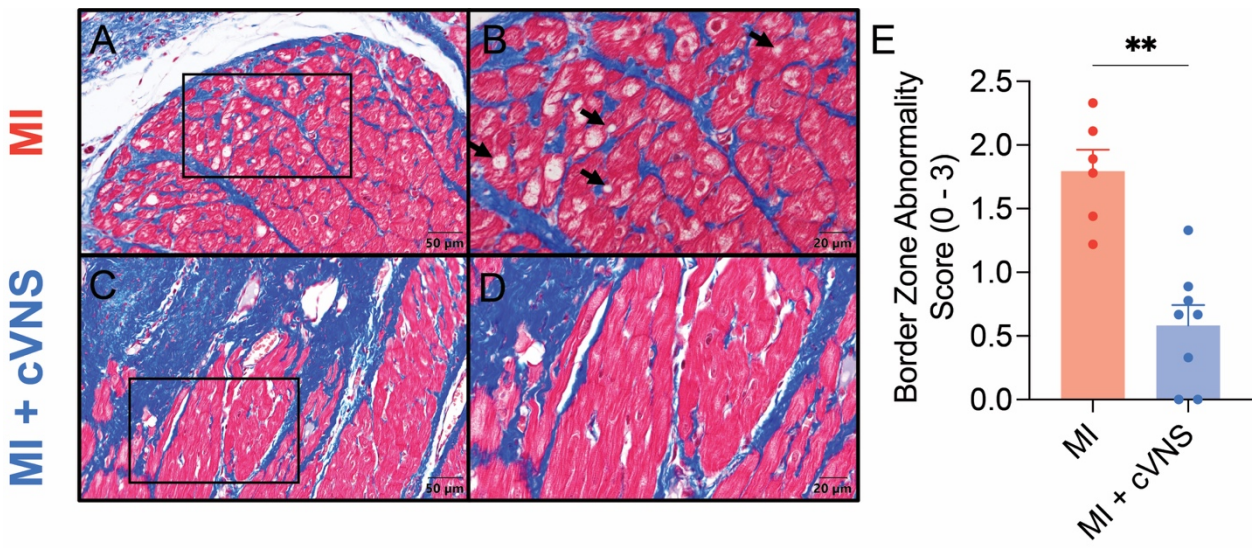

Figure 27. Chronic vagal nerve stimulation mitigates structural remodeling at the scar-border zone. Representative Masson's trichrome stains from MI (A, inset B) and MI + cVNS (C, inset D) animals. MI animals more commonly had myocytolysis (arrow), hypertrophy, and decreased muscle band staining. which was less common in MI + cVNS animals (D, inset E). cVNS, chronic vagal nerve stimulation; MI, myocardial infarction. **p<0.01.

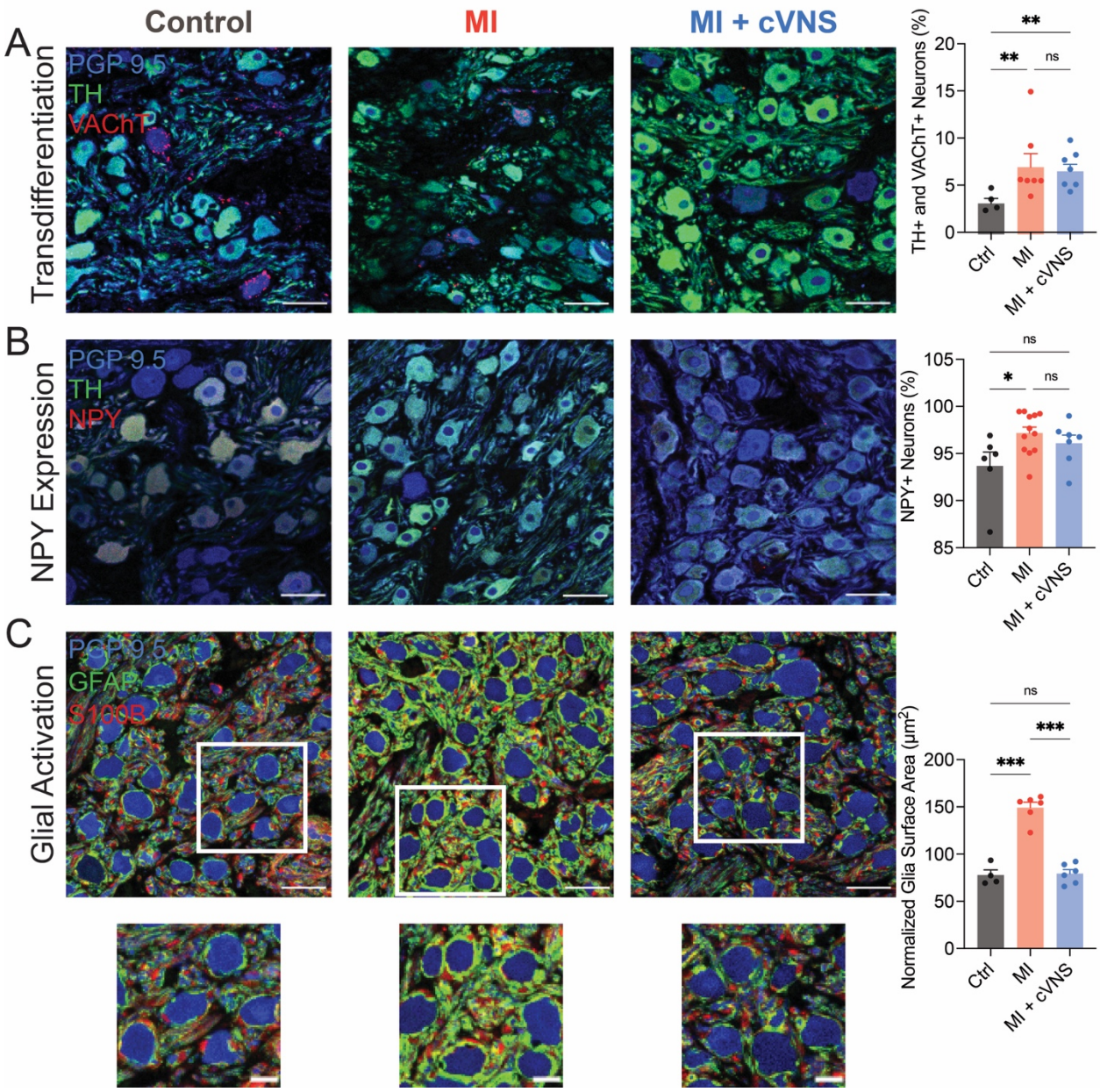

Figure 28. Chronic vagal nerve stimulation reduces extracardiac neural remodeling in the stellate ganglia. (A) Cholinergic transdifferentiation occurred following MI in both MI and MI + cVNS groups, and was unaffected by cVNS therapy. (B) Expression of neuropeptide Y (NPY) in the stellate ganglia was greater in MI animals compared to control, but similar in MI + cVNS pigs relative to control. (C) Glial activation significantly increased in MI animals compared to controls, which was

ameliorated in MI + cVNS. Ctrl, control; cVNS, chronic vagal nerve stimulation; MI, myocardial infarction. Ctrl, control; cVNS, chronic vagal nerve stimulation; GFAP, glial fibrillatory acidic protein; MI, myocardial infarction; NPY, neuropeptide Y; PGP9.5, protein gene product 9.5; S100B, S100 calcium-binding protein B; TH, tyrosine hydroxylase; VAChT, vesicular acetylcholine transporter. Scale bar 50 μm except insets (scale bar 20 μm). *$p<0.05$, **$p<0.01$, ***$p<0.001$.

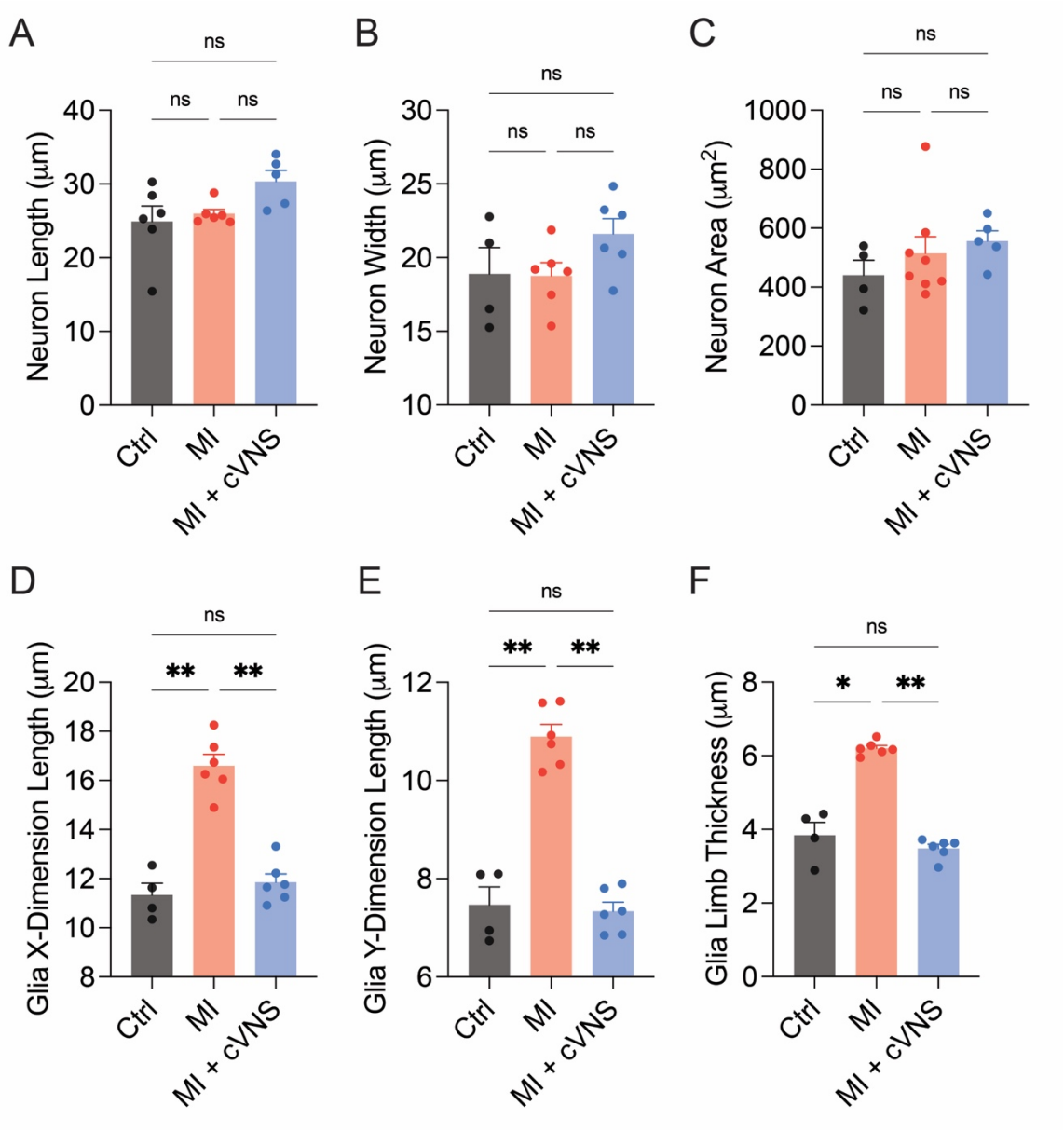

Figure 29. Chronic vagal nerve stimulation primarily impacts glial morphology in the stellate ganglia following myocardial infarction. Stellate ganglia neuron length (A), width (B), and area (C) were comparable across control, MI, and MI + cVNS animals. Stellate ganglia glial size (D, E) and limb thickness (F) significantly increased after MI, which was mitigated by cVNS. Ctrl, control; cVNS, chronic vagal nerve stimulation; MI, myocardial infarction.

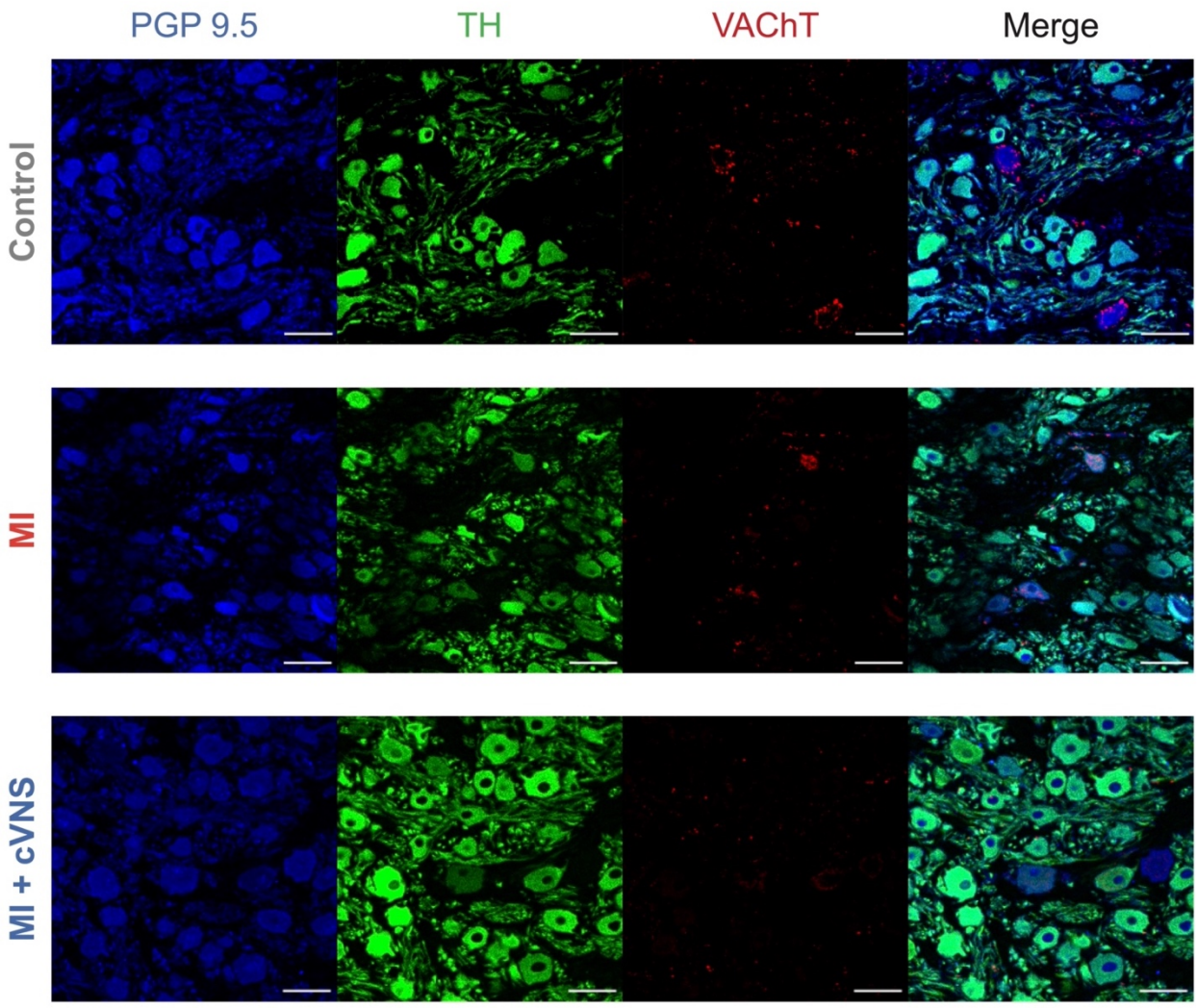

Figure 30. Representative confocal images of stellate ganglia sections for evaluation of cholinergic transdifferentiation. Ctrl, control; cVNS, chronic vagal nerve stimulation; MI, myocardial infarction; PGP9.5, protein gene product 9.5; TH, tyrosine hydroxylase; VAChT, vesicular acetylcholine transporter. Scale bar 50 μm.

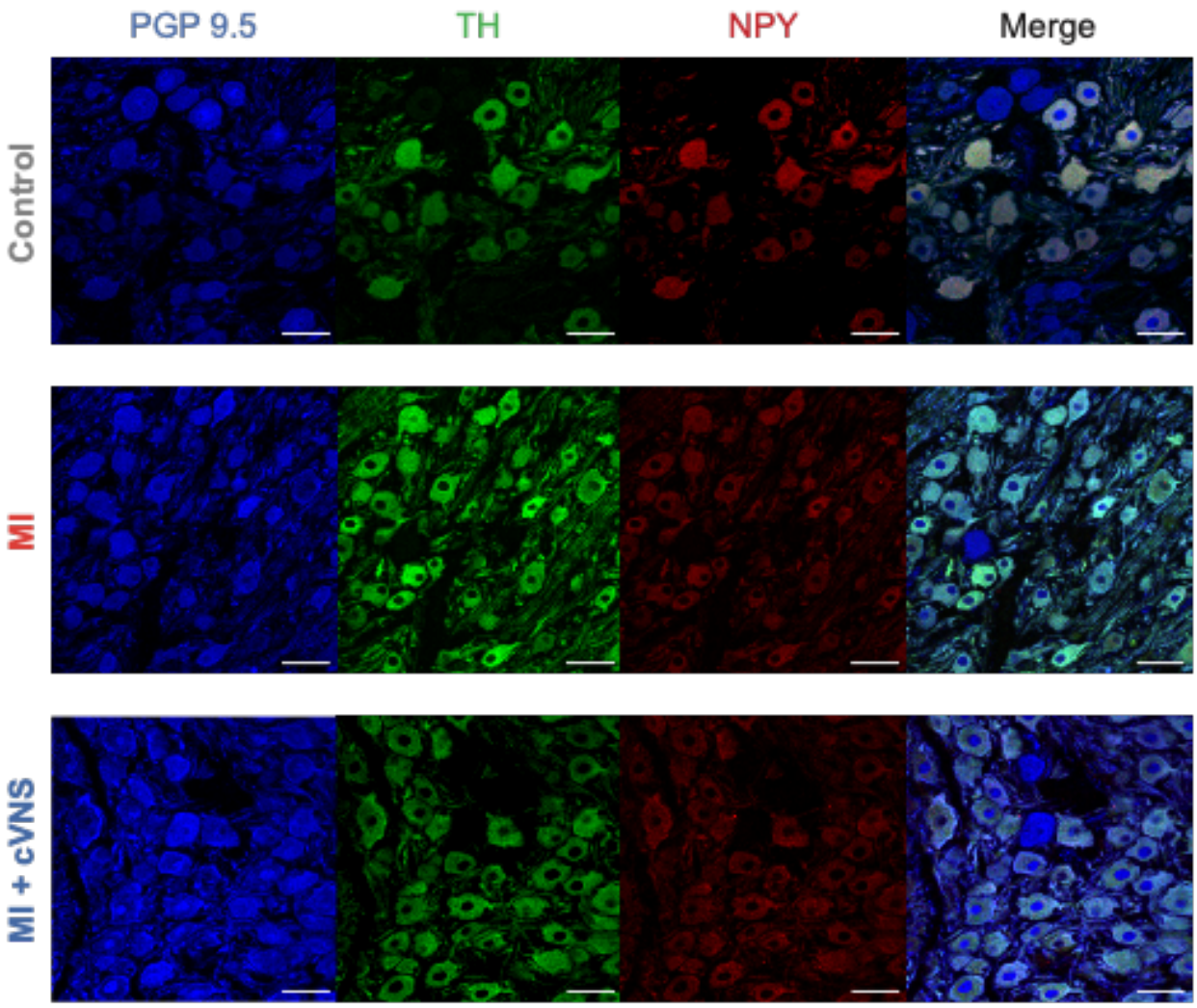

Figure 31. Representative confocal images of stellate ganglia sections for evaluation of neuropeptide Y expression. Ctrl, control; cVNS, chronic vagal nerve stimulation; MI, myocardial infarction; NPY, neuropeptide Y; PGP9.5, protein gene product 9.5; TH, tyrosine hydroxylase. Scale bar 50 μm.

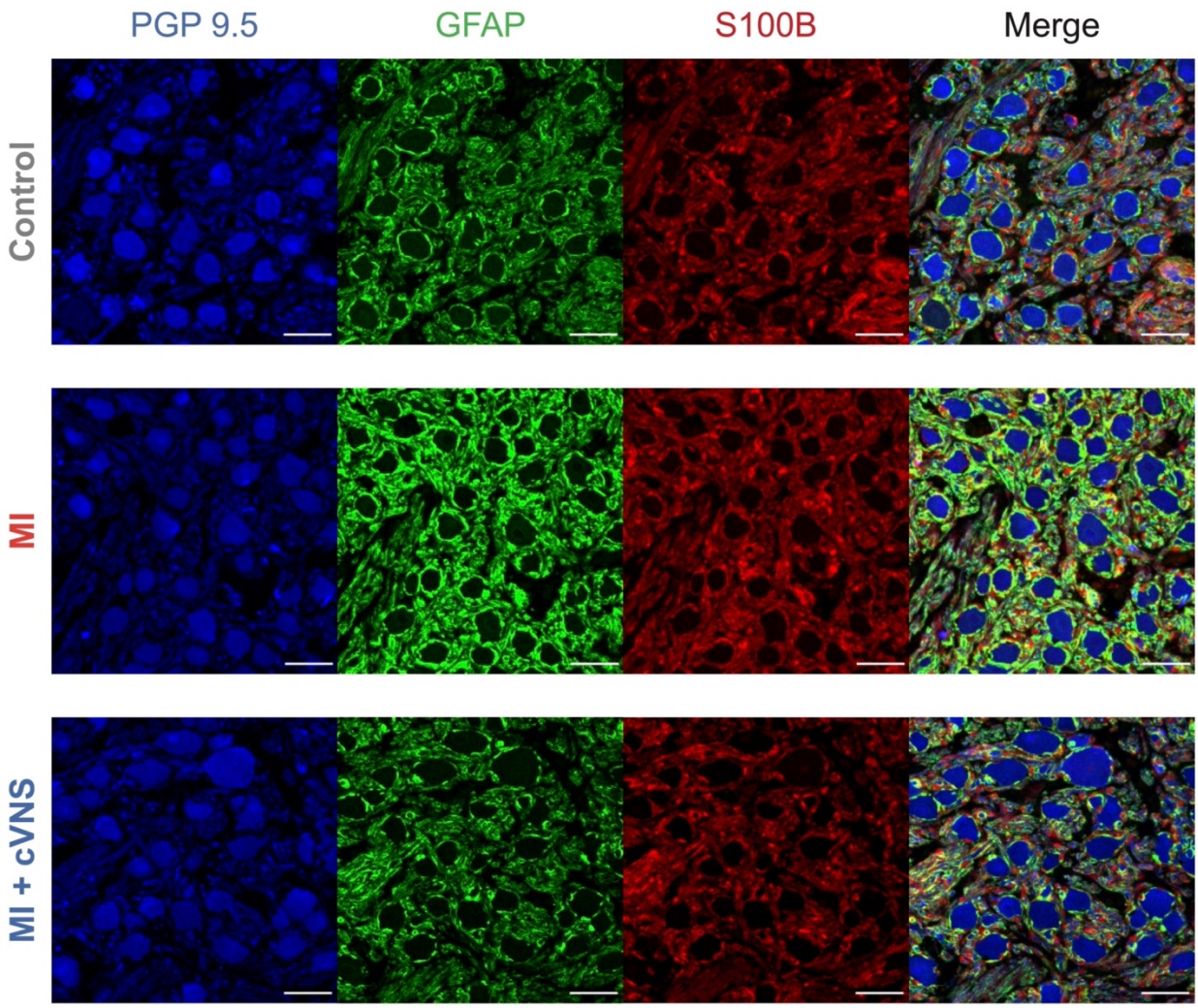

Figure 32. Representative confocal images of stellate ganglia sections for evaluation of glial activation. Ctrl, control; cVNS, chronic vagal nerve stimulation; GFAP, glial fibrillatory acidic protein; MI, myocardial infarction; PGP9.5, protein gene product 9.5; S100B, S100 calcium-binding protein B. Scale bar 50 μm.

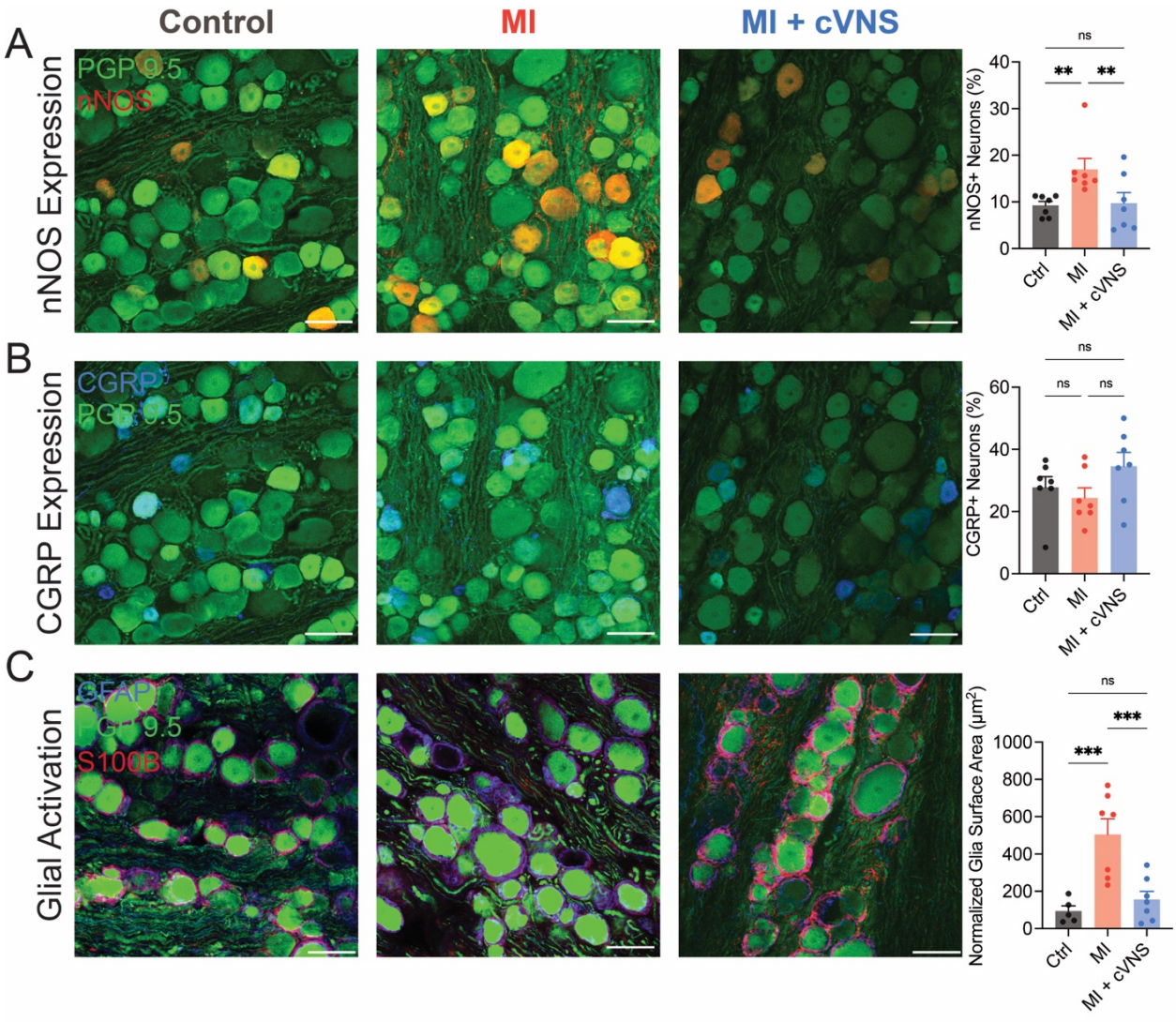

Figure 33. Chronic vagal nerve stimulation reduces glial activation after MI in the thoracic dorsal root ganglia. (A) Neuronal nitric oxide synthase expression significantly increased following MI, which was mitigated by chronic VNS. (B) No difference was evident in calcitonin gene-related peptide expression across study groups. (C) MI resulted in significantly greater glial activation in the thoracic dorsal root ganglia, which was significantly reduced in MI + cVNS animals. CGRP, calcitonin gene-related peptide; Ctrl, control; cVNS, chronic vagal nerve stimulation; GFAP, glial fibrillatory acidic protein; MI, myocardial infarction; nNOS, neuronal nitric oxide

synthase; PGP9.5, protein gene product 9.5; S100B, S100 calcium-binding protein B. Scale bar 50 μm. **p<0.01, ***p<0.001.

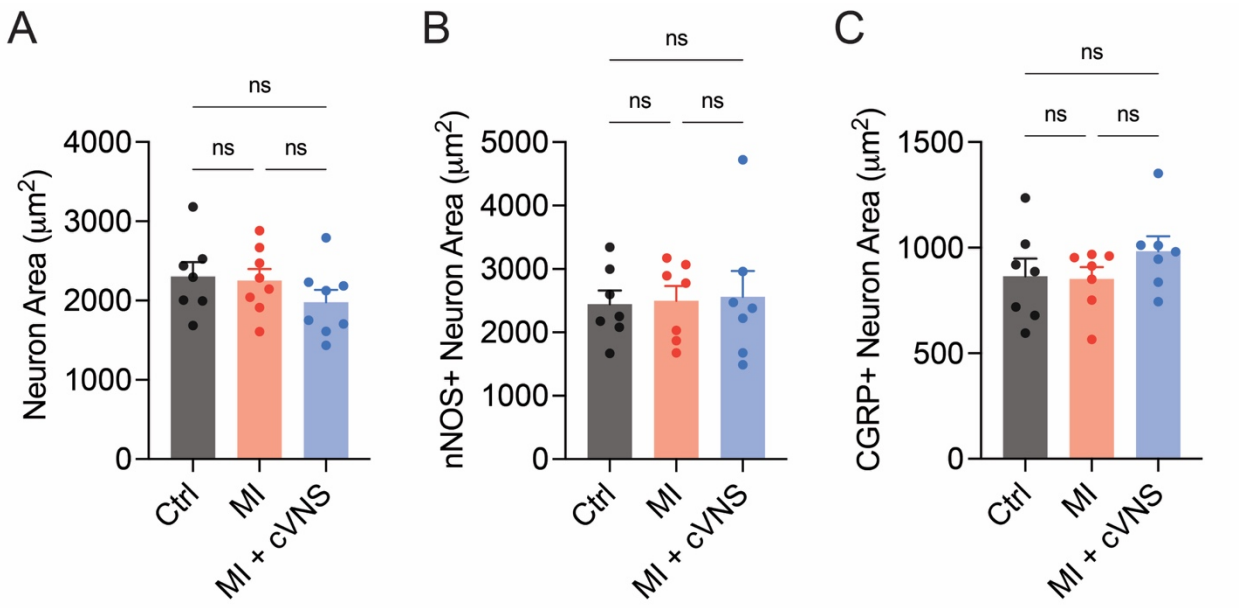

Figure 34. Chronic vagal nerve stimulation does not impact neuron size in the thoracic dorsal root ganglia. No significant differences in overall neuron area (A), nNOS+ neuron area (B), or CGRP+ neuron area (C) were found across study groups. Ctrl, control; cVNS, chronic vagal nerve stimulation; MI, myocardial infarction.

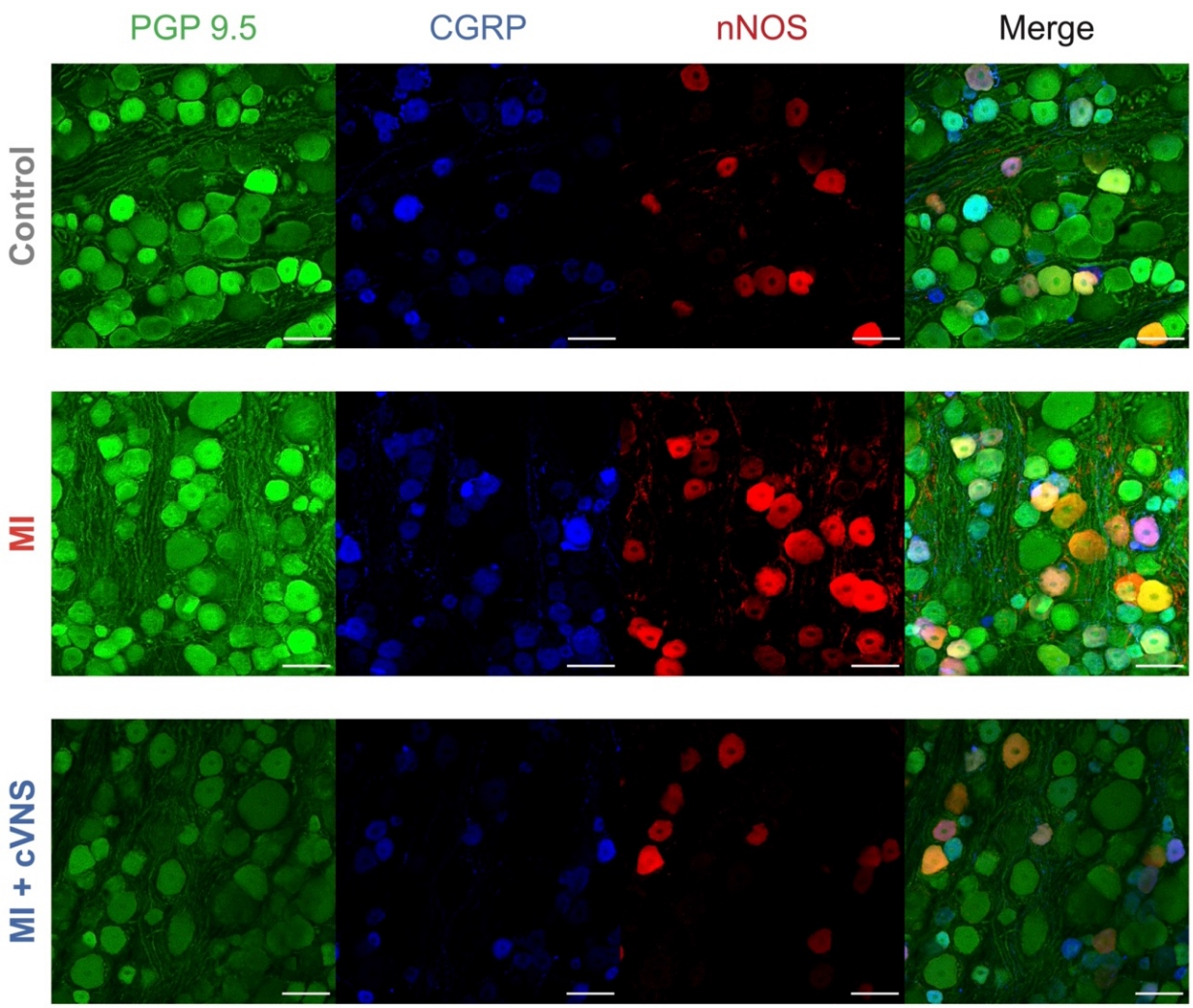

Figure 35. Representative confocal images of first thoracic dorsal root ganglia sections for evaluation neuronal nitric oxide synthase and calcitonin gene related peptide expression. CGRP, calcitonin gene-related peptide; Ctrl, control; cVNS, chronic vagal nerve stimulation; MI, myocardial infarction; nNOS, neuronal nitric oxide synthase; PGP9.5, protein gene product 9.5; Scale bar 50 μm.

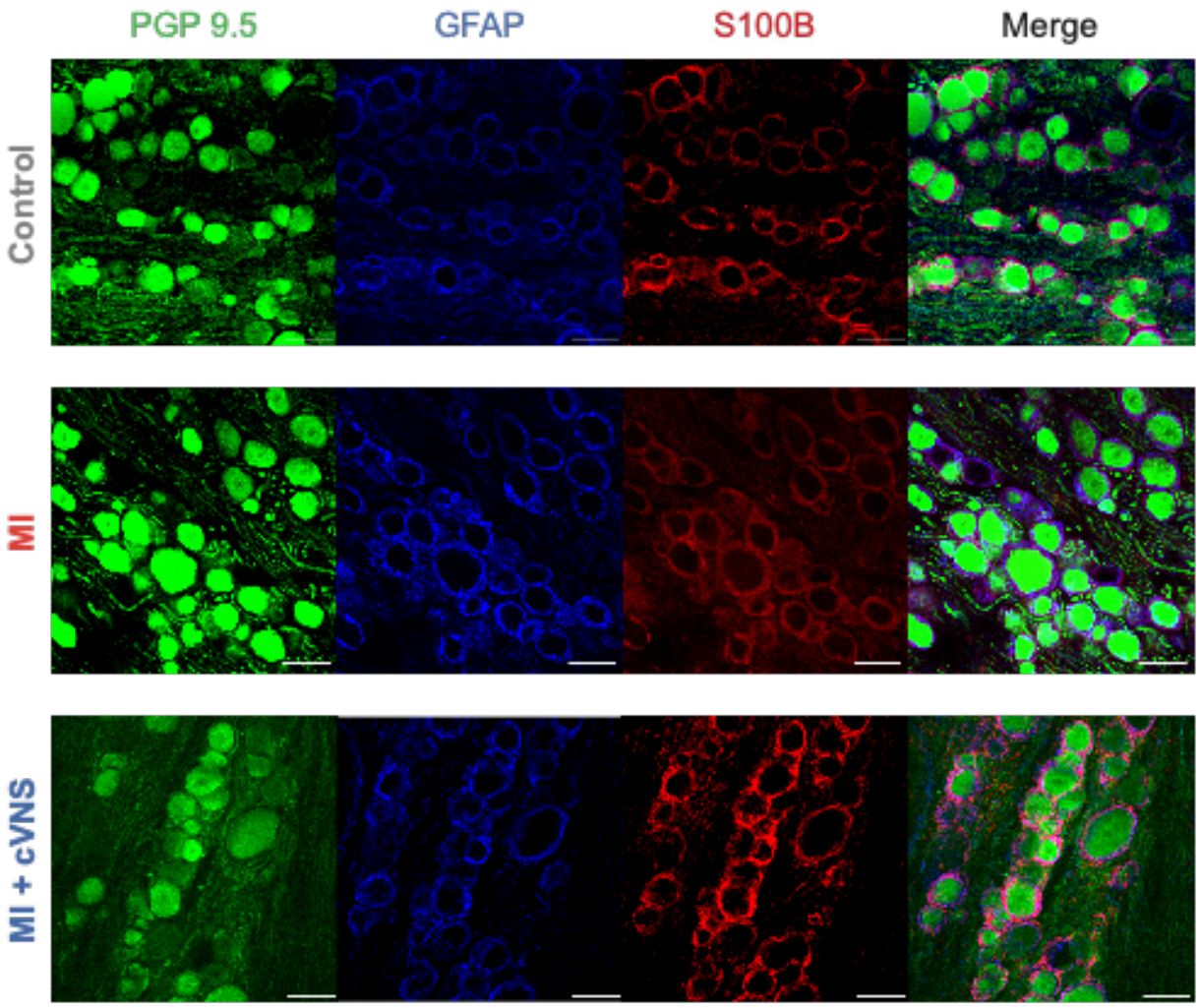

Figure 36. Representative confocal images of first thoracic dorsal root ganglia sections for evaluation of glial activation. Ctrl, control; cVNS, chronic vagal nerve stimulation; GFAP, glial fibrillatory acidic protein; MI, myocardial infarction; PGP9.5, protein gene product 9.5; S100B, S100 calcium-binding protein B. Scale bar 50 μm.

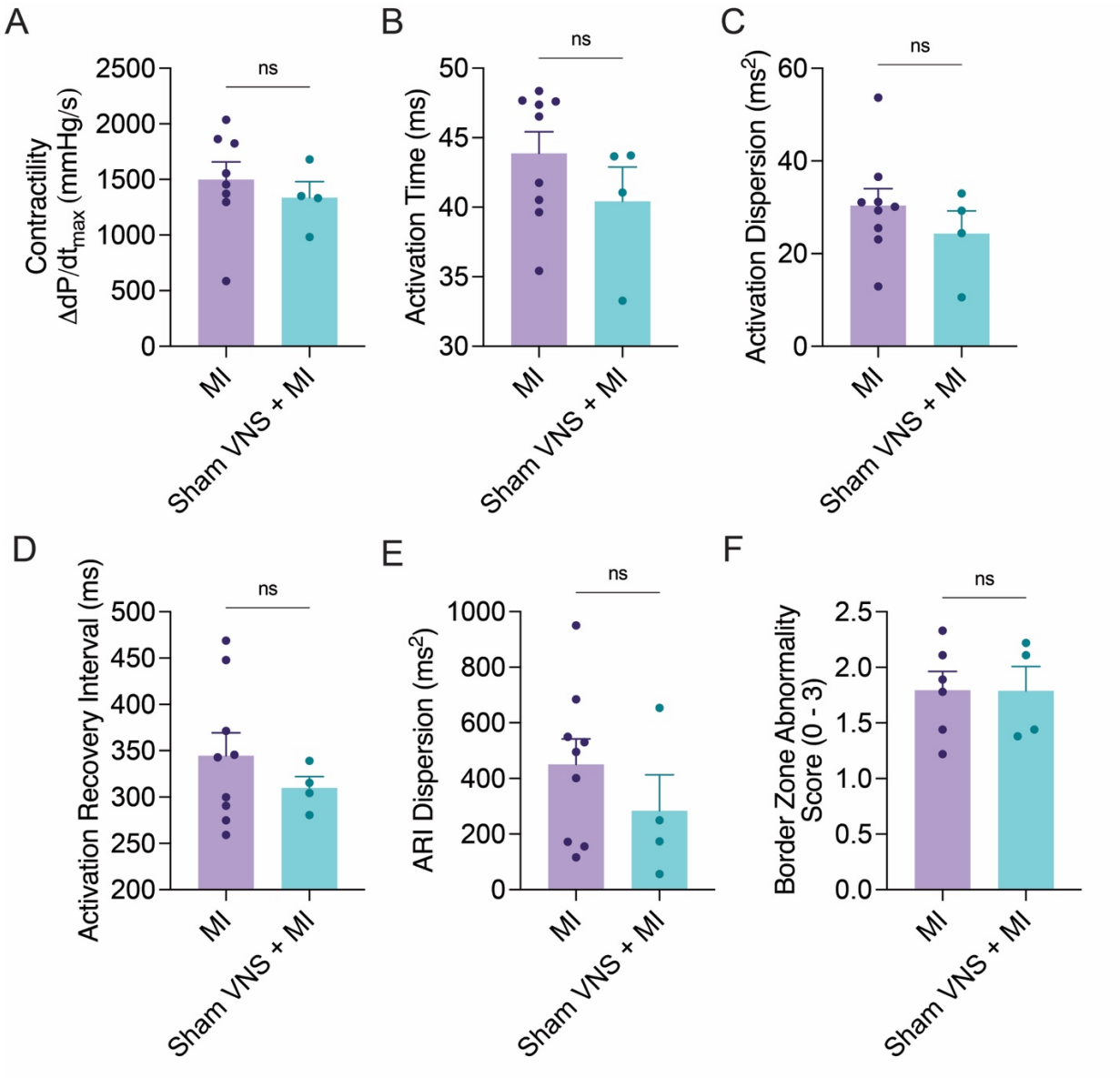

Figure 37. Sham VNS + MI animals were phenotypically comparable to MI animals alone. There were no significant differences in changes in contractility evoked by sympathetic stimulation (A), activation dynamics (B, C), myocardial repolarization properties (D, E), or structural remodeling of the border zone (F) in sham VNS + MI animals compared to MI animals alone. ARI, activation recovery interval; dP/dt_{max}, maximum rate of change of left ventricular pressure (contractility); MI, myocardial infarction; VNS, vagal nerve stimulation.

Primary Antibody	Type	Dilution	Company and Catalog Number
Protein Gene Product 9.5	Polyclonal Guinea Pig	1:500	Neuromics. Edina, Minnesota. GP14104.
Protein Gene Product 9.5	Monoclonal Mouse	1:100	Abcam. Cambridge, Massachusetts. Ab8189.
Tyrosine Hydroxylase	Polyclonal Sheep	1:200	EMD Millipore. Darmstadt, Germany. Ab1542.
Neuropeptide-Y	Polyclonal Rabbit	1:400	Immunostar. Hudson, Wisconsin. 22940.
Vesicular Acetylcholine Transporter	Polyclonal Rabbit	1:200	Synaptic Systems Goettingen, Germany. 139-103.
Neuronal nitric oxide synthase	Polyclonal Goat	1:200	Abcam. Cambridge, Massachusetts. Ab1376.
S100 Calcium Binding Protein B	Polyclonal Rabbit	1:100, 1:200	Abcam. Cambridge, Massachusetts. Ab41548.
Calcitonin Gene Related Peptide	Monoclonal Mouse	1:500	Abcam. Cambridge, Massachusetts. Ab81887.
Glial Fibrillary Acidic Protein	Polyclonal Chicken	1:100, 1:1000	Abcam. Cambridge, Massachusetts. Ab4674.

Table 5. List of primary antibodies.

Secondary Antibody	Type	Dilution	Company and Catalog Number
Alexa Fluor 488 conjugated AffiniPure Donkey Anti-Sheep	Polyclonal Sheep	1:100	Jackson ImmunoResearch. West Grove, PA. 713-545-003.
Cy3 conjugated AffiniPure Donkey Anti-Goat	Polyclonal Goat	1:100	Jackson ImmunoResearch. West Grove, PA. 705-165-147.
Cy3 conjugated AffiniPure Donkey Anti-Rabbit	Polyclonal Rabbit	1:100	Jackson ImmunoResearch. West Grove, PA. 711-165-152.
Alexa Flour 647 AffiniPure Donkey Anti-Mouse	Polyclonal Mouse	1:100	Jackson ImmunoResearch. West Grove, PA. 715-605-151.
Alexa Fluor 488 conjugated AffiniPure Donkey Anti-Chicken	Polyclonal Chicken	1:100	Jackson ImmunoResearch. West Grove, PA. 703-545-155.
Alexa Flour 647 AffiniPure Donkey Anti-Chicken	Polyclonal Chicken	1:100	Jackson ImmunoResearch. West Grove, PA. 703-605-155.
Alexa Fluor 488 conjugated AffiniPure Donkey Anti-Guinea Pig	Polyclonal Guinea Pig	1:100	Jackson ImmunoResearch. West Grove, PA. 706-545-148.

Table 6. List of secondary antibodies.

Variable	Control	MI	MI + cVNS
Heart Rate (bpm)	105 ± 6	103 ± 4	101 ± 8
LVSP (mmHg)	128 ± 8	102 ± 4*	135 ± 7†
dP/dt_{max} (mmHg/s)	1870 ± 116	1435 ± 138*	1947 ± 164†
dP/dt_{min} (mmHg/s)	-1756 ± 131	-1235 ± 81*	-1793 ± 120†

Table 7. Baseline hemodynamics by study group. Values are reported as mean ± standard error for heart rate, left ventricular end-systolic pressure, and the maximum (dP/dt_{max}) and minimum (dP/dt_{min}) rates of change of left ventricular pressure. *$p<0.05$ for control versus MI; †$p<0.05$ for MI versus MI + cVNS; ‡$p<0.05$ for control versus MI + cVNS. cVNS, chronic vagal nerve stimulation; LVSP, left ventricular systolic pressure; MI, myocardial infarction.

Variable	Control	MI	MI + cVNS
Right sympathetic chain stimulation (mA)	0.8 ± 0.2	1.5 ± 0.4	1.3 ± 0.4
Left sympathetic chain stimulation (mA)	1.8 ± 0.5	1.4 ± 0.4	1.3 ± 0.6

Table 8. Thresholds for sympathetic chain stimulations by study group. Values are reported as mean ± standard error for right and left sympathetic chain stimulation. *$p<0.05$ for control versus MI; $^{\dagger}p<0.05$ for MI versus MI + cVNS; $^{\ddagger}p<0.05$ for control versus MI + cVNS. cVNS, chronic vagal nerve stimulation; MI, myocardial infarction.

References

1. Benjamin EJ, Virani SS, Callaway CW, Chamberlain AM, Chang AR, Cheng S, Chiuve SE, Cushman M, Delling FN, Deo R, et al. Heart Disease and Stroke Statistics-2018 Update: A Report From the American Heart Association. *Circulation*. 2018;137:e67-e492.
2. Stecker EC, Reinier K, Marijon E, Narayanan K, Teodorescu C, Uy-Evanado A, Gunson K, Jui J, Chugh SS. Public health burden of sudden cardiac death in the United States. *Circ Arrhythm Electrophysiol*. 2014;7:212-217.
3. Ardell JL, Andresen MC, Armour JA, Billman GE, Chen PS, Foreman RD, Herring N, O'Leary DS, Sabbah HN, Schultz HD, et al. Translational neurocardiology: preclinical models and cardioneural integrative aspects. *J Physiol*. 2016;594:3877-3909.
4. Fukuda K, Kanazawa H, Aizawa Y, Ardell JL, Shivkumar K. Cardiac innervation and sudden cardiac death. *Circ Res*. 2015;116:2005-2019.
5. O'Gara PT, Kushner FG, Ascheim DD, Casey DE, Jr., Chung MK, de Lemos JA, Ettinger SM, Fang JC, Fesmire FM, Franklin BA, et al. 2013 ACCF/AHA guideline for the management of ST-elevation myocardial infarction: executive summary: a report of the American College of Cardiology Foundation/American Heart Association Task Force on Practice Guidelines. *Circulation*. 2013;127:529-555.
6. Ibanez B, James S, Agewall S, Antunes MJ, Bucciarelli-Ducci C, Bueno H, Caforio ALP, Crea F, Goudevenos JA, Halvorsen S, et al. 2017 ESC Guidelines for the management of acute myocardial infarction in patients presenting with ST-

segment elevation: The Task Force for the management of acute myocardial infarction in patients presenting with ST-segment elevation of the European Society of Cardiology (ESC). *Eur Heart J*. 2018;39:119-177.

7. Schwartz PJ, La Rovere MT, Vanoli E. Autonomic nervous system and sudden cardiac death. Experimental basis and clinical observations for post-myocardial infarction risk stratification. *Circulation*. 1992;85:I77-91.
8. La Rovere MT, Bigger JT, Jr., Marcus FI, Mortara A, Schwartz PJ. Baroreflex sensitivity and heart-rate variability in prediction of total cardiac mortality after myocardial infarction. ATRAMI (Autonomic Tone and Reflexes After Myocardial Infarction) Investigators. *Lancet*. 1998;351:478-484.
9. Levy MN, Schwartz PJ. *Vagal Control of the Heart: Experimental Basis and Clinical Implications*. Armonk, NY: Futura Pub. Co.; 1994.
10. Shivkumar K, Ajijola OA, Anand I, Armour JA, Chen PS, Esler M, De Ferrari GM, Fishbein MC, Goldberger JJ, Harper RM, et al. Clinical neurocardiology defining the value of neuroscience-based cardiovascular therapeutics. *J Physiol*. 2016;594:3911-3954.
11. Waxman MB, Wald RW. Termination of ventricular tachycardia by an increase in cardiac vagal drive. *Circulation*. 1977;56:385-391.
12. Ando M, Katare RG, Kakinuma Y, Zhang D, Yamasaki F, Muramoto K, Sato T. Efferent vagal nerve stimulation protects heart against ischemia-induced arrhythmias by preserving connexin43 protein. *Circulation*. 2005;112:164-170.
13. Beaumont E, Southerland EM, Hardwick JC, Wright GL, Ryan S, Li Y, KenKnight BH, Armour JA, Ardell JL. Vagus nerve stimulation mitigates intrinsic cardiac

neuronal and adverse myocyte remodeling postmyocardial infarction. *Am J Physiol Heart Circ Physiol*. 2015;309:H1198-1206.

14. Li M, Zheng C, Sato T, Kawada T, Sugimachi M, Sunagawa K. Vagal nerve stimulation markedly improves long-term survival after chronic heart failure in rats. *Circulation*. 2004;109:120-124.

15. Hamann JJ, Ruble SB, Stolen C, Wang M, Gupta RC, Rastogi S, Sabbah HN. Vagus nerve stimulation improves left ventricular function in a canine model of chronic heart failure. *Eur J Heart Fail*. 2013;15:1319-1326.

16. Radcliffe EJ, Pearman CM, Watkins A, Lawless M, Kirkwood GJ, Saxton SN, Eisner DA, Trafford AW. Chronic vagal nerve stimulation has no effect on tachycardia-induced heart failure progression or excitation-contraction coupling. *Physiol Rep*. 2020;8:e14321.

17. Anand IS, Konstam MA, Klein HU, Mann DL, Ardell JL, Gregory DD, Massaro JM, Libbus I, DiCarlo LA, Udelson JJE, et al. Comparison of symptomatic and functional responses to vagus nerve stimulation in ANTHEM-HF, INOVATE-HF, and NECTAR-HF. *ESC Heart Fail*. 2020;7:75-83.

18. Gold MR, Van Veldhuisen DJ, Hauptman PJ, Borggrefe M, Kubo SH, Lieberman RA, Milasinovic G, Berman BJ, Djordjevic S, Neelagaru S, et al. Vagus Nerve Stimulation for the Treatment of Heart Failure: The INOVATE-HF Trial. *J Am Coll Cardiol*. 2016;68:149-158.

19. Zannad F, De Ferrari GM, Tuinenburg AE, Wright D, Brugada J, Butter C, Klein H, Stolen C, Meyer S, Stein KM, et al. Chronic vagal stimulation for the treatment of low ejection fraction heart failure: results of the NEural Cardiac TherApy foR

Heart Failure (NECTAR-HF) randomized controlled trial. *Eur Heart J*. 2015;36:425-433.

20. Premchand RK, Sharma K, Mittal S, Monteiro R, Dixit S, Libbus I, DiCarlo LA, Ardell JL, Rector TS, Amurthur B, et al. Autonomic Regulation Therapy via Left or Right Cervical Vagus Nerve Stimulation in Patients with Chronic Heart Failure: Results of the ANTHEM-HF Trial. *J Card Fail*. 2014;20:808-816.
21. Hadaya J, Ardell JL. Autonomic Modulation for Cardiovascular Disease. *Front Physiol*. 2020;11:617459.
22. Ardell JL, Nier H, Hammer M, Southerland EM, Ardell CL, Beaumont E, KenKnight BH, Armour JA. Defining the neural fulcrum for chronic vagus nerve stimulation: implications for integrated cardiac control. *J Physiol*. 2017;595:6887-6903.
23. Beaumont E, Wright GL, Southerland EM, Li Y, Chui R, KenKnight BH, Armour JA, Ardell JL. Vagus nerve stimulation mitigates intrinsic cardiac neuronal remodeling and cardiac hypertrophy induced by chronic pressure overload in guinea pig. *Am J Physiol Heart Circ Physiol*. 2016;310:H1349-1359.
24. Yoshie K, Rajendran PS, Massoud L, Mistry J, Swid MA, Wu X, Sallam T, Zhang R, Goldhaber JI, Salavatian S, et al. Cardiac TRPV1 afferent signaling promotes arrhythmogenic ventricular remodeling after myocardial infarction. *JCI Insight*. 2020;5.
25. Rivaud MR, Bayer JD, Cluitmans M, van der Waal J, Bear LR, Boukens BJ, Belterman C, Gottlieb L, Vaillant F, Abell E, et al. Critical repolarization gradients

determine the induction of reentry-based torsades de pointes arrhythmia in models of long QT syndrome. *Heart Rhythm*. 2021;18:278-287.

26. Haws CW, Lux RL. Correlation between in vivo transmembrane action potential durations and activation-recovery intervals from electrograms. Effects of interventions that alter repolarization time. *Circulation*. 1990;81:281-288.

27. Salavatian S, Beaumont E, Longpre JP, Armour JA, Vinet A, Jacquemet V, Shivkumar K, Ardell JL. Vagal stimulation targets select populations of intrinsic cardiac neurons to control neurally induced atrial fibrillation. *Am J Physiol Heart Circ Physiol*. 2016;311:H1311-H1320.

28. Chauhan VS, Downar E, Nanthakumar K, Parker JD, Ross HJ, Chan W, Picton P. Increased ventricular repolarization heterogeneity in patients with ventricular arrhythmia vulnerability and cardiomyopathy: a human in vivo study. *Am J Physiol Heart Circ Physiol*. 2006;290:H79-86.

29. Janse MJ, Coronel R, Opthof T, Sosunov EA, Anyukhovsky EP, Rosen MR. Repolarization gradients in the intact heart: transmural or apico-basal? *Prog Biophys Mol Biol*. 2012;109:6-15.

30. Ajijola OA, Yagishita D, Reddy NK, Yamakawa K, Vaseghi M, Downs AM, Hoover DB, Ardell JL, Shivkumar K. Remodeling of stellate ganglion neurons after spatially targeted myocardial infarction: Neuropeptide and morphologic changes. *Heart Rhythm*. 2015;12:1027-1035.

31. Ajijola OA, Hoover DB, Simerly TM, Brown TC, Yanagawa J, Biniwale RM, Lee JM, Sadeghi A, Khanlou N, Ardell JL, et al. Inflammation, oxidative stress, and

glial cell activation characterize stellate ganglia from humans with electrical storm. *JCI Insight*. 2017;2.

32. Vanoli E, De Ferrari GM, Stramba-Badiale M, Hull SS, Jr., Foreman RD, Schwartz PJ. Vagal stimulation and prevention of sudden death in conscious dogs with a healed myocardial infarction. *Circ Res*. 1991;68:1471-1481.

33. Shinlapawittayatorn K, Chinda K, Palee S, Surinkaew S, Kumfu S, Kumphune S, Chattipakorn S, KenKnight BH, Chattipakorn N. Vagus nerve stimulation initiated late during ischemia, but not reperfusion, exerts cardioprotection via amelioration of cardiac mitochondrial dysfunction. *Heart rhythm*. 2014;11:2278-2287.

34. Shinlapawittayatorn K, Chinda K, Palee S, Surinkaew S, Thunsiri K, Weerateerangkul P, Chattipakorn S, KenKnight BH, Chattipakorn N. Low-amplitude, left vagus nerve stimulation significantly attenuates ventricular dysfunction and infarct size through prevention of mitochondrial dysfunction during acute ischemia-reperfusion injury. *Heart Rhythm*. 2013;10:1700-1707.

35. Seki A, Fishbein MC. Ischemic Heart Disease. In: McManus LM, Mitchell RN, eds. *Pathobiology of Human Disease*. San Diego: Academic Press; 2014:995-1013.

36. Adegboyega PA, Haque AK, Boor PJ. Extensive myocytolysis as a marker of sudden cardiac death. *Cardiovasc Pathol*. 1996;5:315-321.

37. De Ferrari GM, Vanoli E, Stramba-Badiale M, Hull SS, Jr., Foreman RD, Schwartz PJ. Vagal reflexes and survival during acute myocardial ischemia in conscious dogs with healed myocardial infarction. *Am J Physiol*. 1991;261:H63-69.

38. Malliani A, Recordati G, Schwartz PJ. Nervous activity of afferent cardiac sympathetic fibres with atrial and ventricular endings. *J Physiol*. 1973;229:457-469.

39. Hoover DB, Shepherd AV, Southerland EM, Armour JA, Ardell JL. Neurochemical diversity of afferent neurons that transduce sensory signals from dog ventricular myocardium. *Auton Neurosci*. 2008;141:38-45.

40. Nakamura K, Ajijola OA, Aliotta E, Armour JA, Ardell JL, Shivkumar K. Pathological effects of chronic myocardial infarction on peripheral neurons mediating cardiac neurotransmission. *Auton Neurosci*. 2016;197:34-40.

41. Wang L, Olivas A, Francis Stuart SD, Tapa S, Blake MR, Woodward WR, Habecker BA, Ripplinger CM. Cardiac sympathetic nerve transdifferentiation reduces action potential heterogeneity after myocardial infarction. *Am J Physiol Heart Circ Physiol*. 2020;318:H558-H565.

42. Kanazawa H, Ieda M, Kimura K, Arai T, Kawaguchi-Manabe H, Matsuhashi T, Endo J, Sano M, Kawakami T, Kimura T, et al. Heart failure causes cholinergic transdifferentiation of cardiac sympathetic nerves via gp130-signaling cytokines in rodents. *J Clin Invest*. 2010;120:408-421.

43. Olivas A, Gardner RT, Wang L, Ripplinger CM, Woodward WR, Habecker BA. Myocardial Infarction Causes Transient Cholinergic Transdifferentiation of Cardiac Sympathetic Nerves via gp130. *J Neurosci*. 2016;36:479-488.

44. van Weperen VYH, Littman RJ, Arneson DV, Contreras J, Yang X, Ajijola OA. Single-cell transcriptomic profiling of satellite glial cells in stellate ganglia reveals developmental and functional axial dynamics. *Glia*. 2021;69:1281-1291.

45. Feldman-Goriachnik R, Hanani M. The effects of sympathetic nerve damage on satellite glial cells in the mouse superior cervical ganglion. *Auton Neurosci*. 2019;221:102584.

46. Shao LJ, Liang SD, Li GL, Xu CS, Zhang CP. Exploration of P2X3 in the rat stellate ganglia after myocardial ischemia. *Acta Histochem*. 2007;109:330-337.

47. Gurel NZ, Sudarshan KB, Hadaya J, Karavos A, Temma T, Hori Y, Armour JA, Kember G, Ajijola OA. Metrics of High Cofluctuation and Entropy to Describe Control of Cardiac Function in the Stellate Ganglion. *bioRxiv*. 2021:2021.2009.2028.462183.

48. Sudarshan KB, Hori Y, Swid MA, Karavos AC, Wooten C, Armour JA, Kember G, Ajijola OA. A novel metric linking stellate ganglion neuronal population dynamics to cardiopulmonary physiology. *Am J Physiol Heart Circ Physiol*. 2021;321:H369-H381.

49. Shen MJ, Hao-Che C, Park HW, George Akingba A, Chang PC, Zheng Z, Lin SF, Shen C, Chen LS, Chen Z, et al. Low-level vagus nerve stimulation upregulates small conductance calcium-activated potassium channels in the stellate ganglion. *Heart Rhythm*. 2013;10:910-915.

50. Salavatian S, Ardell SM, Hammer M, Gibbons DD, Armour JA, Ardell JL. Thoracic spinal cord neuromodulation obtunds dorsal root ganglion afferent neuronal transduction of the ischemic ventricle. *Am J Physiol Heart Circ Physiol*. 2019.

51. Armour JA, Linderoth B, Arora RC, DeJongste MJ, Ardell JL, Kingma JG, Jr., Hill M, Foreman RD. Long-term modulation of the intrinsic cardiac nervous system by

spinal cord neurons in normal and ischaemic hearts. *Auton Neurosci*. 2002;95:71-79.

52. Wang HJ, Wang W, Cornish KG, Rozanski GJ, Zucker IH. Cardiac sympathetic afferent denervation attenuates cardiac remodeling and improves cardiovascular dysfunction in rats with heart failure. *Hypertension*. 2014;64:745-755.

53. Scherlag BJ, Kabell G, Harrison L, Lazzara R. Mechanisms of bradycardia-induced ventricular arrhythmias in myocardial ischemia and infarction. *Circulation*. 1982;65:1429-1434.

54. Zhang Y, Popovic ZB, Bibevski S, Fakhry I, Sica DA, Van Wagoner DR, Mazgalev TN. Chronic vagus nerve stimulation improves autonomic control and attenuates systemic inflammation and heart failure progression in a canine high-rate pacing model. *Circ Heart Fail*. 2009;2:692-699.

55. Nearing BD, Libbus I, Amurthur B, Kenknight BH, Verrier RL. Acute Autonomic Engagement Assessed by Heart Rate Dynamics During Vagus Nerve Stimulation in Patients With Heart Failure in the ANTHEM-HF Trial. *J Cardiovasc Electrophysiol*. 2016;27:1072-1077.

56. Premchand RK, Sharma K, Mittal S, Monteiro R, Dixit S, Libbus I, DiCarlo LA, Ardell JL, Rector TS, Amurthur B, et al. Extended Follow-Up of Patients With Heart Failure Receiving Autonomic Regulation Therapy in the ANTHEM-HF Study. *J Card Fail*. 2016;22:639-642.

57. Sharma K, Premchand RK, Mittal S, Monteiro R, Libbus I, DiCarlo LA, Ardell JL, Amurthur B, KenKnight BH, Anand IS. Long-term follow-up of patients with heart

failure and reduced ejection receiving autonomic regulation therapy in the ANTHEM-HF pilot study. *Int J Cardiol*. 2020.

58. De Ferrari GM, Stolen C, Tuinenburg AE, Wright DJ, Brugada J, Butter C, Klein H, Neuzil P, Botman C, Castel MA, et al. Long-term vagal stimulation for heart failure: Eighteen month results from the NEural Cardiac TherApy foR Heart Failure (NECTAR-HF) trial. *Int J Cardiol*. 2017;244:229-234.

59. Billman GE. A comprehensive review and analysis of 25 years of data from an in vivo canine model of sudden cardiac death: implications for future anti-arrhythmic drug development. *Pharmacol Ther*. 2006;111:808-835.

60. Collins MN, Billman GE. Autonomic response to coronary occlusion in animals susceptible to ventricular fibrillation. *Am J Physiol*. 1989;257:H1886-1894.

CHAPTER 4

Conclusions, future directions, and clinical implications

Conclusions

The autonomic nervous system plays a major role in the progression of cardiovascular disease including ventricular arrhythmias and cardiac dysfunction following myocardial infarction.[1,2] Pathophysiologically, aberrant remodeling following cardiac injury leads to excess sympathoexcitation and parasympathetic withdrawal (Figure 38). These processes may clinically manifest as inadequate cardiac output, ventricular systolic or diastolic dysfunction, ventricular arrhythmias, and the risk for sudden death. The present work mechanistically evaluates autonomic dysregulation and therapeutic strategies using a porcine model. The principal findings of this dissertation are as follows:

1. MI leads to substantial impairments in cardiac mechanical function and a greater propensity toward ventricular arrhythmias in Yucatan minipigs.
2. At the tissue level, MI promotes anisotropic electrical propagation and conduction block, increases repolarization heterogeneity, and leads to steep repolarization gradients at the scar border-zone.
3. At the cellular level, MI leads to aberrant structural remodeling of the border zone, as well as changes in neuronal phenotypes and glial activation in the stellate and thoracic dorsal root ganglia.
4. Sympathetic blockade using kilohertz frequency alternating current induces a high degree of sympathetic efferent block and reduces norepinephrine release at the level of the heart.
5. Ipsilateral sympathetic blockade is efficacious in the setting of contralateral sympathectomy, reducing norepinephrine release and its end effect on the heart.

6. Chronic vagal nerve stimulation (VNS) substantially improves mechanical function and reduces ventricular arrhythmias post-MI, partly by stabilizing heterogeneity in activation and repolarization in the scar border-zone.
7. Chronic vagal nerve stimulation substantially reduces glial activation in the stellate and thoracic dorsal root ganglia after MI, but also influences neuronal phenotypes.

For the first time, we demonstrate the cardioprotective benefits of chronic VNS on cardiac function, ventricular arrhythmia inducibility, and cardiac structural and extracardiac neural remodeling after MI in a large mammal. This work sets forth a foundation upon which further studies can mechanistically evaluate how restoration of parasympathetic tone improves cardiac function post-MI.

Future Directions

Mechanistic evaluation of autonomic dysregulation at the border-zone

Myocardial infarction and its associated structural and electrical abnormalities contribute to the risk of life-threatening ventricular arrhythmias.[3-5] These arrhythmias represent complex interactions between altered myocardial structure, including scar formation and abnormal myocyte properties, and changes in neural input to the myocardium.[6] The scar border-zone is of particular significance as it is hypothesized to be the source of ventricular arrhythmias following MI. Notably, a majority of clinical interventions that target the myocardium aim to localize scar and border-zone regions and modify the substrate using catheter ablation.[7-11] In the present work, we found that electrophysiologic function at the border-zone was significantly impaired post-MI, with

formation of areas of slow conduction, anisotropic impulse propagation, and steep repolarization gradients. In murine hearts, these border-zone regions colocalize with dense areas of small nerve fibers that are tyrosine hydroxylase positive, suggesting that sympathetic input to this region of the heart is impaired.[12] However, studies examining the functional role of these nerve sprouts have not been evaluated; importantly, whether these sprouts release norepinephrine, and to what degree, has never been directly demonstrated.

To evaluate how myocardial infarction alters catecholamine release in the heart, we evaluated norepinephrine release in response to bilateral sympathetic chain stimulation in vivo in 6 normal Yucatan minipigs and 6 Yucatan minipigs with myocardial infarction. Fast scanning cyclic voltammetry (FSCV) probes were placed in scar and border zone regions of the infarcted hearts and the same corresponding anatomic area in normal hearts (Figure 39). Representative tracings demonstrate a significant increase in NE with bilateral sympathetic chain stimulation (BSS), as expected. In the setting of MI, we found evidence of greater NE release in response to BSS in the border-zone and reduced NE release in scar, compared to the same anatomic region in controls. These findings suggest that sympathetic activation may amplify heterogeneity in the scar border-zone by heterogenous catecholamine release, increasing the propensity toward ventricular arrhythmias. Further ongoing work to map these border zone regions using a combination of tissue-clearing (immunolabeling-enabled three-dimensional imaging of solvent-cleared organs), high-density electrophysiologic mapping, and evaluation of catecholamine release may clarify the role of sympathetic input in border-zone dysfunction following MI.

Identifying subpopulations of myocytes in the border zone for therapeutic targets

Further work to understand properties of border-zone myocytes may not only improve our understanding of cardiac dysfunction following MI, but may identify new therapeutic targets. In the present work, we found that MI resulted in aberrant electrophysiologic remodeling that led to impaired impulse propagation as well as abnormal myocardial repolarization sequences in the left ventricle, which was improved with chronic vagal nerve stimulation. While these analyses reflect underlying function at the myocyte level, these assessments ultimately best represent tissue-level properties rather than those of isolated myocytes. Our laboratory's future work will utilize patch clamping techniques to evaluate repolarization properties and triggered activity among myocytes from border-zone regions of the heart in MI animals with or without chronic VNS. These studies will further build upon findings from this dissertation and evaluate cellular-level electrophysiologic remodeling post-MI.

Heterogeneity of myocytes in the left ventricle post-MI leads to challenges in precise phenotyping of populations of border-zone myocytes.[13-15] Until recently, most single-cell transcriptomic techniques required dissociation of samples, resulting in loss of spatial relationships, which are critical to understanding cardiac remodeling post-MI. Recent advances in sequencing technologies now allow for characterization of transcriptomics profiles in situ, without disruption of tissue architecture or relationships.[16] Evaluation of the spatial transcriptome of scar, border-zone, and remote regions of the myocardium may identify pathways unique to the border-zone that can be targeted post-MI. Moreover, comparison of the border-zone transcriptome in chronic VNS treated animals versus MI alone may identify cellular pathways or targets through

which chronic VNS exerts its cardioprotective effects. These pathways can be further studied to characterize subcellular mechanisms of VNS or to evaluate whether activation or blockade of these pathways through pharmacologic agents can mitigate post-MI cardiac structural or electrical remodeling.

Role of non-neuronal cell populations in afferent and efferent ganglia in remodeling following MI

While neural dysfunction has been increasingly recognized as a contributor to the progression of cardiovascular disease, the majority of studies have focused on evaluation of neural function in vivo, or neuronal phenotypes in vitro, with minimal work evaluating non-neuronal cell types. In the central nervous system, glial cells, particularly astrocytes, are involved in neuron development and maturation, and also become activated in response to pathology or local injury.[17] In the peripheral nervous system, satellite glial cells are found in autonomic and sensory ganglia and are involved in formation and maintenance of synapses.[18] These glial cells diverse, generally considered non-excitable, but can influence activity of neurons in a paracrine manner or directly through cellular coupling via gap junctions.[19-22] In the present work, we found evidence of glial activation following MI in both the stellate ganglia and dorsal root ganglia, the primary source of sympathetic efferent and general visceral afferent fibers to the heart. Activation of these glial cells was mitigated by chronic vagal nerve stimulation in both sets of ganglia, suggesting a central role for glial cells in post-MI neural remodeling. Further work to study cellular mechanisms and consequences of glial dysfunction may identify non-neuronal cell populations that can be therapeutically targeted. Such work may integrate single cell sequencing of satellite glial cells and

selective activation of these cell types using chemogenetic approaches in murine models, where genetic manipulation is readily feasible.[23] Furthermore, as glial activation has been described in humans with ischemic cardiomyopathy,[24] approaches to further study these cells from explanted ganglia or cadaveric donors may inform future work.

Cardiac afferent dysfunction in myocardial infarction and associated disorders

While most studies have focused on either the end-organ or efferent autonomic dysfunction, recent work has evaluated afferent dysfunction as it relates to cardiovascular disease. For example, disruption of transient receptor potential cation subfamily V member 1 (TRPV1)-positive fibers using epicardial resiniferatoxin at the time of MI has been previously shown to mitigate myocardial structural remodeling in both rats and pigs, directly implicating afferent dysfunction in remodeling after MI.[25,26] Although the present dissertation can not differentiate afferent versus efferent function due to its design, efforts to elucidate afferent versus efferent autonomic dysfunction may lead to more mechanistic approaches to disease therapy.

Given the role of the autonomic nervous system in regulation of multiorgan function, several studies have evaluated autonomic dysfunction in diseases that are often comorbid with heart failure or myocardial infarction. In cardiorenal syndrome type 2 (CRS2), underlying primary chronic cardiac disease such as congestive heart failure (CHF) leads to chronic kidney dysfunction, and is strongly associated with greater hazard of all-cause mortality in direct proportional to the degree of decline in renal function.[27] In a rat model of congestive heart failure, disruption of cardiac afferent fibers by epicardial application of resiniferatoxin at the time of MI reduced the CSAR and ameliorated cardiac dysfunction.[28] Importantly, renal dysfunction, as evaluated through

urine output, microalbuminuria, and renal blood flow significantly improved with chronic cardiac afferent ablation compared to vehicle.[28] This process was partly related to reduced central venous congestion, less cortical and medullary injury, and downregulation of genes involved in inflammation, apoptosis, and hypoxia. Taken together, these findings strongly suggest that cardiac afferent activation not only contributes to cardiac dysfunction but also renal disease post-MI. The authors further found that a proportion of these afferent fibers travel through the stellate ganglia, and that disruption of afferents at the level of the stellate mitigates changes in markers of renal dysfunction post-MI.[28] As such, another therapeutic strategy for both cardiac and renal dysfunction after MI includes targeting cardiac afferents. Further research regarding cardiac afferents in large mammals and in conjunction with existing medical therapy are necessary to fully define the translational potential of such approaches for cardiovascular disease and its associated disorders

Clinical Implications

This work provides evidence that chronic vagal nerve stimulation, when delivered in a rationale and neuroscientifically-guided manner, can improve cardiac dysfunction and reduce the propensity toward ventricular arrhythmias following myocardial infarction. The large animal model utilized in the present work readily recapitulates the clinical phenotype of ischemic cardiomyopathy, and exhibits sudden cardiac death in an ambulatory setting. Furthermore, chronic vagal nerve stimulation is feasible in patients, as devices are approved by the United States Food and Drug Administration for epilepsy and depression, and phase III clinical trials are currently underway for heart

failure with reduced ejection fraction. As such, this work provides strong translational evidence for chronic VNS as a therapeutic modality post MI, and we hope this study will aid in implementation of such trials in patients.

Beta adrenergic receptor blockade and inhibition of the renin-angiotensin-aldosterone system are the two most common pharmacologic agents for congestive heart failure and post-MI cardiac dysfunction. The present work supports the existing body of literature that implicates sympathetic dysfunction in the pathogenesis and progression of cardiovascular disease. While existing clinical therapies primarily target components of efferent sympathetic signaling, a growing body of literature has implicated cardiac afferent dysfunction in animal models of cardiovascular disease, and may represent a novel therapeutic approach.

Finally, the present work suggests that the general concept of restoration of parasympathetic tone has substantial cardioprotective effects. No pharmacologic or device-based therapy currently exists to target parasympathetic dysfunction post myocardial infarction. While this could be accomplished with conventional vagal nerve stimulation, further molecular work and mechanistic studies may identify therapeutic pathways through which vagal nerve stimulation acts. Such an approach would facilitate the development of unique, targeted pharmacologic agents and may lead to neuroscientifically-inspired approaches to treat cardiovascular disease.

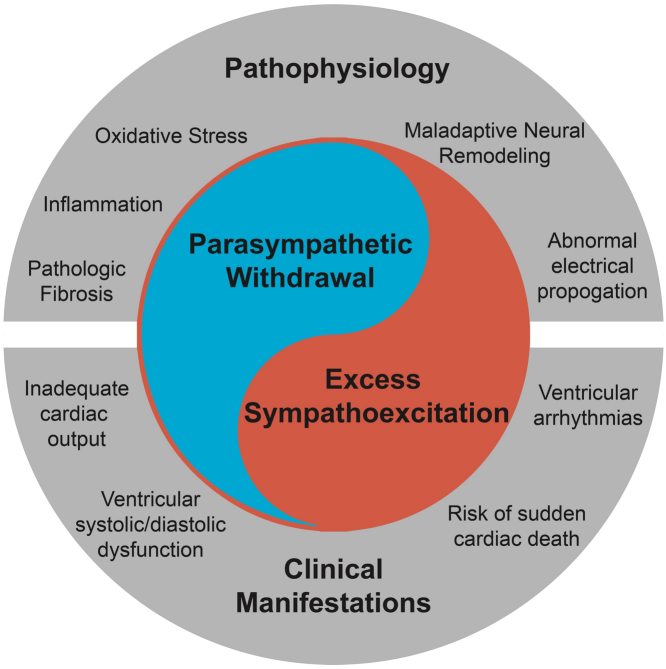

Figure 38. Autonomic dysfunction in cardiovascular disease is characterized by excess sympathoexcitation and parasympathetic withdrawal. Following myocardial infarction, remodeling at the level of the myocardium includes pathologic fibrosis, inflammation, and oxidative stress, as well as maladaptive neural remodeling at the stellate and dorsal root ganglia. These processes lead to inadequate cardiac output, ventricular arrhythmias, and risk for sudden cardiac death.

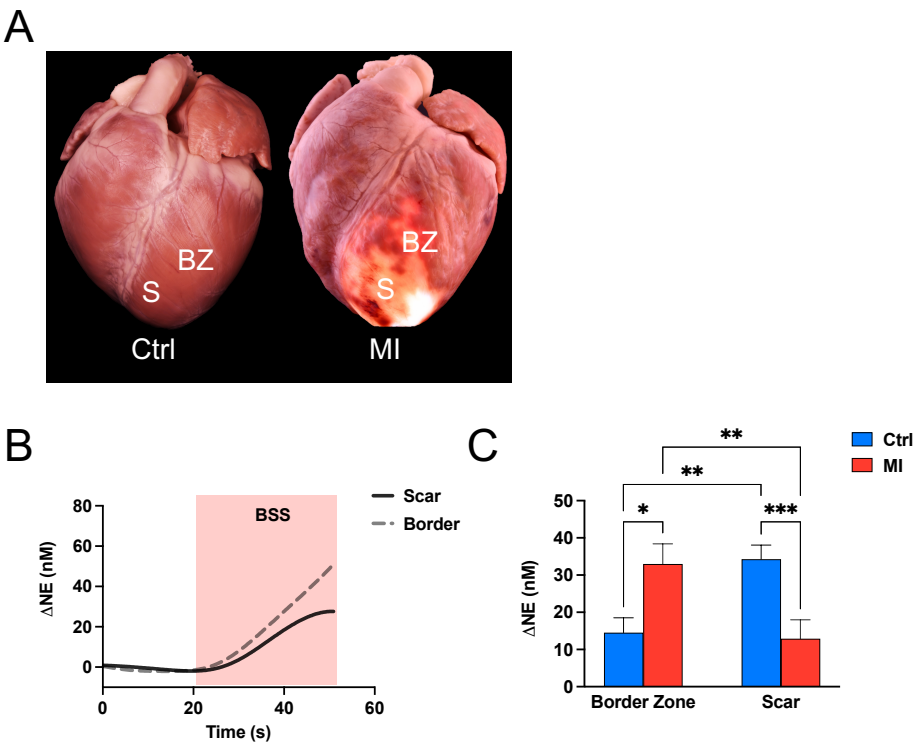

Figure 39. Myocardial infarction (MI) alters catecholamine release in the scar and border zone. Areas of scar (S) and border zone (BZ) and corresponding anatomic regions in normal hearts (A) were evaluated for NE release during bilateral sympathetic chain stimulation (BSS). Representative tracings (B) demonstrate increases in NE with BSS in both scar and border-zone regions in an MI animal. Across 6 control and 6 MI pigs, NE release was greater in the border-zone in MI animals compared to the same anatomic region in controls (C). Moreover, NE release was greater in border zone regions compared to scar in MI animals, potentially exacerbating existing structural heterogeneity and promoting ventricular arrhythmogenesis. *p<0.05, **p<0.01, ***p<0.001.

References

1. Shivkumar K, Ajijola OA, Anand I, Armour JA, Chen PS, Esler M, De Ferrari GM, Fishbein MC, Goldberger JJ, Harper RM, et al. Clinical neurocardiology defining the value of neuroscience-based cardiovascular therapeutics. *J Physiol*. 2016;594:3911-3954.
2. Ardell JL, Andresen MC, Armour JA, Billman GE, Chen PS, Foreman RD, Herring N, O'Leary DS, Sabbah HN, Schultz HD, et al. Translational neurocardiology: preclinical models and cardioneural integrative aspects. *J Physiol*. 2016;594:3877-3909.
3. Zhou S, Chen LS, Miyauchi Y, Miyauchi M, Kar S, Kangavari S, Fishbein MC, Sharifi B, Chen PS. Mechanisms of cardiac nerve sprouting after myocardial infarction in dogs. *Circ Res*. 2004;95:76-83.
4. Janse MJ, Wit AL. Electrophysiological mechanisms of ventricular arrhythmias resulting from myocardial ischemia and infarction. *Physiol Rev*. 1989;69:1049-1169.
5. Billman GE. A comprehensive review and analysis of 25 years of data from an in vivo canine model of sudden cardiac death: implications for future anti-arrhythmic drug development. *Pharmacol Ther*. 2006;111:808-835.
6. Ajijola OA, Lux RL, Khahera A, Kwon O, Aliotta E, Ennis DB, Fishbein MC, Ardell JL, Shivkumar K. Sympathetic modulation of electrical activation in normal and infarcted myocardium: implications for arrhythmogenesis. *Am J Physiol Heart Circ Physiol*. 2017;312:H608-H621.

7. Nakahara S, Tung R, Ramirez RJ, Gima J, Wiener I, Mahajan A, Boyle NG, Shivkumar K. Distribution of late potentials within infarct scars assessed by ultra high-density mapping. *Heart Rhythm*. 2010;7:1817-1824.

8. Nakahara S, Tung R, Ramirez RJ, Michowitz Y, Vaseghi M, Buch E, Gima J, Wiener I, Mahajan A, Boyle NG, et al. Characterization of the arrhythmogenic substrate in ischemic and nonischemic cardiomyopathy implications for catheter ablation of hemodynamically unstable ventricular tachycardia. *J Am Coll Cardiol*. 2010;55:2355-2365.

9. Nakahara S, Vaseghi M, Ramirez RJ, Fonseca CG, Lai CK, Finn JP, Mahajan A, Boyle NG, Shivkumar K. Characterization of myocardial scars: electrophysiological imaging correlates in a porcine infarct model. *Heart Rhythm*. 2011;8:1060-1067.

10. Mathuria N, Tung R, Shivkumar K. Advances in ablation of ventricular tachycardia in nonischemic cardiomyopathy. *Curr Cardiol Rep*. 2012;14:577-583.

11. Shivkumar K. Catheter Ablation of Ventricular Arrhythmias. *N Engl J Med*. 2019;380:1555-1564.

12. Zhu C, Rajendran PS, Hanna P, Efimov IR, Salama G, Fowlkes CC, Shivkumar K. High-resolution structure-function mapping of intact hearts reveals altered sympathetic control of infarct border zones. *JCI Insight*. 2022;7.

13. Decker KF, Rudy Y. Ionic mechanisms of electrophysiological heterogeneity and conduction block in the infarct border zone. *Am J Physiol Heart Circ Physiol*. 2010;299:H1588-1597.

14. Rutherford SL, Trew ML, Sands GB, LeGrice IJ, Smaill BH. High-resolution 3-dimensional reconstruction of the infarct border zone: impact of structural remodeling on electrical activation. *Circ Res*. 2012;111:301-311.
15. Hegyi B, Bossuyt J, Griffiths LG, Shimkunas R, Coulibaly Z, Jian Z, Grimsrud KN, Sondergaard CS, Ginsburg KS, Chiamvimonvat N, et al. Complex electrophysiological remodeling in postinfarction ischemic heart failure. *Proc Natl Acad Sci U S A*. 2018;115:E3036-E3044.
16. Vickovic S, Eraslan G, Salmen F, Klughammer J, Stenbeck L, Schapiro D, Aijo T, Bonneau R, Bergenstrahle L, Navarro JF, et al. High-definition spatial transcriptomics for in situ tissue profiling. *Nat Methods*. 2019;16:987-990.
17. Allen NJ, Lyons DA. Glia as architects of central nervous system formation and function. *Science*. 2018;362:181-185.
18. Hanani M. Satellite glial cells in sensory ganglia: from form to function. *Brain Res Brain Res Rev*. 2005;48:457-476.
19. Spray DC, Iglesias R, Shraer N, Suadicani SO, Belzer V, Hanstein R, Hanani M. Gap junction mediated signaling between satellite glia and neurons in trigeminal ganglia. *Glia*. 2019;67:791-801.
20. Hanani M, Spray DC. Emerging importance of satellite glia in nervous system function and dysfunction. *Nat Rev Neurosci*. 2020;21:485-498.
21. Chen Z, Huang Q, Song X, Ford NC, Zhang C, Xu Q, Lay M, He SQ, Dong X, Hanani M, et al. Purinergic signaling between neurons and satellite glial cells of mouse dorsal root ganglia modulates neuronal excitability in vivo. *Pain*. 2021.

22. Souza GR, Talbot J, Lotufo CM, Cunha FQ, Cunha TM, Ferreira SH. Fractalkine mediates inflammatory pain through activation of satellite glial cells. *Proc Natl Acad Sci U S A*. 2013;110:11193-11198.

23. Hirbec H, Deglon N, Foo LC, Goshen I, Grutzendler J, Hangen E, Kreisel T, Linck N, Muffat J, Regio S, et al. Emerging technologies to study glial cells. *Glia*. 2020;68:1692-1728.

24. Ajijola OA, Hoover DB, Simerly TM, Brown TC, Yanagawa J, Biniwale RM, Lee JM, Sadeghi A, Khanlou N, Ardell JL, et al. Inflammation, oxidative stress, and glial cell activation characterize stellate ganglia from humans with electrical storm. *JCI Insight*. 2017;2.

25. Wang HJ, Wang W, Cornish KG, Rozanski GJ, Zucker IH. Cardiac sympathetic afferent denervation attenuates cardiac remodeling and improves cardiovascular dysfunction in rats with heart failure. *Hypertension*. 2014;64:745-755.

26. Yoshie K, Rajendran PS, Massoud L, Mistry J, Swid MA, Wu X, Sallam T, Zhang R, Goldhaber JI, Salavatian S, et al. Cardiac TRPV1 afferent signaling promotes arrhythmogenic ventricular remodeling after myocardial infarction. *JCI Insight*. 2020;5.

27. Smith GL, Lichtman JH, Bracken MB, Shlipak MG, Phillips CO, DiCapua P, Krumholz HM. Renal impairment and outcomes in heart failure: systematic review and meta-analysis. *J Am Coll Cardiol*. 2006;47:1987-1996.

28. Xia Z, Vellichirammal NN, Han L, Gao L, Boesen EI, Schiller AM, Pellegrino P, Lisco SJ, Guda C, Zucker IH, Wang HJ. Cardiac spinal afferent denervation

attenuates renal dysfunction in rats with cardio-renal syndrome type 2. *JACC Basic Transl Sci*. 2022;7.